UNIVERSITY OF LIVERPOOL

An Investigation into the Hydration and Growth of Ice Layers on Metal Surfaces using Low Temperature Scanning Tunnelling Microscopy

Thesis of Nikki Louise Gerrard

October 2019

Supervisors:

Professor Andrew Hodgson

Dr George Darling

Thesis Contents

List of Abbreviations

PEMFC – Polymer Exchange Membrane Fuel Cell

UHV – Ultra High Vacuum

SPM – Scanning Probe Microscopy

STM – Scanning Tunnelling Microscopy

DFT – Density Functional Theory

AFM – Atomic Force Microscopy

LEED – Low Energy Electron Diffraction

ML – Monolayer

TPD - Temperature Programmed Desorption

ESDIAD – Electron Stimulated Desorption Ion Angular Distribution

XPS – X-ray Photoelectron Spectroscopy

UPS – Ultraviolet Photoelectron Spectroscopy

HREELS – High Resolution Electron Energy Loss Spectroscopy

FTIR – Fourier-Transform Infrared Spectroscopy

VASP – Vienna Ab initio Simulation Package

PBE – Perdew-Burle-Ernzerhof

vdW – van der Waals

SXRD – Surface X-Ray Diffraction

SnPt – $(\sqrt{3}x\sqrt{3})R30°$-SnPt(111) alloy surface

P – Pinched

Z – Zigzag

MD – Molecular Dynamics

Acknowledgements

There are so many people I would like to thank for the large or small part they have played in supporting me during my doctorate studies, all of which have led me to where I am today, and for that, I will forever be grateful.

I naturally have to start with my supervisor, Professor Andrew Hodgson, as without him believing I was the right candidate for this studentship, I would not be here today. I have so many things to be thankful for, your endless stream of knowledge and expertise in this field, your insightful intelligence in Chemistry as a whole and all you have taught me during my time at the SSRC. You have passed on many skills and words of wisdom which I will utilise during my entirety of my career from hereon, and have made sure that the importance of Surface Science (and particularly water!) will always have an important place in my heart. But putting the science aside, you have been an amazing role model who has encouraged me throughout. Our research group has always felt like a supportive team and I will always be grateful for the kind and friendly atmosphere you created. Your endless support, care and encouragement have helped me to get through the darker days in the lab when I may otherwise have lost hope and helped me to believe in myself again. I have been so lucky to have such an influential person as a supervisor and I will forever be thankful to you.

Dr Shamsal Haq, without you I'm unsure I would have survived the dark art of STM! Thank you for your endless training and support through my PhD studies, for picking me up on the darker days in the lab and always encouraging me to achieve. For fixing any problems I could not solve and answering my never-ending list of questions! For showing me the ins and outs of a rotary pump, how to change a gasket and all the trivial things required to become a true experimentalist! I will be forever grateful for your mentoring Sam, and all of the time you took to help me, but also your friendship and the many times of laughter we had. You never failed to brighten my day, thank you.

Now I move on to the amazing lady who has kept me sane over the last four and a half years, Dr Fiona McBride. We sparked a great friendship as soon as we met and I am sure we will remain friends for the rest of time. Thank you for our mentor/mentee lunches; I'm going to miss our trips to Moose Coffee for sure and our complaints

about daily life in the lab whilst eating curly fries at The Font! Thank you being the person I can come to with my ‘stupid questions’ when I cannot find the answer elsewhere and would not dare to ask someone else in case they laughed! Thankful for your continued interest in water and your database-filled brain for when I ask about a particular paper from many years ago and expect you to remember it in detail! I will forever be thankful to you for your kindness, humour and friendship. I have so many lovely memories from my time at the SSRC and they will always hold a place in my heart. Thank you for your endless encouragement, support and the ‘are you alive?’ moments when I had been working non-stop in the lab and missed coffee breaks. I hope every student completing a PhD has someone like you to pull them through the highs and lows, thank you Fi.

Dr George Darling and Dr Gita Sedghi, I thank you both for your encouragement and support throughout the many years I have been at the University of Liverpool, both undergraduate and postgraduate. George, thank you for your advice throughout my time at the SSRC and the collaboration of your theoretical calculations and insight to support my experimental results. Gita, thank you for teaching me how to communicate well with other students and pass my knowledge onto others. These are skills I will use throughout my career.

The past and present members of the Hodgson group, Chenfang and Ed, thank you for your words of wisdom, extended STM knowledge and all of your help and support during my studies. You brought great expertise to the group and I wish you the best of luck with your excelling careers. To the other members of the SSRC who I have had the pleasure of working with, thank you for your fruitful conversations at tea break and lunch time throughout the last four years. I will always be grateful for your friendship and kindness and I wish you all the best of luck in the future.

Leaving the best till last, I thank the most important people in my life. The ones who provide unconditional love, support and encouragement throughout. To my amazing husband who has supported me throughout my many years of studying, for pushing me through the hard times and celebrating with me through the good. To my darling daughter, you bring so much happiness to my life and motivate me to achieve more and more every day. You will forever be my inspiration and thanks to you, I know I

can succeed in all I do. To my loving parents, for always encouraging me to follow my dreams and teaching me that I can do anything I set my mind to. To the remainder of my family and friends, thank you all for your encouragement, support and love.

Finally to any readers of this thesis, thank you for your time. I hope these topics provide you with as much interest and insightfulness as they did me.

Chapter 1

Introduction

1. Introduction

1.1. Introduction to Water/Solid Interfaces

Water plays a huge role in everyday life where it is largely taken for granted and its importance often forgotten. Being present in the majority of environments, it influences many aspects of nature, science and technology. One often forgets about its vital role within the world's ecosystem, with 71 %[1] of earth covered with water and its act as an essential source of nutrition for animals and plants. Although essential to maintain life on earth, it also plays a huge role in undesirable situations, including more contemporary issues of corrosion, energy shortages and climate change[2]. This has led to a great desire to understand the interactions and influence of water/solid interfaces and how to utilise this knowledge to improve the earth's environment. Over recent years, there has consequently been a vast amount of research performed to analyse and assess interfacial water layers in the hope of developing an insight into the complicated nature of this simple molecule.

If we discuss the more contemporary issues of water in more detail, one huge area of research over recent years has been focused on preventing the corrosion of metallic pipework[3-5]. It is well known that water will easily corrode iron, regardless of its composition, and there has consequently been great attention into the investigation of anticorrosion coatings for pipework to extend their lifetime and reduce costs within this industry. Completing this to a high standard requires an understanding of this water/metal interface and the application of this knowledge to ensure successful manufacturing of an appropriate coating composition. Another issue that has been of great interest in recent years is the role of water in fuel cells, including the Proton Exchange Membrane Fuel Cell (PEMFC)[6,7]. To create high performance and high energy efficient PEMFCs, it is essential to understand the transport of water across the membrane and how heat transfer from different water phases aids the fuel cell's

overall performance[8]. For the role in which water plays in these issues to be understood, it is essential to recognise the importance of water at the water/solid interfacial layer, before one can begin to conquer these issues in the near future.

The activity and reactivity of water/solid interfaces is often a result of the hydrogen-bonding networks that form at the interface, their ability to solvate ions and the ease of proton transfer (or charge) across a hydrogen-bonding network to the surface. Theoretical models for many electrochemical interfaces show that the local hydrogen-bonding network of surface adsorbates with water changes their stability and conformation[9], modifying reaction barriers and changing the chemistry that can occur. In particular, important surface processes that depend on hydrogen-bonding include low temperature fuel cell reactions[10-12], water-gas shift catalysis[13,14], and various other commercial processes[15,16]. However, aqueous or water containing interfaces are difficult to characterise, largely due to their disorder and the difficulty in determining the position of hydrogen atoms, which makes it challenging to locate all of the atoms at an interface. As a consequence, little is known directly about the structure of the reaction intermediates involved, which are instead often inferred from theoretical models[2,17-22]. Current experimental measurements are however unable to properly test or support such theoretical descriptions, leaving uncertainty about the validity of the models used.

To understand the interactions at water/solid interfaces, one needs to also appreciate the unusual physical and chemical properties of water in the interfacial layer. Most experimental studies have therefore focused on the use of Ultra High Vacuum (UHV) systems to limit contaminants, enabling the possibility to investigate the surface reaction of water at a particular water/metal interface and the structure it forms without the influence of other surface species. This is essential as one needs to gain an insight on a molecular scale to understand the favourable environment of water within this interfacial layer, before taking into account additional factors which can influence surface wetting on a macroscopic scale.

To gain a clear insight into these water/metal interfaces on a molecular level, it is important to understand the structure of the initial wetting layer which binds to the surface before one can articulate how it transforms its structure from the surface layer

into a thick ice film. Much work has been done which focuses on the structures that form at these interfaces, with great attention to different symmetry faces of various transition metals[2,17,18,23,24]. In light of these studies, the general outcome is that a single model cannot be used to describe the first wetting layer of different metal surfaces. Instead, several structures have been proposed over recent years through a combination of experimental and theoretical investigations, which include a variety of hydrogen-bonding structures, none of which closely resemble the structure of bulk ice.

With ice growth on solid surfaces inevitably involving a degree of mismatch between the lattice parameter of the surface and that of bulk ice, discussions have focused on the idea that the structure of the surface layer must provide a suitable template on which ice can nucleate[25-30]. This has led to the suggestion that while a good ice nucleating surface will cause the first few water layers to adopt the registry of the underlying surface, this will in itself create strain between the interfacial layer and a bulk ice film as the layer grows into a continuous multilayer film. Our understanding of how the first few layers accommodate this strain is presently minimal, with no experiments available to describe the hydrogen bonding structure of the interfacial layer in detail. In fact, despite many simulations, both the understanding of first layer water and how this water structure relaxes into the bulk ice film remains ambiguous for water/solid interfaces.

High-resolution Scanning Probe Microscopy (SPM) provides a direct route to gain detailed information on the bonding geometries of water adsorbed at a surface, allowing direct investigation of water and its hydration at solid interfaces. As water forms different structures on metal surfaces with different symmetry faces, this thesis discussion involves the study of a combination of close-packed, open-faced and stepped surfaces to give a general insight into surface wetting and the exploration of whether there are similarities between the different interfacial layers that form. The discussion explores how the reactivity of a surface affects the hydrogen-bonding network, dependant on dissociation, or whether the influence of reactive step sites provides favourability in the bonding site and geometry of water. It also deliberates factors that make a good ice nucleating agent and whether a surface can act as a template to grow an ordered multilayer film.

1.2. The Structure of Water and its Unique Properties

Water exists in all three forms in our environment, ice (solid), water (liquid) and vapour (gas), making it a highly unusual species[31]. Although covalently bonded, water is a highly polar molecule with an incredibly high boiling and freezing point for its low molecular weight. These properties are a consequence of the strong hydrogen-bonding interactions present between neighbouring water molecules, requiring considerably more energy than other molecules of its size to break these strong hydrogen-bonds. Another consequence of its strong hydrogen-bonding network is its high surface tension and exceptionally high heat of vaporisation, giving water a lower vapour pressure than many large molecules. A final, unique property to discuss is its low density in its solid form. Water expands as it freezes, which causes its solid ice form to float above its liquid water form. Water is one of the only molecules that is able to do this and this has dramatic implications for many systems, ranging from environmental weathering processes through to practical engineering applications[31]. It is these unique properties associated with the strong water-water hydrogen bond, along with the ubiquitous presence of water in our environment, that make water a particularly interesting molecule to study.

Water has a simple atomic arrangement, consisting of only two hydrogen atoms and one oxygen atom. The oxygen atom of a water molecule has two lone pairs of electrons which repel the hydrogen atoms downwards to give water its bent shape and C_{2v} symmetry, in turn creating a bond angle of 104.5 °[23]. Oxygen has a partial negative charge, being able to attract electrons more efficiently than hydrogen, which in turn has a partial positive charge. This means that the oxygen atom of a single water molecule is attracted to the hydrogen atoms of other water molecules, in the same way that the hydrogen atoms are attracted to the oxygen atoms in neighbouring water molecules. With each molecule having two covalent O-H bonds, water can form two hydrogen bonds with its surrounding water molecules within a water network.

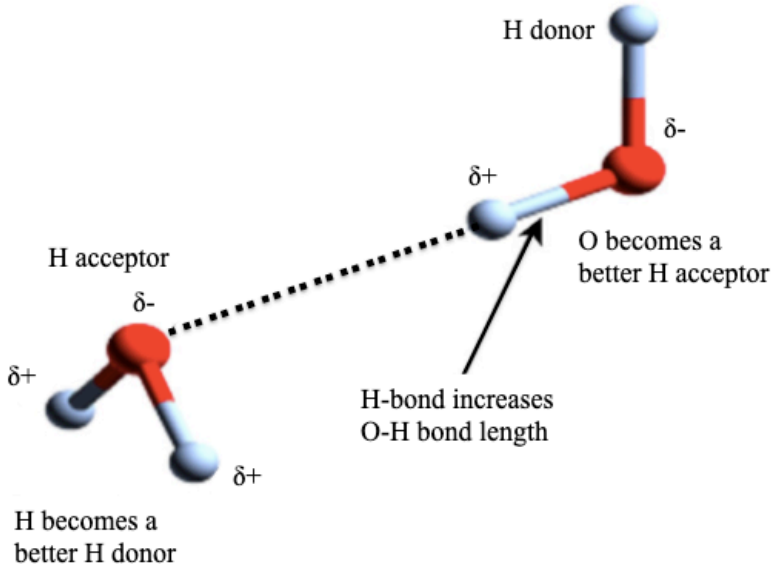

Figure 1. Hydrogen-bonding arrangement between two neighbouring water molecules, showing the partial negatively charged oxygen and partial positively charged hydrogen atoms.
Adapted from A. Hodgson *et al.*, *Surface Science Reports*, 2009, **64**, 381-451.

Hydrogen-bonding is the most important aspect of water in all of its states and also the reason why it has such unique properties. A hydrogen-bond is a relatively strong intermolecular interaction, and when occurring between neighbouring water molecules, this also has an effect on the water molecule in question. By forming a hydrogen-bonding interaction with an adjacent water molecule, this increases the change separation (dipole) of water[18,23,32], making the hydrogen atom involved a better proton donor, and in turn, the oxygen atom of the neighbouring water molecule becomes a better proton acceptor. By doing so, this increases the overall strength of the collective hydrogen-bonding network and results in cooperative hydrogen-bonding, as illustrated in Figure 1.

When it comes to investigating the structure which forms at these water/metal interfaces, the most stable structure is not always one with the maximum number of hydrogen bonds[2]. Stabilising the water layer involves a compromise between maximising both the water-water hydrogen-bonding and the water interaction with the solid surface. This creates a sensitive competition between the two interactions, adding to the interesting properties of the interfacial layer and suggesting just how much work needs to be done to understand the structure resulting from these complex hydrogen-bonding networks.

1.3. Studying Wetting Layer Structures

1.3.1. Experimental Requirements

In order to study the detailed structure of water/solid interfaces, it is crucial to prepare clean atomically flat surfaces where water can be deposited under UHV conditions. Various experimental techniques can then be implemented to examine the structure of water that forms at this interfacial layer. To gain a thorough understanding of surface wetting, it is useful to combine a range of experimental techniques, as each technique will provide different structural information. Together, it is then possible to gain an insight into the symmetry of the resulting wetting layer, an indication as to whether dissociation has occurred and also information regarding the growth of multilayer films. This thesis study concentrates on the use of Scanning Tunnelling Microscopy (STM) to gain a molecular level understanding of the interfacial layer of a small number of key water/metal interfaces.

The Scanning Tunnelling Microscope was invented by Binnig, Rohrer, Gerber and Weibel in 1981, originally intended as an imaging instrument[33,34]. It is now known that STM can accomplish much more due to the development of new state of the art, low temperature instruments, which can achieve atomic resolution and also manipulate atoms and molecules at low thermal mobility. This has been an invaluable tool for the imaging of water monomers and small clusters on metal surfaces at low temperature, allowing investigation into the formation of a variety of water structures on various metal surfaces[23,35-37]. A detailed discussion of this technique is presented in the Experimental Chapter.

1.3.2. Supportive Theoretical Calculations

Theoretical calculations have provided a vast amount of support in the discussion of wetting layer structures and are widely used to interpret experimental results[17,19-23]. In combination with experimental data, Density Functional Theory (DFT) calculations give an insight into the feasibility of different water arrangements within a wetting layer, calculating the most favourable bonding network and also an insight into the most probable proton arrangement in terms of stability. These calculations do however have their limitations, and although one particular structural model may be calculated as the most favourable in terms of binding energy, this may not always agree with experimental results. Therefore, rather than relying solely on the lowest

energy structure calculated, STM and other experimental techniques often use DFT to predict several low energy structures. These can then be compared against that already known about the wetting layer to provide a structure that is believed to be the most likely to form at the interface. George Darling, Angelos Michaelides and Chiara Gattinoni performed the calculations provided in this thesis to support the experimental studies.

1.4. The Rise and Fall of the Bilayer Model

The structure of water that forms on different metal surfaces has been studied extensively for many years with an initial breakthrough in the understanding of surface wetting being the proposal of the Bilayer Model in the 1980s. Studying the adsorption of water on a Ru(0001) surface, Doering and Madey[38] suggested that the first wetting layer forms a hexagonal 2D structure similar to that of bulk ice, I_h. As displayed in Figures 2a-b, this structure consists of a buckled network of hexagonal water rings, arranged so that each water molecule shares hydrogen bonds with its three nearest neighbours. This buckled arrangement is often referred to as a 'bilayer' because the water molecules are sited at two distinct heights. The water molecules in the lower layer lie flat and bond directly to the metal substrate via electron donation. This occurs through the lone pair of electrons on the oxygen atom and allows these water molecules to lie close to the metal surface, forming a strong bonding interaction. The water molecules in the upper half of the bilayer, meanwhile, are connected to the lower half via the hydrogen-bonding network. With one of the hydrogen atoms in each water molecule orientated parallel to the topmost surface layer, the other hydrogen atom can orient down towards the metal surface in a H-down geometry (Figure 2a), or orient upwards into vacuum, known as H-up (Figure 2b). In the original study, this bilayer was assumed to be H-up[38] and it was this which became the standard model for the adsorption of water on all metal surfaces during the rest of the 1980s and 1990s.

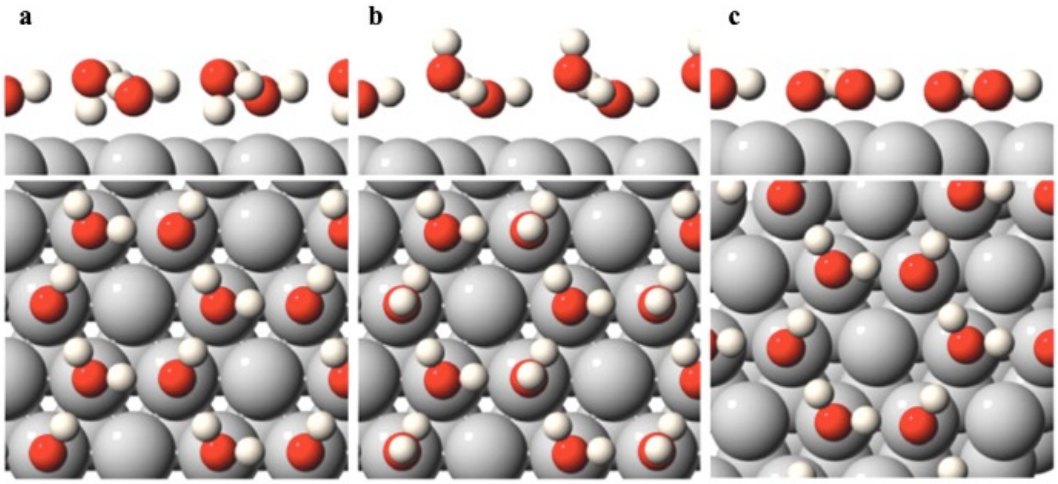

Figure 2. The (√3x√3)R30° hexagonal arrangement of a first wetting layer adsorbed on a close-packed metal surface, known as the Bilayer Model, where a) represents the H-down geometry, b) the H-up geometry and c) the partially dissociated OH-H_2O structure in a √3 unit cell.
Adapted from A. Hodgson *et al.*, *Surface Science Reports*, 2009, **64**, 381-451.

In contrast to the model structure proposed, later studies proved that the hexagonal (√3x√3)R30° diffraction pattern observed for the surface wetting of many metal substrates, including Ru(0001), was actually a result of a partially dissociated water-hydroxide overlayer[23,39-43]. As seen in Figure 2c, this overlayer is much less buckled than the H-down and H-up arrangements observed in Figures 2a-b, respectively. A LEED-IV investigation by Held and Menzel in the 1990s was the first publication to pinpoint inconsistencies with the Bilayer Model during an investigation of the first wetting layer on Ru(0001)[40]. They found that the best model fit for their data was actually a structure containing co-planar oxygen atoms, rather than the buckled arrangement of oxygen proposed by the Bilayer Model. A theoretical study by Feibelman, using DFT calculations in 2002, found evidence that this wetting layer was partially dissociated on Ru(0001), with a 2D overlayer containing both hydroxide and water found to be the most stable arrangement from theoretical calculations[41]. This generated many questions regarding the feasibility of the Bilayer Model as a general model for the adsorption of water on metal surfaces. It also opens the discussion of how complicated surface wetting actually is, with the wettability of the metal surface in question playing a huge role in the structure that forms.

Although now proved to be incorrect, the Bilayer Model is still frequently used as a starting point to interpret the first layer wetting of metal surfaces[2,18,23]. Since this

study, there has been a vast amount of research to gain an insight into the most favourable binding site of water, with several studies in this research area performed by Michaelides *et al*. Concentrating on close-packed transition and noble metal surfaces[17], they found that water preferentially adsorbs at an atop site, binding almost parallel to the surface with an average, small tilt angle of 10°, as presented in Figure 3[44]. DFT calculations predict that this binding site is the most favourable as a result of the interaction between the lone pair $1b_1$ orbital of oxygen with the metal surface. Multilayer adsorption of water, on the other hand, has been studied in much less detail from both a theoretical and experimental view, with many unanswered questions still remaining.

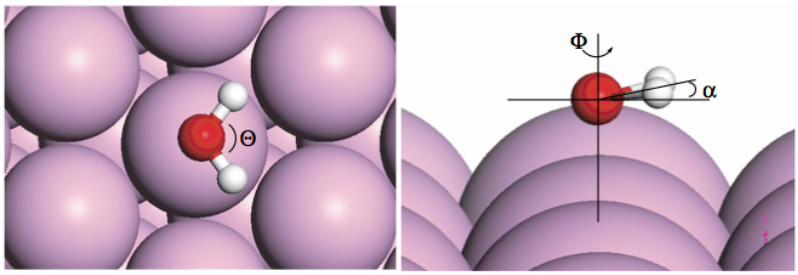

Figure 3. The most favourable adsorption site for a water monomer adsorbed on a close packed metal surface, a) top view and b) side view.
Adapted from A. Michaelides *et al.*, *Applied Physics A*, 2006, **85**, 415-425.

1.5. Bernal-Fowler-Pauling Ice Rules

Following the fall of the Bilayer Model, other structural models have been developed to describe intact water at water/metal interfaces, often based on the Bernal-Fowler-Pauling ice rules[45-47]. Developed by Bernal and Fowler in 1933, and later modified with the inclusion of the statistical model produced by Pauling in 1935[48], these rules were developed to understand the structure of bulk ice, defined by the following four points:

a) Each oxygen atom is bonded to two hydrogen atoms at a distance of 0.95 Å to form a molecule of water.
b) Each water molecule is orientated with two hydrogen atoms towards two of the four neighbouring oxygen atoms in a tetrahedral coordination.
c) The orientation of adjacent water molecules allows only one hydrogen atom to lie between each pair of oxygen atoms.

d) Bulk hexagonal ice, I_h, can exist in a large number of configurations, each corresponding to a certain distribution of hydrogen with respect to the oxygen atoms.

These rules have been widely applied to describe and interpret the structure of water/metal interfaces, and by using evidence from both experimental studies and theoretical calculations, detailed structural models for water have been published on various different metal surfaces as discussed below.

1.6. Monolayer Wetting Structures

Experimental and theoretical investigations have led to immense advances in the field of surface wetting, revealing several different structural arrangements for the adsorption of a first wetting layer. Whilst 1D pentagonal chains have been observed on Cu(110)[49], a 2D overlayer built from a combination of hydrogen-bonded pentamer, hexamer and heptamer units has been reported on Pt(111)[50,51]. 3D structures, on the other hand, form on hydrophobic surfaces which exhibit a non-wetting behaviour, such as Ag(111), Cu(111) and Au(111)[52-54], rather than the growth of a continuous water film. Although some structural aspects of water/metal interfaces are becoming better understood, the growth of a second and further wetting layers to form multilayer ice films, is much more complex and has barely been studied in comparison. There is also the question of strain relief within the wetting structures of these thick ice films and how the first layer of water compensates hydrogen order, density and lateral strain to stabilise bulk ice.

1.6.1. One-Dimensional Water Structures

An example of a one-dimensional ice structure is seen in the nucleation of 1 nm wide chains grown on Cu(110), displayed in Figure 4a[49]. These chains are built from face-sharing pentamers, rather than the simple hexagonal arrangement of water molecules initially proposed[55,56]. Favoured by the smaller size of the water rings and their assembly on the Cu(110) surface, this structure maximises the water-metal bonding and maintains a strong hydrogen-bonded network[49]. The slightly smaller size of these pentagonal units, compared to that of larger hexagonal rings, enables a good fit of the overlayer to the underlying Cu(110) substrate, while maximising the number of water molecules bonded flat above the Cu atoms[2]. In this case, the increased

interaction with the metal offsets the reduced hydrogen bond coordination of water in the 1D chain. This structure was the first arrangement built exclusively from pentagonal rings that was proposed in the field and prompted the consideration of ring sizes other than an ideal hexagonal arrangement to model superstructures in the adsorption of water on metal surfaces.

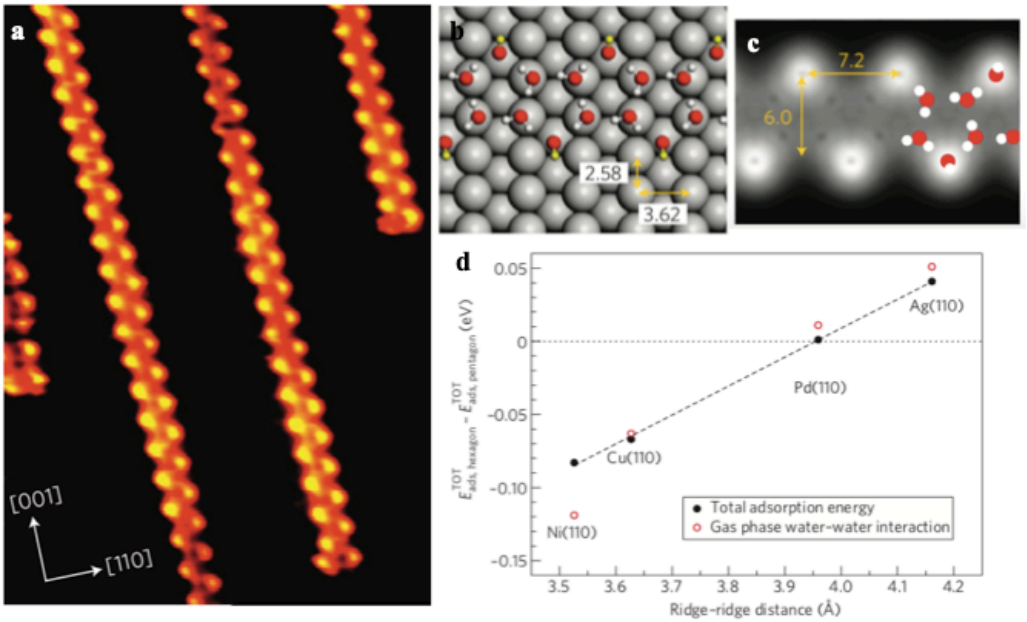

Figure 4. a) STM image of the 1D pentagonal chains on Cu(110) (120 x 140 Å^2, 100 K, -196 mV, -630 pA), b) the most stable structure calculated by DFT, c) STM simulation of b) and d) a plot to show the stability of hexamer versus pentamer units for metals with different lattice parameters.
Adapted from J. Carrasco *et al.*, *Nature Materials*, 2009, **8**, 427-431.

When assessing this pentagonal water structure on other open-faced metal surfaces, DFT calculations indicate a strong correlation between the metal lattice parameter and relative stability of water hexamers versus pentamers, which is displayed in Figure 4d[49]. The results conclude that surfaces with a larger lattice constant, such as Ag(110), have a clear preference for hexamers, whilst those with smaller lattice parameters, like Cu(110) and Ni(110), are expected to favour smaller pentagonal units. This alone portrays the complexity of surface wetting and how one general model for ice growth cannot be expected for all metal substrates.

1.6.2. Two-Dimensional Water Structures

Nie *et al*. recently used a combination of STM and DFT to investigate the structure of the two-dimensional (√37x√37)R25.3° and (√39x√39)R16.1° wetting phases observed on Pt(111)[50,51]. The bonding motif for this water monolayer is comprised of two types of hexagonal rings, bridged by a combination of water pentamers and heptamers, where the dangling hydrogen bonds are arranged to point towards the metal surface to preserve a complete hydrogen-bonded network[2].

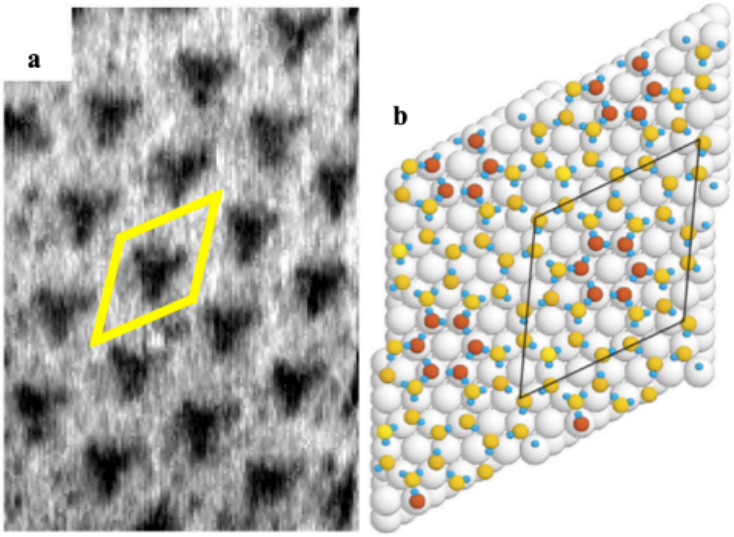

Figure 5. a) STM image of an ordered area of water deposited on Pt(111) at 140 K, b) DFT calculated model of the (√37x√37)R25.3° wetting phase.
Adapted from S. Nie *et al.*, *Physical Review Letters*, 2010, **105**, 026102.

As seen in Figure 5, this first layer structure contains ordered flat-lying water molecules, arranged in hexagonal rings and bonded to the underlying surface through the water oxygen atoms. The structure of these flat hexamers enables the water molecules to lie close atop Pt, remaining in registry with the underlying substrate. It is these low-lying water hexamers which encourage the surface wetting of Pt(111) by anchoring the interfacial layer to the metal substrate[57]. The other type of water hexamer proposed in this structure is a higher-lying ring of water molecules, arranged in a H-down orientation. In contrast to the flat-lying hexamers, these hexagonal rings are only weakly bound to the metal surface and are rotated 30 ° relative to the tightly bound, low-lying water hexamers. It is these H-down units that complete the hydrogen-bonding network, but they do not lie in registry with the substrate, interacting with the surface only by polarization of the OH bond and charge

interactions. The bridging units that connect these two types of water hexamers are proposed to be a combination of pentagonal and heptagonal rings. This study demonstrates the importance of modeling these complex structures which form at water/metal interfaces to gain a clearer picture of the solid/water interface, and how this is key to understanding surface wetting on a larger scale.

1.6.3. Three-Dimensional Water Structures

3D structures are formed on several non-wetting surfaces, such as Au(111), Ag(111) and Cu(111). These hydrophobic surfaces do not exhibit the same behaviour as the wetting surfaces discussed above, with water adsorbing intact to form 3D ice clusters, where the size of the clusters depend on the temperature at which water adsorbs[23]. These clusters continue to grow in the three-dimension rather than forming a continuous water film[58], leaving regions of bare metal exposed. This occurs as a result of weak water-metal interactions, which have been extensively studied by Morgenstern *et al*. over recent years using high-resolution STM[23,52-54,59-62]. With smaller clusters being difficult to analyse, research has turned to the growth of multilayer films on these surfaces to understand the behaviour and structures which form on these non-wetting surfaces.

1.7. Multilayer Surface Wetting

In contrast to first layer water, an in-depth look into multilayer wetting has proved extremely challenging, both from an experimental and theoretical view. There is limited information about the early stages of ice growth at a molecular level, partly because multilayer ice is extremely sensitive to electron beam damage. Its insulating character has provided difficulty in imaging films nondestructively with SPM, where it is challenging to maintain a sufficient current for imaging without damaging the ice layers in the process[27,58,63,64]. Water is also easily disturbed by scanning because its large dipole moment and the low energy of a hydrogen-bond again make it difficult to image ice without disturbance[58,60]. As a consequence, multilayer wetting remains unexplored, where the results from successful investigations have only demonstrated the complexity of crystalline ice growth[23].

Before recent experiments, it was generally assumed that a continuous ice film could grow above an initial first wetting layer with a hexagonal (√3x√3)R30° structure, similar to that of bulk ice, I_h[18,23]. However, this idea was proved too simplistic after investigations of crystalline ice growth on some common metal surfaces, Ru(0001), Pd(111) and Pt(111)[23]. Hodgson *et al*. discuss how multilayer adsorption is extremely sensitive to the binding energy of the first wetting layer and how easily this first layer can reconstruct to accommodate thick film growth[23]. This idea was further emphasised in a discussion by Carrasco *et al*. describing how the presence of OH groups facilitates the nucleation of second layer water above a first contact layer. It is thought that these dangling hydroxide bonds are either arranged to stick out of the contact layer away from the surface, or that they must form by reconstruction upon adsorption of multilayer water[2]. This question has prompted detailed studies using a combination of experimental techniques and theoretical investigations to examine the formation of multilayer water structures.

The first of three publications to knowledge which show molecularly resolved STM images of multilayer water adsorption, investigates the thermally activated transition of amorphous to crystalline ice clusters on a hydrophobic Cu(111) surface. Mehlhorn *et al*. found three different ice superstructures, being a faceted surface, pyramidal islands and nanocrystallite structures, for the annealing of amorphous solid water up to 149 K[65]. These diverse structures were observed with no indication of a terminating Ih(0001) bilayer at any anneal temperature between the crystallization and desorption temperature, being 130 K and 149 K, respectively[65]. These results provide an indication that more complex structures need to be considered, both in theoretical calculations and the analysis of experimental findings, when investigating ice growth on metal surfaces.

Another publications in mind is a recent study by Maier *et al*. using low temperature STM to investigate the structure of the first ice layers grown on Ru(0001) and Pt(111)[66]. The first wetting layer on both of these surfaces is composed of a hexagonal water network, connected by pentagonal and heptagonal units, which lie mutually in and out of registry with the underlying substrate. On Ru(0001), which has only a small 3.5 % mismatch to ice, this initial wetting layer is found to rearrange to form a simple, hexagonal honeycomb unit to facilitate further ice growth. Maier *et al*.

report the adsorption of additional water to form ordered second layer patches that possess this hexagonal (√3x√3)R30° structure[66]. Moreover, further water adsorption results in additional third layer water molecules appearing as the brightest sites in Figures 6a-b. Highlighted by the black circle in Figure 6b, these third layer molecules appear to consistently adsorb at the same site, which suggests a preferential binding site above the second wetting layer. The second wetting layer is removed by the tip after repeated scanning, which is seen towards the edges of the water island. As a result, this exposes a hexagonal network of first layer water molecules which appear to lie in registry with the underlying Ru(0001) substrate. It also suggests that the restructuring of the initial wetting layer, composed from a network of 5, 6 and 7 membered water rings, into a commensurate hexagonal structure, is required to facilitate further ice growth[66].

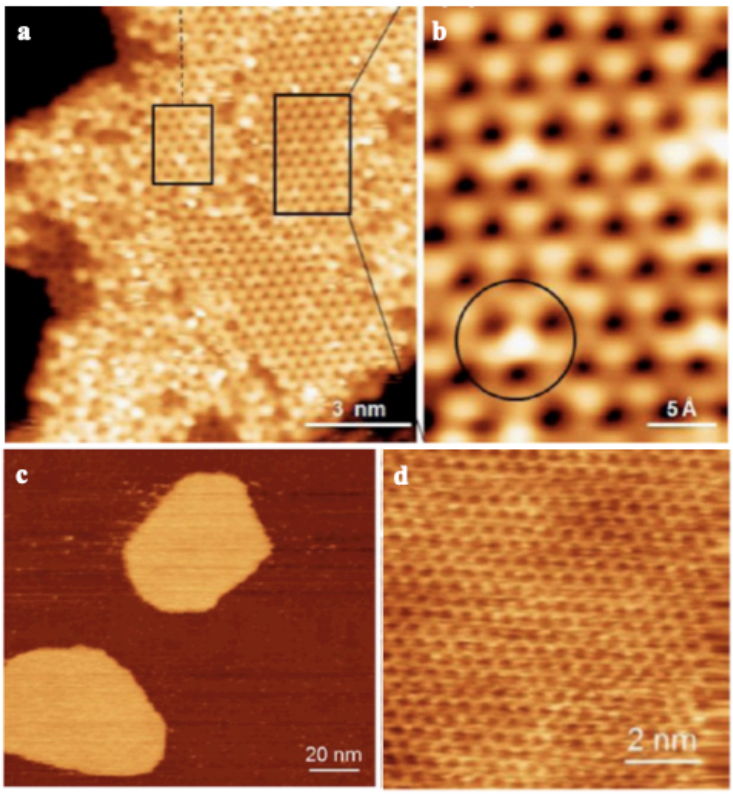

Figure 6. a-b) STM images showing two complete layers of water plus additional third layer water molecules adsorbed on Ru(0001), where b) shows a magnified area of a), with the black circle highlighting these additional third layer water molecules (77 K, -263 mV, 3.3 pA). c-d) STM images showing complete first and partial second layer wetting on Pt(111) in the presence of residual hydrogen to form a (√3x√3)R30° hexagonal structure, with d) showing the resolved structure of a second layer island, c) (77 K, 201 mV, 17.5 pA), d) (77 K, -243 mV, 22.9 pA).

Adapted from S. Maier *et al.*, *Journal of the American Chemical Society*, 2016, **138**, 3145-3151.

The (√39x√39)R16.1° wetting phase observed for a complete monolayer of water on Pt(111) is also found to be an unsuitable substrate to facilitate ice growth. Not only is this two-dimensional phase quite tightly bound to the underlying substrate, but previous STM studies by Thürmer *et al*. found that multilayer ice films dewet Pt(111) to form (√3x√3)R30° islands[27]. These are reported to be several layers thick, embedded within (√39x√39)R16.1° single bilayer domains. The STM images reported in the study by Maier *et al*., also support Pt(111) being a poor template for ice growth, with the disordered second layer islands which form being difficult to resolve as a result of water mobility and strong water-tip interactions[66]. Instead, it is reported that exposure of the Pt(111) surface to a background atmosphere of residual hydrogen forms a (√3x√3)R30° multilayer water film, as seen in Figures 6c-d. With this second layer structure being similar to hexagonal bulk ice, I_h, and thought to be in registry with the underlying Pt(111) substrate, ordered growth of crystalline multilayer films can proceed[66].

A detailed investigation of thick ice films on Pt(111) by Thürmer *et al*., found that isolated 3D clusters of hexagonal ice begin to grow by layer nucleation after the completion of a first wetting layer[67]. During subsequent adsorption of water, the steps of the Pt(111) substrate become buried as the film gets thicker, and this results in the growth of spirals, created by screw dislocations above the Pt(111) steps. As the stacking registry is the same for all bilayers that are connected by this screw dislocation, cubic ice is initially formed rather than the alternating stacking sequence of hexagonal ice[23]. These screw dislocations then accelerate ice growth, avoiding the need to nucleate a new water layer, with the presence of double spirals controlling preferential formation back to hexagonal ice as the film thickness grows above 20 nm[67]. This therefore argues that hexagonal ice is the equilibrium structure formed at low temperature, in this case 140 K, but there is still much work needed to be done to investigate this in more detail.

The final recent publication which probes multilayer surface wetting is the growth of two water layers on a stepped surface of Cu(511)[30,68]. With narrow three-atom wide terraces, water preferably binds to the favourable low coordinate step sites, bridging across the hydrophobic (100) terraces to create a highly corrugated, 2D first wetting layer, as seen in Figures 7a,d. This (3 1, $\overline{3}$ 1) structure forms at a water coverage ≤

0.83 ML, built from a combination of pentamer, hexamer and octamer units[68]. DFT suggests that the network is stabilized by the four flat water molecules bound at the hydrophilic Cu step sites and also the presence of three water molecules orientated H-down next to the step. These are in turn stabilized by the step dipole with the remaining three water molecules completing the hydrogen-bonding network, as seen in Figure 7d.

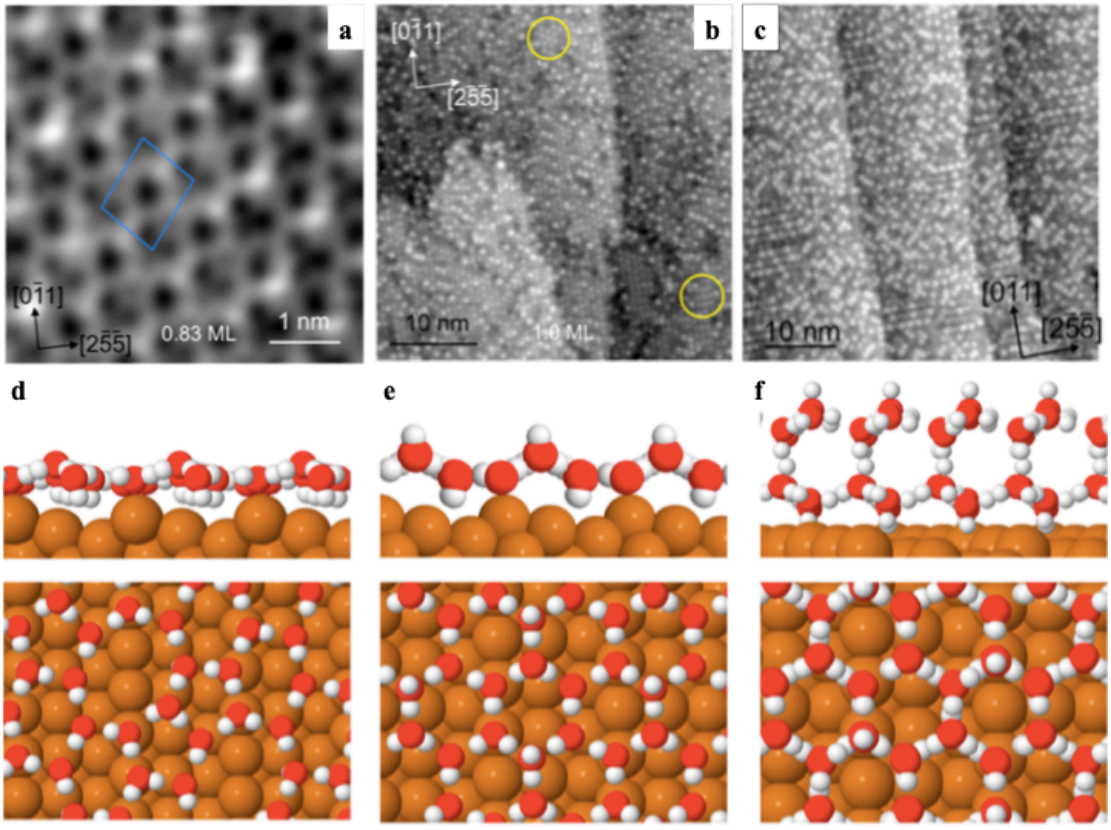

Figure 7. STM images of water adsorbed on a stepped Cu(511) surface, at a coverage of a) 0.83 ML to give a (3 1, $\bar{3}$ 1) unit cell after annealing to 138 K (77 K, -0.11 V, 100 pA), b) 1 ML to give a (3 0, $\bar{1}$ 1) ordered water film after annealing to 138 K (77 K, 0.11 V, 21 pA), and c) 2 ML to give a (5 1, $\bar{4}$ 1) superstructure after annealing to 135 K (77 K, 0.1 V, 21 pA). DFT calculated models d-f) represent the most stable structure for a-c, respectively.
Adapted from C. Lin *et al.*, *Journal of the American Chemical Society*, 2018, **140**, 15804-15811.

Increasing the water coverage to investigate multilayer surface wetting reveals this 2D layer is unstable to the adsorption of further water. Instead, the structure relaxes, becoming compressed to create a buckled hexagonal network, as seen in Figures 7b/e[30]. This ordered film has a (3 0, $\bar{1}$ 1) structure and allows further adsorption to become facile, with the formation of a continuous second wetting layer, displayed in

Figures 7c/f. This can then grow into a commensurate multilayer ice film with a (5 1, $\bar{4}$ 1) superstructure. DFT indicates the importance of the first layer structure to relax and adopt the periodicity and corrugation of bulk ice. The need to form a buckled donor-acceptor first layer, in order to stabilize second layer adsorption, suggests that corrugated surfaces may nucleate ice more effectively than flat surfaces. To our knowledge, these are the only publications with high-resolution STM images that directly probe the growth of multilayer ice, providing only a partial insight into the multilayer wetting of solid surfaces.

1.8. Overview of Thesis

This thesis discusses the resulting structures of water which form during the initial stages of wetting on different metal surfaces and how surface symmetry, lattice parameter and reactivity can all have an effect on how the first wetting layer grows. The inclusion of close-packed, open-faced and stepped surfaces of different metals allows us to probe a variety of different hydrogen-bonding networks to investigate the most favourable water binding site on different symmetry faces. These studies also examine the influence of a substrate's reactivity on the resulting water structure and whether dissociation is initiated on more reactive metal surfaces, and if so, to what extent.

1.8.1. Introduction to Bimetallic Alloys

Bimetallic alloys have become of great interest over recent years as a result their enhanced reactivity, selectivity and resistance to catalytic poisoning, making them tuneable substrates for electrocatalysis[69]. With Pt being an expensive metal that is easily poisoned by the CO bi-product produced in a variety of fuel cell reactions, investigations have focused the alloying of Pt with other transition metals with an aim to create a surface that would reduce, if not completely eliminate, the poisoning of the Pt active site[70-74]. In turn, the hope of increasing the catalyst lifetime and reducing costs may be achieved.

During these studies, it was found that alloying Pt with Sn not only prevents the poisoning of the Pt active site, but also creates a surface with the traditional (√3x√3)R30° structure of bulk hexagonal ice, I_h. Water adsorption on this (√3x√3)R30°-SnPt(111) surface forms a simple, hexagonal structure, commensurate

with the underlying alloy substrate[69,75]. This therefore provides a simple system to probe surface wetting using low temperature STM to investigate the growth of this ordered first wetting layer structure into a thick ice film, pushing the barrier of STM limitations in Chapter 3.

1.8.2. Introduction to Open-Faced Surfaces

Investigations into the structure which forms when water adsorbs on an open-faced metal surface has been of interest over recent years following the discovery of 1D pentagonal intact water chains on Cu(110) at low temperature[49]. Before this publication was released, all structures reported for the wetting of metal surfaces had found water networks built around hexagonal ring structures[55,56]. This led to the suggestion that metals with a small lattice parameter will favour small pentagonal ring structures, with Ni(110) predicted to be one of the most favourable surfaces for the formation of a pentagonal water network[49]. This study did not however consider the reactivity of Ni with respect to Cu, and whether water does indeed ever adsorb intact on Ni(110), or whether dissociation occurs upon adsorption even at low temperature. The Temperature Programmed Desorption (TPD) data reported for the water/Ni(110) system[76,77] is however remarkably similar to that for water/Cu(110), prompting the consideration that the structures which form on Cu(110)[78], also form on Ni(110). The discussion in Chapter 4 debates these ideas along with analysis of the wetting structures which form on Ni(110) with increasing temperature, using low temperature STM.

1.8.3. Introduction to Stepped Surfaces

Recent work has examining the effect of step sites on the structures which form during the surface wetting of ideal stepped metal surfaces[30,68,79-87]. These substrates have small terraces with a distinct width, having regular rows of step sites across the surface layer. With previous investigations finding surface steps to be a favourable binding site for water, it is interesting to analyse whether this is invariably the preferred site during surface wetting and how these surfaces direct water growth.

With recent studies probing the surface wetting of different stepped Pt surfaces, this thesis examines the adsorption of water on a stepped surface of Pt(211) to corroborate data obtained from other experimental techniques which are already published in the

literature[79-83]. Pt(211) has extremely narrow (111) terraces, being only three-atoms wide, separated by (100) step sites. In comparison to Pt(533), which has the same step symmetry but with four-atom wide (111) terraces, Pt(211) has been suggested to have too narrow a terrace width to stabilise water[84-87]. Instead, it is proposed that water will only bind at the reactive (100) step sites in a 1D array, being unfavourable to bridge across the narrow terraces to form a 2D structure[80]. This structural model is considered in Chapter 5 with evidence from low temperature STM studies providing input to a discussion of this system.

1.9. References

[1] https://phys.org/news/2014-12-percent-earth.html

[2] J. Carrasco, A. Hodgson, A. Michaelies, *Nature Materials*, 2012, **11**, 667-674.

[3] W. F. Langelier, *Journal of American Water Works Association*, 1936, **28**, 1500-1521.

[4] T. J. Harvey, F. C. Walsh, A. H. Nahle, *Journal of Molecular Liquids*, 2018, **266**, 160-175.

[5] M. A. Malik, M. A. Hashim, F. Nabi, S. A, AL-Thabaiti, Z. Khan, *International Journal of Electrochemical Science*, 2011, **6**, 1927-1948.

[6] V. Gurau, H. Liu, S. Kakac, *AlChE Journal*, 1998, **44**, 2410-2422.

[7] H. Li, Y, Tang, Z. Wang, Z. Shi, S. Wu, D. Song, J. Zhang, K. Fatih, J. Zhang, H. Wang, Z. Liu, R. Abouatallah, A. Mazza, *Journal of Power Sources*, 2008, **178**, 103-117.

[8] Trung V. Nguyen, Ralph E. White, *Journal of Electrochemical Society*, 1993, **140**, 2178-2186.

[9] S. Haq, J. Harnett, A. Hodgson, *Journal of Physical Chemistry B*, 2002, **106**, 3950-3959.

[10] T. R Ralph, M. P. Hogarth, *Platinum Metals Review*, 2002, **46**, 117-135.

[11] S. Chunshan, *Catalysis Today*, 2002, **77**, 17-49.

[12] E. Antolini, T. Lopes, E. R. Gonzalez, *Journal of Power Source*, 2006, **160**, 957-968.

[13] D. W. Newsome, *Catalysis Reviews*, 2006, **21**, 275-318.

[14] C. Ratnasamy, J. P. Wagner, *Catalysis Reviews*, 2009, **51**, 325-440.

[15] P. Bampoulis, K. Sotthewes, E. Dollekamp, B. Poelseama, *Surface Science Reports*, 2018, **73**, 233-264.

[16] J. B. Baxter, C. Richter, C. A. Schmuttenmaer, *Annual Review of Physical Chemistry*, 2014 **65**, 423-447.

[17] A. Michaelides, *Applied Physics A*, 2006, **85**, 415-425.

[18] M. Henderson, *Surface Science Reports*, 2002, **46**, 5.

[19] P. Hohenberg, W. Kohn, *Physical Review*, 1964, **136**, B864.

[20] W. Kohn, L. Sham, *Physical Review*, 1965, **140**, A1133.

[21] J. P. Perdew, J. A. Chevary, S. H. Vosko, K. A. Jackson, M. R. Pederson, D. J. Singh, C. Fiolhais, *Physical Review B*, 1992, **46**, 6671.

[22] J. P. Perdew, K. Burke, M. Ernzerhof, *Physical Review Letters*, 1996, **77**, 3865.

[23] A. Hodgson, S. Haq, *Surface Science Reports*, 2009, **64**, 281-451.

[24] P. A. Thiel, T. E. Madey, *Surface Science Reports*, 1987, **7**, 211.

[25] A. Massey, F. McBride, G. R. Darling, M.Nakamura, A. Hodgson, *Physical Chemistry Chemical Physics*, 2014, **16**, 24018.

[26] S. Nie, P. J. Feibelman, N. C. Bartelt, K. Thürmer, *Physical Review Letters*, 2010, **105**, 026102.

[27] K. Thürmer, N. C. Bartelt, *Physical Review Letters*, 2008, **100**, 186101.

[28] G. A. Kimmel, N. G. Petrik, Z. Dohnalek, B. D. Kay, *Journal of Chemical Physics*, 2007, **126**, 114702.

[29] S. Nie, N. C. Bartelt, K. Thürmer, *Physical Review B: Condensed Matter and Materials Physics*, 2011, **84**, 035420.

[30] C. Lin, G. Corem, O. Godsi, G. Alexandrowicz, G. R. Darling, A. Hodgson, *Journal of the American Chemical Society*, 2018, **140**, 15804-15811.

[31] http://www1.lsbu.ac.uk/water/water_molecule.html

[32] J. K. Gregory, D. C. Clary, K. Liu, M. G. Brown, R. J, Saykally, *Science*, 1997, **275**, 814.

[33] G. Binning, H. Rohrer, *Reviews of Modern Physics*, 1987, **59**, 615-625.

[34] K. Morgenstern, N. Lorente, K. H. Rieder, *Physica Status Solidi B, Basic Solid State Physics,* 2013, **250**, 1671-1751.

[35] T. Mitsui, M. K. Rose, E. Formin, D. F. Ogletree, M. Salmeron, *Science*, 2002, **297**, 1850.

[36] K. Motobayashi, C. Matsumoto, Y. Kim, M. Kawai, *Surface Science*, 2008, **602**, 3136.

[37] A. Michaelides, K. Morgenstern, *Nature Materials*, 2007, **6**, 597.

[38] D. L. Doering, T. E. Madey, *Surface Science*, 1982, **123**, 305-337.

[39] G. Held, D. Menzel, Surface Science, 1994, 316, 92-102.

[40] G. Held, D. Menzel, *Physical Review Letters*, 1995, **74**, 4221.

[41] P. J. Feibelman, *Science*, 2002, **295**, 99-102.

[42] A. Michaelides, P. Hu, *Journal of the American Chemical Society*, 2001, **123**, 4235-4242.

[43] A. Michaelides, P. Hu, *Journal of Chemical Physics*, 2001, **114**, 513-519.

[44] A. Michaelides, V. A. Ranea, P. L. de Andres, D. King, *Physical Review Letters*, 2003, **90**, 216102.

[45] J. D. Bernal, R. H. Fowler, *Journal of Chemical Physics*, 1933, **1**, 515.

[46] V. Buch, P. Sandler, J. Sadlej, *Journal of Physical Chemistry B*, 1998, **102**, 8641.

[47] J. L. Aragones, L. G. MacDowell, C. Vega, *Journal of Physical Chemistry A*, 2011, **115**, 5745-5758.

[48] L. Pauling, *Journal of the American Chemical Society*, 1935, **57**, 2680.

[49] J. Carrasco, A. Michaelides, M. Forster, S. Haq, R. Raval, A. Hodgson, *Nature Materials*, 2009, **8**, 427-431.

[50] S. Nie, P. J. Feibelman, N. C. Bartelt, K. Thürmer, *Physical Review Letters*, 2010, **105**, 026102.

[51] P. J. Feibelman, N. C. Bartelt, S. Nie, K. Thürmer, *Journal of Chemical Physics*, 2010, **133**, 154703.

[52] K. Morgenstern, *Surface Science*, 2002, **504**, 293-300.

[53] K. Morgenstern, H. Gawronski, T. Mehlhorn, K. H. Rieder, *Journal of Modern Optics*, 2004, **51**, 2813-2819.

[54] H. Gawronski, K. Morgenstern, K. H. Rieder, *European Physical Journal D*, 2005, **35**, 349-353.

[55] T. Yamada, S. Tamamori, H. Okuyama, T. Argua, *Physical Review Letters*, 2006, **96**, 036105.

[56] J. Lee, D. C. Sorescu, K. D. Jordan, J. T. Yates Jr., *Journal of Physical Chemistry C*, 2008, **112**, 17672-17677.

[57] S. Maier, I. Stass, T. Mitsui, P. J. Feibelman, K. Thürmer, M. Salmeron, *Physical Review B*, 2012, **85**, 155434.

[58] M. Mehlhorn, K. Morgenstern, *Physical Review Letters*, 2007, **99**, 246101.

[59] K. Morgenstern, J. Nieminen, *Physical Review Letters*, 2002, **88**, 066102.

[60] K. Morgenstern, J. Nieminen, *Journal of Chemical Physics*, 2004, **120**, 10786-10791.

[61] K. Morgenstern, K. H. Rieder, *Journal of Chemical Physics*, 2002, **116**, 5746.

[62] K. Morgenstern, K. H. Rieder, *Chemical Physics Letters*, 2002, **358**, 250.

[63] K. Thürmer, N. C. Bartelt, *Physical Review B*, 2008, **77**, 195425.

[64] A. Verdaguer, G. M. Sacha, H. Bluhm, M. Salmeron, *Chemical Reviews*, 2006, **106**, 1478-1510.

[65] J. Stachler, M. Mehlhorn, U. Bovensiepen, M. Meyer, D. O. Kusmierek, K. Morgenstern, M. Wolf, *Physical Review Letters*, 2007, **98**, 206105.

[66] S. Maier, B. A. J. Lechner, G. A. Somorjai, M. Salmeron, *Journal of the American Chemical Society*, 2016, **138**, 3145-3151.

[67] K. Thürmer, S. Nie, *Proceedings of the National Academy of Science of the United States of American (PNAS)*, 2013, **110**, 11757-11762.

[68] C. Lin, N. Avidor, G. Corem, O. Godsi, G. Alexandrowciz, G. R. Darling, A. Hodgson, *Physical Review Letters*, 2018, **120**, 076101.

[69] F. McBride, G. R. Darling, K. Pussi, A. Hodgson, *Physical Review Letters*, 2011, **106**, 226101.

[70] E. Antolini, J. R. C. Salgado, E. R. Gonzalez, *Journal of Power Sources*, 2006, **160**, 957-968.

[71] E. Antolini, T. Lopes, E. R. Gonzalez, *Journal of Alloys and Compounds*, 2008, **461**, 253-262.

[72] J. Fearon, G. W. Watson, *Journal of Materials Chemistry*, 2006, **16**, 1989-1996.

[73] C. Panja, N. Saliba, B. E. Koel, *Surface Science*, 1998, **395**, 248-259.

[74] F. Vigier, C. Countanceau, F. Hahn, E. M. Belgsir, C. Lamy, *Journal of Electroanalytical Chemistry*, 2004, **563**, 81-89.

[75] F. McBride, G. R. Darling, K. Pussi, C. A. Lucas, Y. Gründer, M. Darlington, A Brownrigg, A. Hodgson, *Journal of Physical Chemistry C*, 2013, **117**, 4032-4039.

[76] B. W. Callen, K. Griffiths, R. V. Kasza, *Journal of Chemical Physics*, 1992, **97**, 3760.

[77] G. Pirug, O. Knauff, H. P. Bonzel, *Surface Science*, 1994, **321**, 58-70.

[78] M. Forster, R. Raval, J. Carrasco, A. Michaelides, A. Hodgson, *Chemical Science*, 2012, **3**, 93.

[79] C. Badan, M. T. M. Koper, L. B. F. Juurlink, *Journal of Physical Chemistry C*, 2015, **119**, 13551-13560.

[80] C. Badan, Y. Heyrich, M. T. M. Koper, L. B. F. Juurlink, *Journal of Physical Chemistry Letters*, 2016, **7**, 1682-1685.

[81] R. Pekoz, D. Donadio, *Journal of Physical Chemistry C*, 2017, **121**, 16783-16791.

[82] O. Endo, M. Nakamura, R. Sumii, K. Amemiya, *Journal of Physical Chemistry C*, 2012, **116**, 13980-13984.

[83] M. Nakamura, N. Sato, N. Hoshi, J. M. Soon, O. Sakata, *Journal of Physical Chemistry C*, 2009, **113**, 4538-4542.

[84] M. J. Kolb, J. Wermink, F. Calle-Vallejo, L. B. F. Luurlink, M. T. M. Koper, *Physical Chemistry Chemical Physics*, 2016, **18**, 3416-3422.

[85] M. J. Kolb, F. Calle-Vallejo, L. B. F. Juurlink, M. T. M. Koper, *Journal of Chemical Physics*, 2014, **140**, 134708.

[86] M. J. T. C. van der Niet, O. T. Berg, L. B. F. Juurlink, M. T. M. Koper, *Journal of Physical Chemistry C*, 2010, **114**, 18953-18960.

[87] M. L Grecea, E. H. G. Backus, B. Riedmüller, A. Eichler, A. W. Kleyn, M. Bonn, *Journal of Physical Chemistry B*, 2004, **108**, 12575-12582.

Chapter 2

Experimental Overview

2. Experimental Overview

2.1. Ultra High Vacuum

To gain a molecular level understanding of the intermolecular interactions and the resulting structures which form when water wets a metal surface, water adsorption experiments are studied under UHV conditions. This limits potential surface contamination and minimises any residual gas present during the preparation and characterisation of a surface layer. The surface structures that form are therefore a result of only the intended adsorbate or its products, and not a product of side reactions which may have influenced an adsorbed species.

Species can adsorb on a surface in two ways, being either physisorbed or chemisorbed depending on the nature of the adsorbate[1-2]. When directly physisorbed to a metal surface, only weak intermolecular forces are involved where the adsorbate interacts with the surface layer only by Van der Waals interactions. Chemisorption, on the other hand, involves the formation of a chemical bond between the surface and adsorbate and is much stronger, for example, covalent bonding to the surface. This is the case for water dissociation, where hydroxyl groups are tightly bound to the metal surface. In the case of molecular water, however, the physisorption bond is typically of a similar strength to a water-water hydrogen bond. This means the water layer must adapt its structure to optimise both the water-solid interaction and the local hydrogen-bonding arrangement between water molecules, and as a consequence, the hydrogen-bonding network formed for a first wetting layer is specific to the binding energy of water and the symmetry of the surface in question, as reflected in the variety of structures observed for surface wetting[3-6].

2.1.1. *Overview of UHV System*

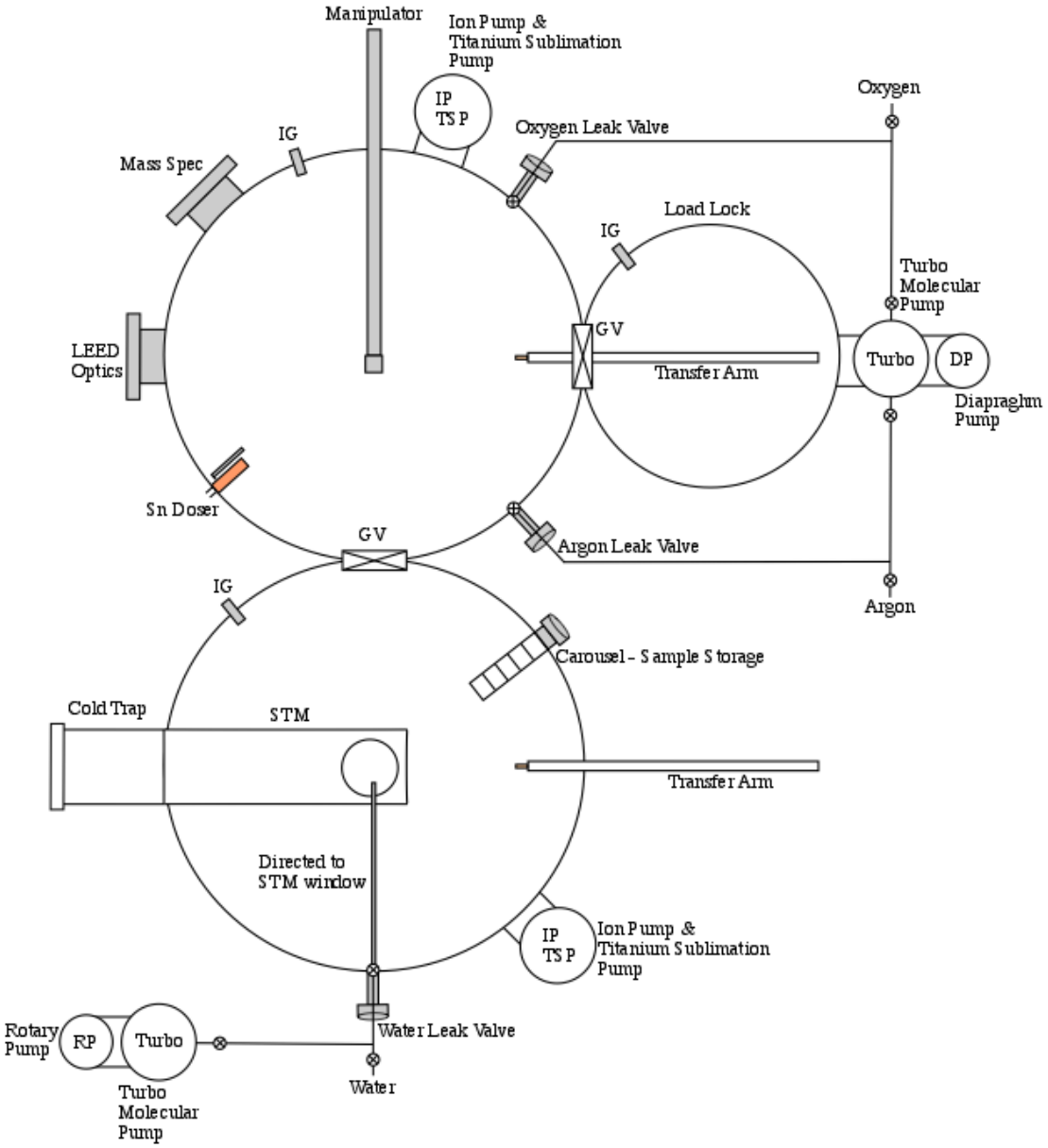

Figure 1. Schematic overview of the CreaTec SPM UHV instrument used for the preparation and surface analysis of the systems studied in this thesis.

Figure 1 shows a schematic of the CreaTec low temperature SPM used during the investigations of this thesis, capable of both STM and AFM. It has three separate chambers used for loading, preparation and characterisation. Firstly, substrates are loaded into the UHV system through the load lock chamber, where it can then be moved into the preparation chamber using the transfer arm and transferred onto the manipulator. The manipulator allows movement through the preparation and

characterisation chambers, allowing precise control over the position of the substrate to optimise experimental conditions. The preparation chamber possesses a LEED optics, mass spectrometer, argon ion gun and Sn doser. The surface can be cleaned in this chamber using the argon ion gun through repeated sputter-anneal cycles, with resulting surface cleanliness checked by LEED. The quality of a species entering the chamber, such as argon for sputtering, can be qualified by the mass spectrometer in the preparation chamber. This is used to ensure that all gases entering the chamber are clean, again minimising contamination. The manipulator can then transfer the substrate into the characterisation chamber, where a wobble stick is used to place the sample into the STM column. The STM column is attached to a cold trap to aid pumping and allow sample cooling to temperatures as low as 4 K.

2.1.2. Overview of System Pumping

The chamber is equipped with a variety of pumps to maintain UHV conditions, which are labelled in the schematic shown in Figure 1. Ion pumps are used for the main pumping of the preparation and characterisation chambers, with the load lock having its own pumping system equipped with a turbo molecular pump, backed by a diaphragm roughing pump. This provides oil-free pumping of the system. The preparation and characterisation chambers are each equipped with titanium sublimation pumps to further aid the removal of residual gas from the system. The characterisation chamber is equipped with a cold trap situated above the STM head. This condenses gaseous species residing in the chamber to ensure a good vacuum within the system. This cold trap also has a unique design in which it has an inner and outer jacket. The inner jacket can be filled with liquid nitrogen or liquid helium to reach temperatures of 77 K or 4 K, respectively, within the STM head, providing the outer shield is filled with liquid nitrogen to reduce boil off from the inner jacket. Overall, this allows the maintenance of a clean UHV system and a vacuum within the 10^{-11} mbar range is easily achieved.

2.2. Sample Preparation

2.2.1. Preparation of a Clean Metal Surface

It is essential that the surface of the metal is clean and well-ordered before water adsorption. This requires the surface to be bombarded with a beam of monatomic Ar^+ ions at an energy ranging typically between 0.5-1 keV, which is known as surface

sputtering. With argon being an inert gas, it does not react with the surface material and instead, removes the topmost layers of the surface, in turn removing contaminants. The surface is then annealed to provide sufficient energy for the surface atoms to move and reorder, which creates an ordered topmost surface layer. This process is repeated as necessary with the conditions used dependent on the metal in question.

2.2.2. Alloy Preparation

For the investigation of the (√3x√3)R30°-SnPt(111) alloy, a Pt(111) crystal was used as the starting substrate. The surface was subject to repeated cleaning cycles, as explained above, to obtain a well-ordered Pt(111) surface layer. To create the bimetallic alloy of interest, an external Sn doser was mounted onto one of the external ports of the preparation chamber, demonstrated in Figure 2. This consisted of a Sn wire wrapped around a W filament, so that as a filament current was applied, the Sn metal wire was heated to its melting point resulting in the evaporation of Sn into the chamber. The Pt(111) substrate was positioned with its surface directly aligned and orientated towards the Sn doser to optimise the evaporation of Sn onto the Pt(111) surface.

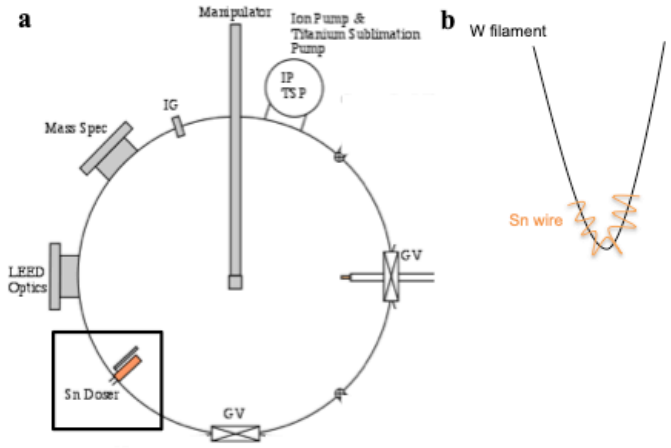

Figure 2. Schematic of the preparation chamber highlighting the Sn doser used for the preparation of the (√3x√3)R30°-SnPt(111) alloy surface discussed in Chapter 3, a) highlights the position of the Sn doser within the preparation chamber and b) a simplified schematic of the Sn doser discussed in Section 2.2.2.

To form the (√3x√3)R30°-SnPt(111) monolayer surface alloy, a coverage ≥ 0.33 ML of Sn was deposited followed by annealing to 700-1000 K to desorb the excess Sn[7-9]. After the surface structure was analysed with LEED to confirm formation of the correct monolayer alloy, the sample was transferred into the STM column where it was left to cool to 77 K. The resulting surface structure could then be analysed by STM to obtain structural information of the clean surface layer before beginning water adsorption experiments.

2.2.3. Water Adsorption

The substrates were cooled to 77 K before beginning water adsorption experiments. When cold, water was dosed onto the surface via a molecular beam, allowing controlled growth of water films. A simplified overview of the water doser is seen in Figure 1 which shows the pumping system for the doser. The doser was set up with a capillary tube aligned with the STM window, directly positioned towards the sample surface. Exposure was firstly quantified by the adsorption of one complete ML, following which the conditions could be adjusted to allow slow and controlled growth of a water film. This allowed for a coverage of less than 1 ML to be examined to analyse the initial surface wetting of different substrates.

2.3. Surface Characterisation

UHV provides a way to study the adsorption of species on a surface without the influence of residual gas and surface contaminants affecting the desired surface reaction. The resulting products can then be analysed using a mixture of techniques to examine the structure of the surface layer. The main techniques used throughout this thesis were LEED and STM, which are discussed in detail below.

2.3.1. Low Energy Electron Diffraction

LEED is a valuable analysis tool used to ensure the creation of an ordered surface structure. It utilises a beam of low energy electrons to create a back-scattered electron diffraction pattern of the surface layer. With only elastically-scattered electrons contributing to the diffraction pattern observed, LEED can be used to gain information about the cleanliness of the surface and how ordered the surface layer is, or to gain information about the symmetry of an adsorbate with respect to the substrate surface.

Figure 3a gives a simple schematic of the process which occurs within a LEED optics unit. It consists of an electron gun directed at a substrate surface, which uses a beam of low energy electrons, typically ranging between 20-200 eV. As the electron beam hits the surface, the elastically scattered electrons from the surface atoms hit a phosphor screen to generate an electron diffraction pattern. These electrons have not lost energy when leaving the surface, unlike the inelastically scattered electrons which are filtered out by the grids positioned in front of the phosphor screen[10-12].

LEED can be used in two ways, qualitatively or quantitatively. For the investigations reported in this thesis, only qualitative LEED analysis was used for an indication of the symmetry and order of the surface layer and rotational alignment with adsorbates. Quantitative LEED, on the other hand, which is known as LEED-IV, records the intensity of the diffracted beams as a function of electron beam energy to give accurate information on atomic positions.

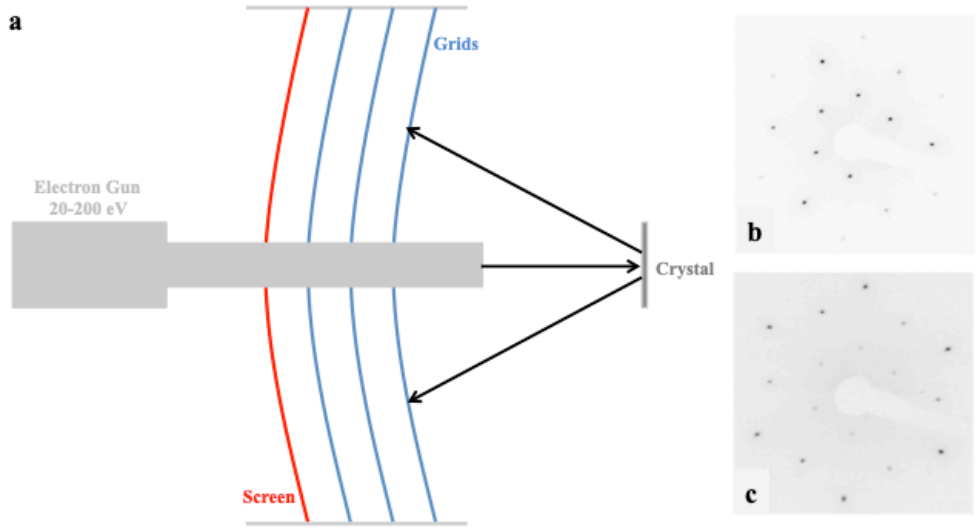

Figure 3. a) Simplified schematic of a LEED optics unit, b) LEED pattern obtained for a clean (√3x√3)R30°-SnPt(111) alloy surface and c) after the adsorption of 1 ML water.
a) Adapted from reference [10].

2.3.2. Scanning Tunnelling Microscopy

When the creation of a clean, ordered surface has been established or a surface reaction has occurred, the resulting surface can be examined by STM in hope of gaining an atomic understanding of the surface structure. STM is a largely utilised

technique used in surface science as it allows the atomic resolution of surface atoms and therefore provides details of structural formation[13].

When an atomically sharp metal tip is brought within several Å of a conducting surface and a bias voltage is applied, electrons can tunnel from the tip to surface, or vice versa, depending on the polarity of the applied bias. This process is usually forbidden by classical mechanics, but when the tip-surface separation is small, these laws are overcome and quantum tunnelling can occur. The tip scans the surface to image the density of states of the surface and/or adsorbates, from which current and height information can be obtained and atomic resolution of the surface species can be achieved.

Invented by Binnig and Rohrer in 1981, they developed the first working STM at IBM Zurich Research Laboratories and later won the Nobel Prize in Physics in 1986[14]. The polarity of the bias voltage applied influences the direction of the tunnelling electrons. In the case of the CreaTec STM system described in this thesis, the bias voltage is applied to the sample. Therefore, when a positive bias voltage is reported, this denotes a positive bias on the sample allowing electrons to flow from the tip to sample, and thus imaging the unoccupied states of the sample.

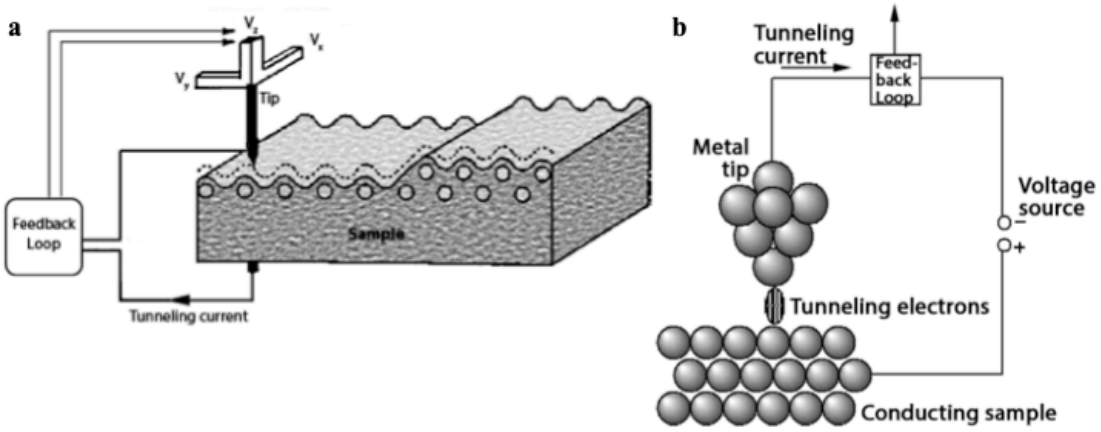

Figure 4. a) Schematic of STM, b) highlighting the feedback loop.
Adapted from reference [15].

STM can be operated in two modes, constant-current or constant-height. In the case of constant-current mode, a desired tunnelling current is set and the feedback loop changes the tip-surface separation to maintain this current while the tip is scanned

over the surface. The vertical movements of the tip are recorded and this gives a topographic image containing surface height information. Constant-height mode, on the other hand, uses a set tip-surface separation where the feedback loop is turned off. The tip scans the surface at this set height and gives a topographic image using the variations in tunnelling current. This requires a very stable system with minimal noise, usually at a temperature of 4 K with a flat surface to prevent damage to the tip. The images reported in this thesis were all recorded in constant-current mode.

2.4. Conclusions

A variety of experimental techniques are essential to provide a clear picture of the structures being examined. Further information regarding the experimental procedures used for the preparation and characterisation of each surface is detailed in the individual chapters to which they apply. This information also contains details of image processing and calibration.

2.5. References

[1] K. W. Kolasinski, *Foundations of Catalysis and Nanoscience (Second Edition)*, Wiley, New Jersey, 2008.

[2] G. Attard, C. Barnes, *Surfaces*, Oxford Chemistry Primers, Oxford Science Publications, 1998.

[3] A. Hodgson, S. Haq, *Surface Science Reports*, 2009, **64**, 381-451.

[4] J. Carrasco, A. Hodgson, A. Michaelies, *Nature Materials*, 2012, **11**, 667-674.

[5] A. Michaelides, *Applied Physics A*, 2006, **85**, 415-425.

[6] M. Henderson, *Surface Science Reports*, 2002, **46**, 5.

[7] F. McBride, G. R. Darling, K. Pussi, A. Hodgson, *Physical Review Letters*, 2011, **106**, 226101.

[8] F. McBride, G. R. Darling, K. Pussi, C. A. Lucas, Y. Gründer, M. Darlington, A. Brownrigg, A. Hodgson, *Journal of Physical Chemistry C*, 2013, **117**, 4032-4039.

[9] S. H. Overbury, D. R. Mullins, M. T. Paffet, B. E. Koel, *Surface Science*, 1991, **254**, 45.

[10]https://chem.libretexts.org/Bookshelves/Physical_and_Theoretical_Chemistry_Textbook_Maps/Supplemental_Modules_(Physical_and_Theoretical_Chemistry)/Surface_Science/6%3A_Overlayer_Structures_and_Surface_Diffraction/6.2%3A_Low_Energy_Electron_Diffraction_(LEED)

[11] M. A. VanHove, W. H. Weinberg, C. Chan, *Low-Energy Electron Diffraction*, Springer Series in Surface Sciences, Springer-Verlag, Berlin, **Volume 6**, 1986.
[12] M. A. VanHove, S. Y. Tong, *Surface Crystallography by LEED*, Springer Series in Chemical Physics, Springer-Verlag, Berlin, **Volume 2**, 1979.
[13] K. Morgenstern, N. Lorente, K. H. Rieder, *Physica Status Solidi B, Basic Solid State Physics,* 2013, **250**, 1671-1751.
[14] G. Binnig, H. Rohrer, *Review of Modern Physics*, 1987, **59**, 615-625.
[15] https://www.nanoscience.com/techniques/scanning-tunneling-microscopy/

Chapter 3

Strain Relief during the Growth of an Ice Film on a Hexagonal (√3x√3)R30°-SnPt(111) Template Surface

3.1. Introduction

The need for clean and sustainable power has led to vast research into the production of fuel cells over recent years, with the objective to create highly efficient energy converting devices with low or zero emission[1,2]. This attraction arose from numerous issues including fossil fuel shortages, high energy demands and environmental pollution. Although many fuels cells operate well under ambient conditions using a Pt catalyst, the surface is easily poisoned by reaction intermediates, often CO, which block the Pt active sites and make the catalyst inactive. This in turn increases costs and as Pt is an expensive metal, there have been many investigations to reduce or replace the amount of Pt within the catalytic material, in hope of reducing costs and creating of a CO resistant catalytic Pt surface[3-7].

The catalytic surface poisoning of Pt is an issue that has been under investigation in Direct Alcohol Fuel Cells (DAFCs)[2,8-11]. DAFCs use methanol or ethanol as a fuel and source of hydrogen, being advantageous because liquid alcohols are easy to handle and transport and are relatively non-toxic compared to possible alternatives[7,12]. When an active Pt metal catalyst is used in the dissociative adsorption of the alcohol, however, the surface is readily poisoned by a CO intermediate produced during the oxidation reaction. CO strongly adsorbs on Pt, blocking and limiting the number of surface active sites, which in turn reduces cell performance. Recent studies have therefore focused on the surface alloying of Pt with a variety of transition metals in the hope of preventing this surface poisoning[2,13,14].

PtSn is a promising catalytic alloy surface in DAFCs, which has shown remarkable activity and resistance to CO poisoning by activation of adsorbed water[11,15,16]. CO oxidation on PtSn is proposed to occur via a bifunctional mechanism, where an OH species on Sn oxidises the CO molecules preferentially adsorbed on Pt[13,17]. This frees the Pt active sites and optimises

the activity of the catalyst by preventing surface poisoning. Although the exact reaction mechanism remains unknown, it has been suggested that hydroxide is produced by activation of water at low potentials[18].

McBride *et al*. have investigated how the (√3x√3)R30°-SnPt(111) alloy surface responds to both hydroxide and water adsorption using a combination of LEED-IV and DFT studies, in hope of gaining a better understanding as to why this surface prevents poisoning of the Pt active site[13]. They report that for the bare alloy substrate, the larger atomic size of Sn causes the Sn atoms to protrude out of the surface plane by approximately 0.2 Å[13,19-22]. The adsorption of an intact water film on this surface further increases this outward displacement of Sn to 0.36 Å[13], which is an increase of 80 %. Theoretical studies into the adsorption of hydroxide, on the other hand, whether it be purely hydroxide or a mixed water-hydroxide layer, find it causes a displacement of Sn above the surface layer by approximately 0.8 Å. This is much larger than that found by electrochemical studies and a comparison of these results with previous Surface X-Ray Diffraction (SXRD) measurements[13,16,23], indicates that the displacement of Sn is most likely a result of water adsorption rather than hydroxide. This therefore questions the adsorption mechanism of hydroxide on Sn which was proposed in previous models, and shows that there is still much work to be done to fully understand the interfacial interactions occurring during the surface wetting of SnPt.

With SnPt forming a monolayer surface alloy with a (√3x√3)R30° structure, it possesses similarities in terms of symmetry with hexagonal ice and therefore became a compelling system to study the adsorption of a simple water film[24-26]. McBride *et al*. found that water adsorbs intact on this surface to form an ordered hexagonal hydrogen-bonded network[13,26]. LEED-IV and DFT have provided evidence to support a (√3x√3)R30° H-down bilayer with water adsorbed flat atop Sn and H-down on Pt, commensurate with the underlying substrate[26]. Further from this, LEED experiments by Massey *et al*. found that the adsorption of additional wetting layers forms an ordered ice structure[27]. This PtSn template therefore represents a promising system to investigate multilayer wetting.

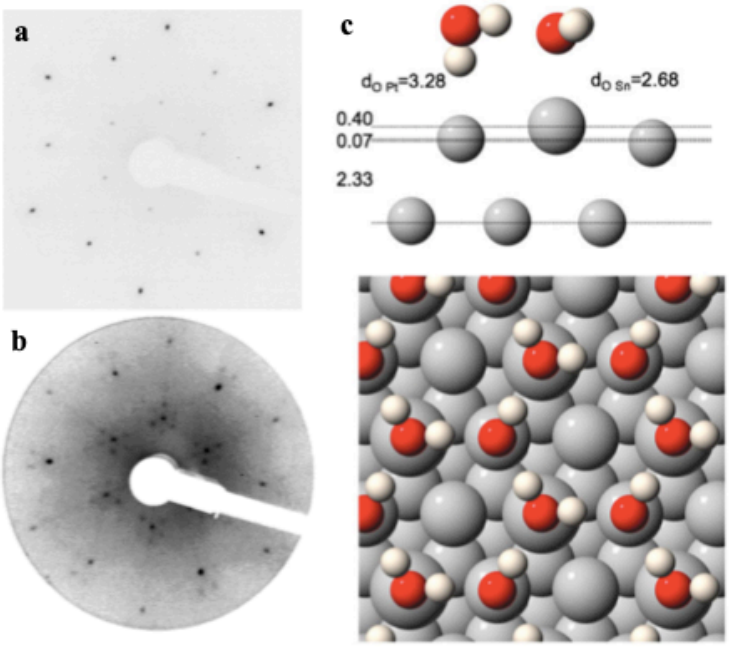

Figure 1. LEED images recorded at 90 eV with increasing water coverage on the (√3x√3)R30°-SnPt(111) alloy surface at a) 1 ML and b) 6.2 ML water and c) water structure calculated by DFT[26].
c) Adapted from F. McBride *et al.*, *Physical Review Letters*, 2011, **106**, 226101.

The creation of a template surface with a similar periodicity to bulk ice should theoretically allow the growth of an ordered wetting layer, in registry with the underlying substrate, to corroborate reports by McBride and Massey *et al*[13,26,27]. The objective of this study is to investigate the surface structure with STM in hope of gaining evidence to support H-down wetting, and in turn explore the adsorption of further wetting layers. With the alloy surface and first wetting layer having the same lattice periodicity, the water film should be pinned and held by the substrate, which will hopefully aid the imaging of further wetting layers with STM. This provides an opportunity to examine the multilayer wetting of a simple template surface and gain an insight into the growth of an ice film.

3.2. Experimental

3.2.1. Preparation of Clean Pt(111) Surface

A Pt(111) surface (99.999 %, Surface Preparation Laboratory) was polished to within 0.25° of the (111) face and cleaned by cycles of Ar^+ ion sputtering at 0.9 keV and annealing to approximately 1200 K. The surface was repeatedly treated in an oxygen atmosphere ($5x10^{-7}$ mbar) and subsequently annealed to remove carbon contamination. The surface quality was determined using a low current MCP LEED and STM before beginning alloy preparation.

3.2.2. Preparation of (√3x√3)R30°-SnPt(111) Alloy Surface

Tin (99.995 %) was deposited from a thermal source to adsorb slightly in excess of 0.33 ML and the surface annealed to approximately 1000 K to form a (√3x√3)R30° monolayer surface alloy. Surface preparation was characterised by LEED and STM to confirm the formation of this (√3x√3)R30° ordered structure over the complete Pt(111) surface, and to assess surface cleanliness before beginning water adsorption. Full conditions for this preparation are detailed in Chapter 2.

3.2.3. Water Adsorption

Water adsorption was studied in an UHV chamber with a base pressure of $4x10^{-11}$ mbar, using a CreaTec low-temperature STM with a separate preparation chamber. Water films were grown using a molecular beam directed through the STM housing aperture towards the crystal face. Water exposure was quantified by STM, with one layer defined as covering the complete (√3x√3)R30°-SnPt(111) surface. The surface was then annealed within the STM housing at various temperatures to order or desorb the water structure.

Initially, a surface coverage of less than 1 ML was prepared to investigate the first layer wetting structure, before proceeding to explore more complex multilayer wetting. For sub-monolayer growth, the alloy surface was exposed to a background of 0.1 Langmuir water at 77 K. This was quantified to be approximately 0.7 ML of water following STM analysis. The surface was then annealed to 120 K to order the water network before further examination by STM. After analysing this first wetting layer structure, the next objective was to investigate multilayer wetting. For growth of a multilayer film, the surface was held at a temperature of 130 K whilst exposed to duplicate small additions of 0.05 Langmuir water. STM analysis was again used to determine the relative coverage and structure of the multilayer film.

For the imaging of multilayer water films, a low tunnel current was used to prevent tip-induced restructuring or dissociation of the water structures, with the exact I_t and V_t values stated in the figure captions. Applying a negative bias voltage to the sample was found to give the best resolution of the second wetting layer, imaging the occupied states of the water molecules.

3.2.4. Theoretical Calculations

DFT calculations were carried out by our collaborators (Michaelides, *UCL London*, and Gattinoni, *ETH Zurich*) with VASP[28-30] using the optB86b-vdW functional[31]. This functional is a revised version of the van der Waals (vdW) density functional of Dion *et al.*[32], which has shown good agreement with experimental data for water adsorption on metals[33-37]. Further tests were performed with the Perdew-Burke-Ernzerhof (PBE) functional[38], both with and without the D3 vdW correction[39]. Core electrons were replaced by projector augmented wave potentials[40], whereas the valence states were expanded in plane-waves with a cut-off energy of 500 eV. All calculations were performed using a four layer thick (4×3) Pt(111) slab. In the top layer, 1/3 of the surface Pt atoms were substituted with a Sn atom. Periodic images were separated by approximately 15 Å of vacuum in the direction perpendicular to the surface. The metal atoms in the bottom layer were fixed to the bulk optB86b-vdW optimal positions ($a^{Pt}_{optB86b\text{-}vdW}$ = 3.950 Å), whereas all other atoms were allowed to relax. A Monkhorst−Pack k-point grid of (3×6×1) was used in all calculations. A dipole correction along the direction perpendicular to the metal surface was applied and geometry optimizations were performed with a residual force threshold of 0.005 eV/Å.

STM images were simulated using the Tersoff−Hamann approach[41], with a voltage of −500 mV and at a height of 8 Å above the metal surface for the two-layer structures, and a voltage of +1 eV and at a height of 6 Å for the one-layer structure. Simulated images for different voltages and tip heights show similar results, demonstrating that the conclusion does not depend on the choice of these parameters.

Adsorption energies per molecule, E_{ads}, were computed with a standard definition, $E_{ads}=(E_{water/PtSn} - E_{PtSn} - n \times E_{H2O})/n$, where the total energies of the n-water system, relaxed bare metal slab, and an isolated gas phase water molecule are $E_{water/PtSn}$, E_{PtSn}, and E_{H2O}, respectively. Favorable (exothermic) adsorption corresponds to negative values of the adsorption energy. It should be noted that energy differences between different adsorbed systems can be rather small, *i.e.* below 10-20 meV, which is generally considered the lower limit of reliability of DFT calculations. Therefore, in order to identify the experimental structure, comparisons between experimental and DFT calculated workfunction changes have also been considered, as well as the compatibility of the STM images. The workfunction for the bare metal slab and the adsorbed system was estimated by computing the total local potential along the direction perpendicular to the surface, and considering the value for the

vacuum above the slab. The workfunction difference was then obtained by subtracting the two.

3.3. Results and Discussion

3.3.1. (√3x√3)R30°-SnPt(111) Template Surface

Before investigating the surface wetting of (√3x√3)R30°-SnPt(111), it was essential to characterise the bare surface layer. This monolayer alloy structure has been previously examined using other characterisation techniques, but has not been analysed by STM[13,18,22,26,27,42-45]. Imaging with STM allows an assessment of the clean surface before the adsorption of a water film.

The data reported in this section reveals the growth of an ordered (√3x√3)R30° alloy surface, in agreement with data reported in previous studies[13,26]. The surface layer is imaged with two different contrasts, either imaging Sn as bright protrusions surrounded by dark neighbouring Pt atoms, or as a hexagonal honeycomb lattice where Pt is imaged as a bright matrix and Sn as the dark ring centres. Both contrasts have the same structure and are found to be a result of tip condition, not bias voltage. The bare surface shows faults such as vacant Sn sites and domain boundaries, all of which are expected during the formation of this substitutional alloy surface, which is described in detail below.

3.3.1.1. Structural Analysis

A STM image of the (√3x√3)R30°-SnPt(111) surface is displayed in Figure 2a, formed by depositing ≥ 0.33 ML Sn on a Pt(111) surface and annealing to around 1200 K. This image reveals an arrangement of bright circular protrusions which correspond to the larger Sn atoms within the surface structure. As the surface is corrugated, Sn protrudes out of the topmost layer by approximately 0.2 Å[26] and is therefore appearing as an increased tunnel current. The dark regions surrounding these bright Sn features correspond to the neighbouring Pt atoms which complete the (√3x√3)R30° alloy structure. The measured Sn-Sn spacings are in good agreement with that of the expected (√3x√3)R30°-Sn distance at 4.72 Å, hence confirming the formation of an ordered substitutional alloy surface. This structure is seen for a range of tunnelling conditions over the complete surface layer.

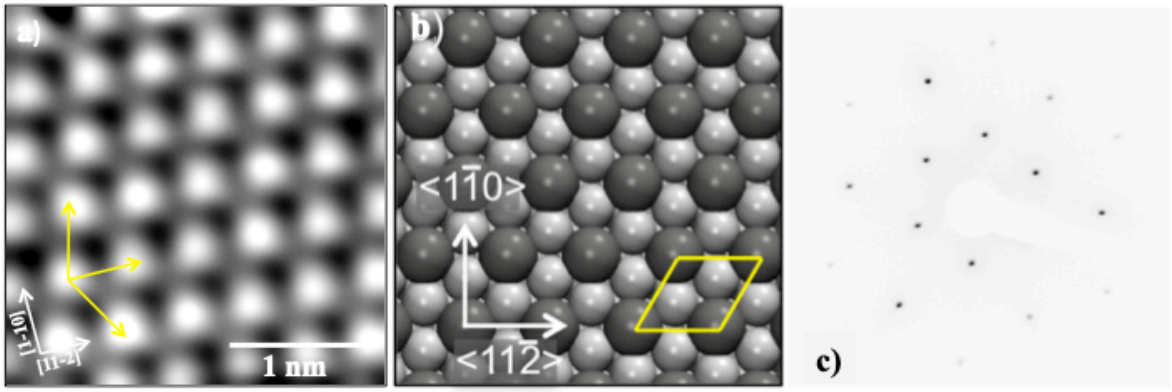

Figure 2. a) STM image, b) structural schematic and c) LEED pattern of the clean (√3x√3)R30°-SnPt(111) surface. The bright protrusions in a) correspond to Sn whilst Pt is imaged dark (77 K, 201 mV, 807 pA).

Sn has three nearest-neighbour directions within the (√3x√3)R30° surface structure, highlighted by the yellow arrows in Figure 2a. These correspond to the [11$\bar{2}$] azimuths, a result of the alloying substitution mechanism, with a surface Pt atom being substituted for a Sn atom at every (√3x√3)R30° site. As discussed, the observed bright protrusions in Figure 2a correspond to the larger buckled Sn atoms within the surface layer. These atoms must provide a tunnelling pathway with a higher tunnel current, and so, appear brighter in the STM images. The darker regions of the image therefore represent the smaller Pt atoms which have a lower tunnel current and appear at a lower height within the corrugated surface layer. LEED-IV data obtained from McBride *et al*. supports this surface corrugation, revealing an outward expansion of Sn by 0.20±0.03Å above the topmost layer[13].

Although Sn appears as an increased tunnel current in Figure 2a, changing the tip condition can reverse this contrast. This can be seen in Figure 3b, where a change in the state of the tip apex results in a change in the imaging contrast, and consequently, the surface is imaged as a honeycomb lattice. Figure 3b displays a network of bright hexagonal rings, each with a dark ring centre. In this arrangement, it surface Pt is imaged with an increased tunnel current to reveal the matrix of the honeycomb lattice, whilst the dark ring centres correspond to Sn. Although the bare alloy surface is being imaged differently here, both possess the same (√3x√3)R30° periodicity, simply imaging the same structure with a different contrast. With both imaging contrasts seen for a range of tunnelling conditions, it is not thought to be an effect of sample bias. Instead, it is thought to be a change in the tip state, most likely caused by the adsorption/desorption of an adsorbate at the tip apex.

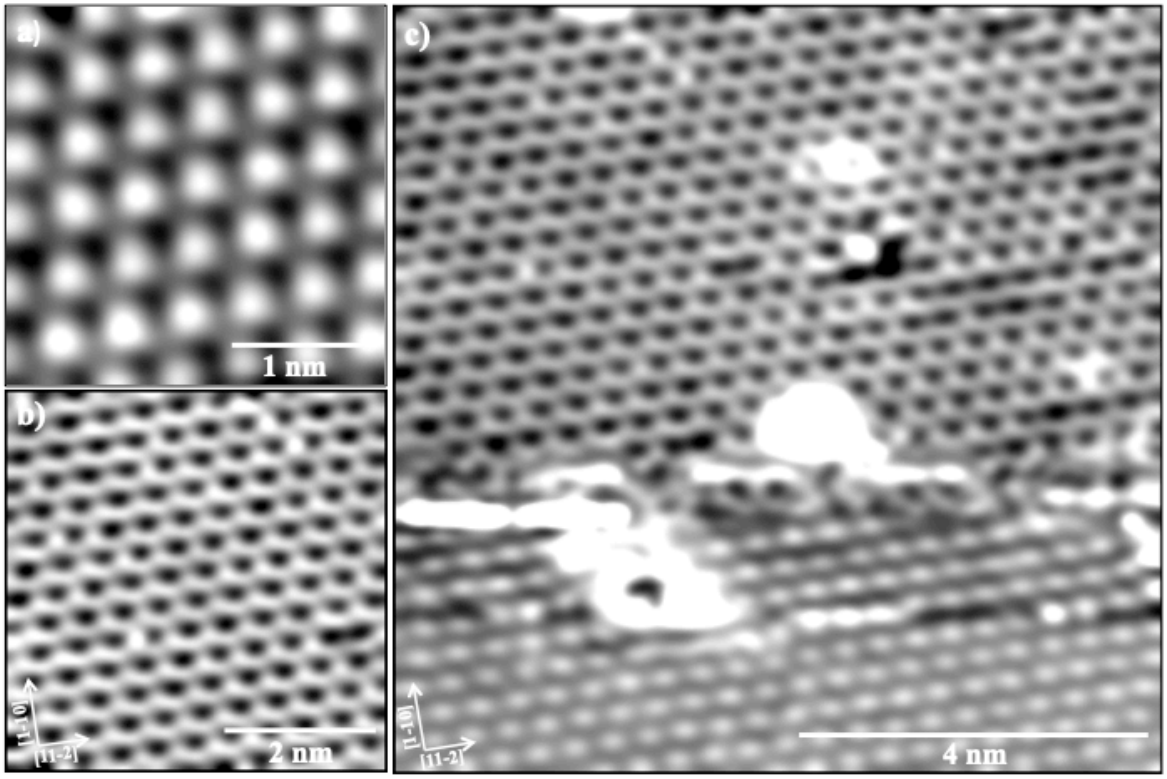

Figure 3. The different imaging contrasts observed for the (√3x√3)R30° SnPt(111) surface, a) Sn images as bright protrusions and Pt as dark (77 K, 201 mV, 807 pA), b) honeycomb lattice where Pt images as the bright hexagonal matrix and Sn as the dark ring centres and c) an STM image showing a tip change during scanning with both contrasts displayed in one image (77 K, 670 mV, 242 pA).

Figure 3c provides further evidence to support the different imaging contrasts being a result of tip change rather than bias dependency. Here, both imaging contrasts are seen in the same image under the same tunnelling conditions. Scanning over the large bright protrusion seen in the centre of the image is most likely the cause for the change in tip state, inducing a change in imaging contrast. As there has been no change in bias voltage or tunnel current, this provides further evidence to support the idea that the change in imaging contrast cannot be a result of bias dependency or tunnelling conditions.

Analysis of the (√3x√3)R30°-SnPt(111) alloy surface on a larger scale reveals the formation of domain pits. These are single layer depressions observed within the surface plane, as seen in Figure 4a. These growth features support alloy formation as they are not seen when imaging clean Pt(111). Characterisation of these structural features by STM confirms a (√3x√3)R30° periodicity across the complete surface layer. As alloying proceeds, Pt atoms are removed from the surface layer where they are substituted for Sn. These atoms then form a new topmost layer with Sn, having a (√3x√3)R30° surface structure, and so the surface of

the domain pits are at the same height as the original clean Pt(111) surface layer, before the adsorption of Sn. This results in the formation of these domain pits across the surface layer to allow complete alloy termination to occur.

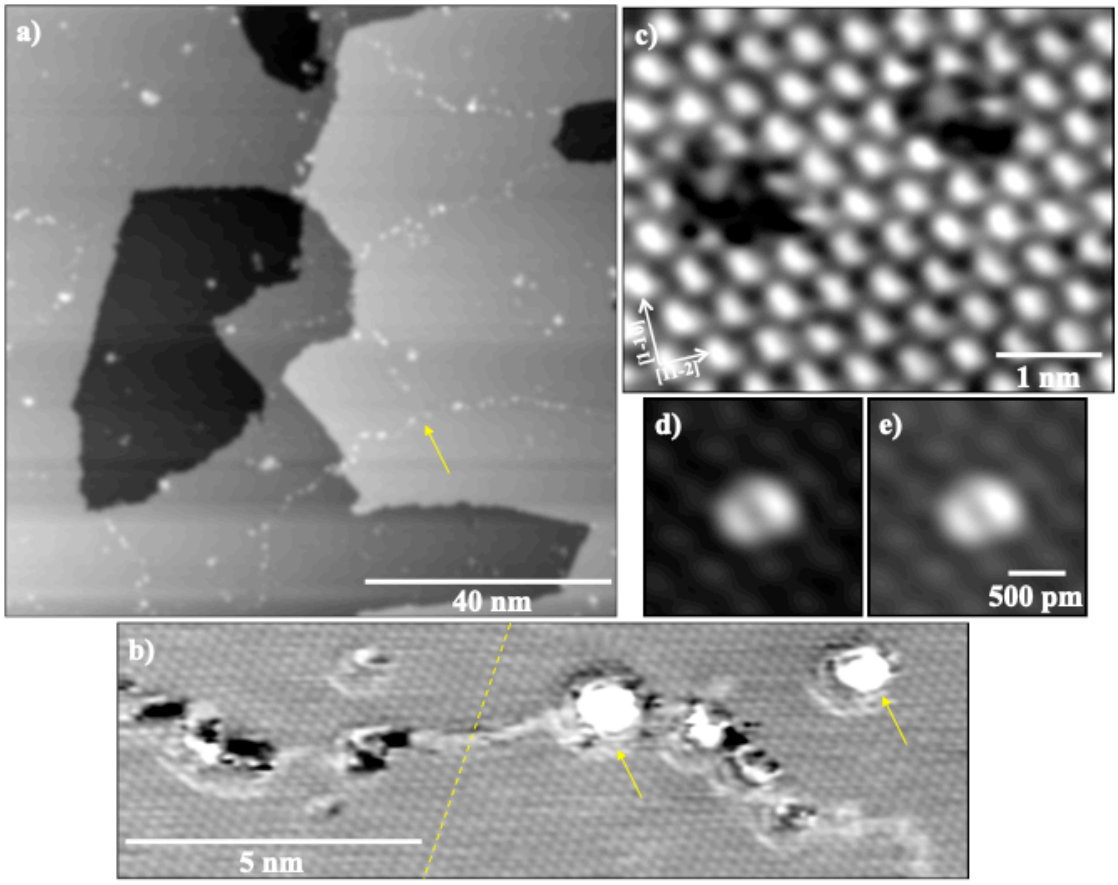

Figure 4. STM images to show the formation of a) domain pits and boundary walls (also highlighted in b), c) Sn vacant sites and d-e) CO adsorbates, a) (77 K, 1.24 V, 79 pA), b) (RT, 808 mV, 366 pA), c) (77 K, -604 mV, 559 pA), d/e) (77 K, -942 mV, 201 pA).

The surface layer also exhibits domain boundaries, which are seen as the irregular lines running along the topmost layer, highlighted by the yellow arrows in Figure 4a. These boundary walls separate two different (√3x√3)R30° domains, where one boundary is displayed in more detail in Figure 4b. When two regions meet out of registry, an anti-phase boundary wall is formed. This is further emphasised by the shift in atomic registry across the boundary, highlighted by the dashed yellow line in Figure 4b. This yellow line is superimposed above Sn on the bottom half of the image, but above Pt on the top half of the image, which confirms that the two areas are out of phase. These growth characteristics relieve strain within the surface layer to allow alloy termination to occur across the surface.

Again, this is another feature not observed for clean Pt(111), which confirms that alloy formation has occurred over the complete surface.

Small dark features are occasionally observed when imaging the (√3x√3)R30°-SnPt(111) surface with STM. These features, highlighted by the yellow arrows in Figure 4c, appear to disrupt the close-packed Sn rows along the surface layer. As discussed above, the bright protrusions represent surface Sn. The dark depressions observed in Figure 4c must therefore correspond to sites of missing Sn atoms. An error during the substitution of surface Pt for Sn can result in a Pt atom residing at a site where Sn should be, creating a Sn vacancy in the topmost layer. With Pt having a lower tunnel current, it appears dark in STM. Therefore, the dark region present in Figure 4c corresponds to a Pt atom positioned at this site, with no nearest neighbour Sn atoms. This is plausible as structural defects are expected to occur during surface substitution across such a large area of substrate.

The large bright protrusions highlighted by the arrows in Figure 4b are proposed to be islands of excess Sn. As they make up only a small minority of the surface layer, they are not observed by LEED or regularly in STM. The small double features observed in Figure 4d/e are thought to be a surface contaminant such as CO. Except for the possibility of damaging or modifying the STM tip apex, these adsorbates do not affect imaging this system with STM.

3.3.1.2. Structural Comparisons to Other Systems

Imaging the (√3x√3)R30° surface reconstruction of the $Pt_3Sn(111)$ bulk alloy also reveals a similar honeycomb network to that observed in Figure 3b[44,46]. As discussed earlier, when the (√3x√3)R30° network is imaged as a honeycomb lattice, the bright hexagonal matrix corresponds to surface Pt and the dark ring centres to surface Sn. The imaging of this honeycomb structure was observed for $Pt_3Sn(111)$ by Kuntze *et al*. at room temperature for a range of tunnelling conditions, using a bias voltage and tunnelling current of ±(0.1-0.9) V and 0.5-3.0 nA, respectively. They do not however report the atomically resolved imaging contrast displayed in Figure 3a, where the bright protrusions correspond to surface Sn and the surrounding dark area to surface Pt. As they are imaging the bulk alloy, which has an increased lattice parameter compared to Pt, the surface layer may not have the same degree of corrugation as the monolayer surface alloy being reported in this chapter. The surface Sn atoms therefore do not have an increased tunnelling pathway, as seen in Figure 2a, and instead the surface layer is, apparently, only imaged with the honeycomb contrast.

Kuntze *et al*. also observe similarities in the features present within the surface layer, such as domain boundaries[44,46]. They report the boundary walls to be an irregular line separating two (√3x√3)R30° domains, similar to that seen in Figure 4b, which also display the same shift in atomic registry across the boundary wall[46]. The large bright protrusions displayed in Figure 4b have similarly been observed by Kuntze *et al*. during their investigation of $Pt_3Sn(111)$. They also suggested these features are surplus Sn in the surface layer, as the clusters were found to disappear upon oxygen adsorption to form a Sn-O overlayer[44,46,48]. Overall, the $Pt_3Sn(111)$ bulk alloy provides only a comparison for discussion as its surface periodicity is similar to that of the monolayer surface alloy produced from the deposition of Sn on Pt(111)[20,43,47].

Surface pit formation has been reported for other systems, such as during the mass transport of surface Cu in oxygen-induced reconstruction of Cu(110). In the presence of oxygen, Cu atoms are removed from the surface terraces to form chains of Cu-O, which results in the formation of pitted regions[49,50]. When imaging clean Cu(110) with STM, the step edges display a 'fringed' appearance as a result of Cu surface diffusion[50,51]. These mobile Cu atoms are removed from step edges on adsorption of oxygen to produce a (2x1)-O structure. After adsorption of a large quantity of oxygen, the coverage of the (2x1)-O phase increases and this adatom supply from the step edges is reduced, until approximately 50% of the surface has formed the (2x1)-O structure and the supply and transport of Cu adatoms then becomes restricted as the oxygen coverage is further increased[50,51]. This results in the removal of surface Cu from the terrace, rather than step edges, creating holes in the terraces of the topmost Cu layer. Although a different explanation for surface pitting than that proposed for the formation of the (√3x√3)R30°-SnPt(111) alloy in this chapter, pitting in this system is again a result of atom removal from the surface terraces.

3.3.1.3. Mechanism of Surface Alloying

Information regarding the formation mechanism of the (√3x√3)R30°-SnPt(111) alloy structure is limited, except that it occurs by surface substitution of Pt for Sn in a (√3x√3)R30° arrangement. Inspection of X-ray Photoelectron Diffraction (XPD) data by Galeotti *et al*. reveals all Sn atoms in the alloy structure lie in the topmost surface plane[22]. The Sn XPD 3d peak appears similar to the Pt XPD 4f peak, indicating that the Sn and Pt atoms are in the same local environment. This confirms surface substitution, but gives no information as to the mechanism of how it occurs.

A recent paper by Schmid *et al*. studying the surface alloying of Cu(111) with Sn investigated the reaction kinetics using Low Energy Electron Microscopy (LEEM) and STM[52]. They proposed the formation of bronze via a cooperative mechanism, where ordered 2D Sn islands spontaneously sweep across the surface leaving behind alloyed bronze islands. As these Sn islands move across the Cu(111) surface, Sn randomly exchanges with the surface Cu atoms. These Cu atoms are then ejected from the Sn islands as 2D ordered bronze crystals. This process is driven by surface free energy, occurring when surface diffusion is faster than exchange into the surface, and this may be the mechanism occurring during formation of this SnPt(111) system.

3.3.1.4. Summary of Alloy Formation

This section describes the growth of an ordered template surface with a (√3x√3)R30°-SnPt(111) structure. With alloy formation occurring over the complete surface layer, analysis by STM supports previous data reported by McBride *et al*[13,26]. This topmost layer forms domain pits as a result of the mechanism for alloy formation. These pitted regions are seen to exhibit boundary walls across the surface layer, which correspond to anti-phase boundaries separating different (√3x√3)R30° domains. Atomic resolution of the surface structure by STM allows the substrate to be imaged in two contrasts. As a result of the appreciable corrugation of Sn above the surface, imaging is dominated by the observation of bright circular protrusions corresponding to the larger surface Sn atoms which image with an increased tunnel current. A change in the tip apex, however, changes the contrast to produce a honeycomb lattice, now imaging surface Pt with an increased tunnel current and Sn as the dark ring centres. Additionally, surface features have been assigned as Sn vacant sites, surplus Sn and other adsorbates, thought to be CO molecules. This understanding of the surface structure and the resulting images underpins the following investigation of surface wetting by STM imaging of the water film.

3.3.2. The Adsorption of a Water Monolayer on (√3x√3)R30°-SnPt(111)

It is possible to restrict the growth of a water film by controlling surface exposure. This allows the surface to be decorated with only small islands of water, followed by subsequent annealing to coalesce and order the water molecules into large ordered islands, with repeated exposure leading to the growth of one complete monolayer. This single water layer can then be analysed by STM before adsorption to further wetting layers.

The wetting of (√3x√3)R30°-SnPt(111) sees the formation of a complete 2D first layer network before the formation of an additional second layer. This first layer structure contains a hexagonal arrangement of water molecules, built from interconnected 6-membered water rings. Further analysis reveals a 3-fold symmetry of the hexagonal network, which is a result of water adsorbed flat on Sn, whilst H-down water on Pt completes the hydrogen-bonding network.

3.3.2.1. Structural Analysis

STM was used to investigate the growth of an ordered first wetting layer on (√3x√3)R30°-SnPt(111). The initial deposition of water sees the growth of small islands, which appear to change shape over the range of scan images indicating the mobility of water for this low coverage at 77 K. The small water islands image with low resolution until the surface is annealed to promote coalescence into large ordered islands.

Figure 5 reveals a water island grown on (√3x√3)R30°-SnPt(111) after adsorption of approximately 0.7 ML and surface annealing to 120 K. The bright regions of Figure 5a correspond to the water islands and the dark surrounding area to the bare alloy surface. The STM image in Figure 5b shows a higher resolution image, revealing a network of water molecules arranged into hexagonal rings. Each ring contains six water molecules, having a water molecule adsorbed at each ring corner. Hydrogen-bonding between these water molecules creates a complete hexagonal lattice across the water island. The spacing of the hexagonal rings is in agreement with the (√3x√3)R30° spacing expected, confirming the formation of a commensurate first wetting layer.

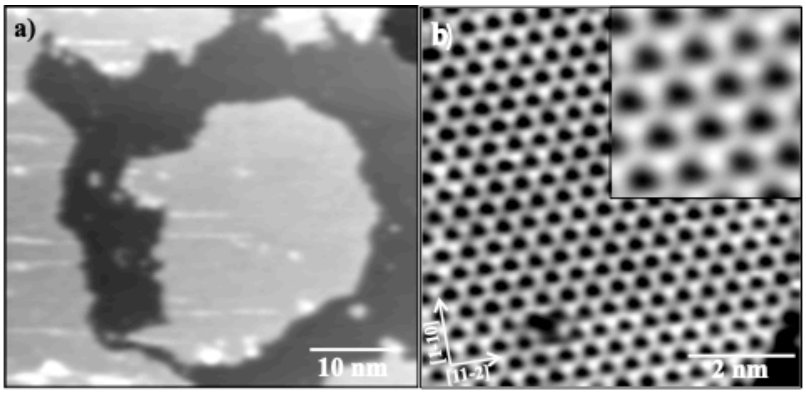

Figure 5. STM images of a) first wetting layer islands (bright) on a bare surface of SnPt (dark) after annealing to 120 K, where b) shows the island structure imaged with higher resolution, a) (77 K, 808 mV, 168 pA), b) (77 K, 268 mV, 101 pA).

A closer examination of the water structure in Figure 5b reveals alternate water sites show a slightly higher contrast than their neighbouring water sites. With each hexagonal ring containing 6 water molecules, 3 of these sites are imaged as bright sites and 3 less bright. These surround a dark ring centre, giving a 3-fold symmetry to the hexagonal ring structure. As this characteristic symmetry is seen regardless of tunnelling conditions, it is not a result of bias dependency. This is the first instance to our knowledge that a 3-fold symmetric, hexagonal first wetting layer has been imaged with STM, and confirms the stability and compatibility of the water film on this template surface.

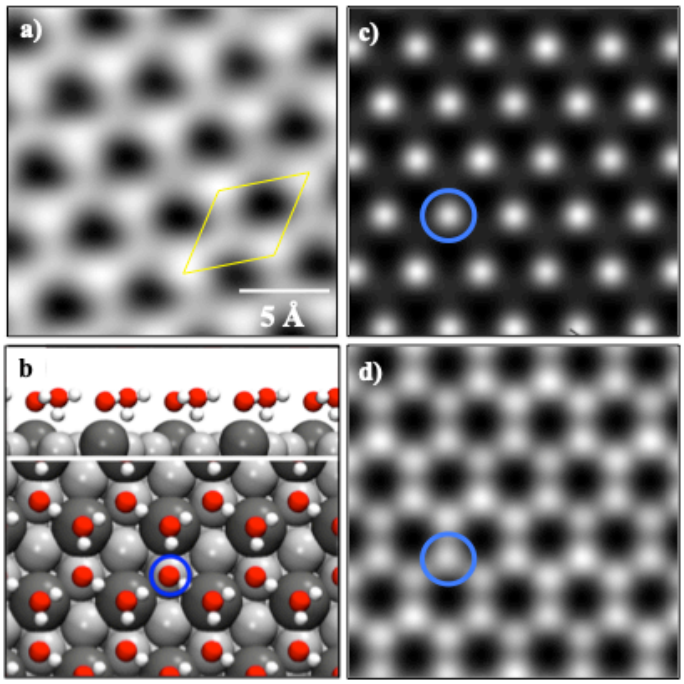

Figure 6. a) STM image of the first wetting layer (77 K, 268 mV, 101 pA), b) lowest energy structure calculated for a single layer of water, showing water adsorbed flat above Sn and H-down above Pt, c) STM simulation for water arranged in the alternative H-up structure, showing the H-up site in blue and d) STM simulation of a H-down water layer, with the H-down site highlighted in blue. The simulated voltage is +1 V and the tip-surface distance is 6 Å (calculations were performed by C. Gattinoni).

A DFT study to investigate the structure of this H-down wetting layer on (√3x√3)R30°-SnPt(111) supports the conclusions drawn from the STM images. Calculations reveal a binding energy of -0.76 eV/water, which is 0.14 eV/water more stable than the H-up arrangement. The STM simulated images for the calculated H-up and H-down structures are shown in Figure 6c and 6d, respectively. Although the higher contrast site above Pt is seen in both structures, the STM simulation for the H-up arrangement is dominated by the hydrogen atoms that point out from the surface. This makes the flat lying water molecules barely

visible, directly opposing the experimental STM images which find only a small difference in contrast between the two water sites. The H-down structure is therefore preferred, in agreement with the LEED-IV data and workfunction assignment as a H-down wetting layer by McBride *et al*.

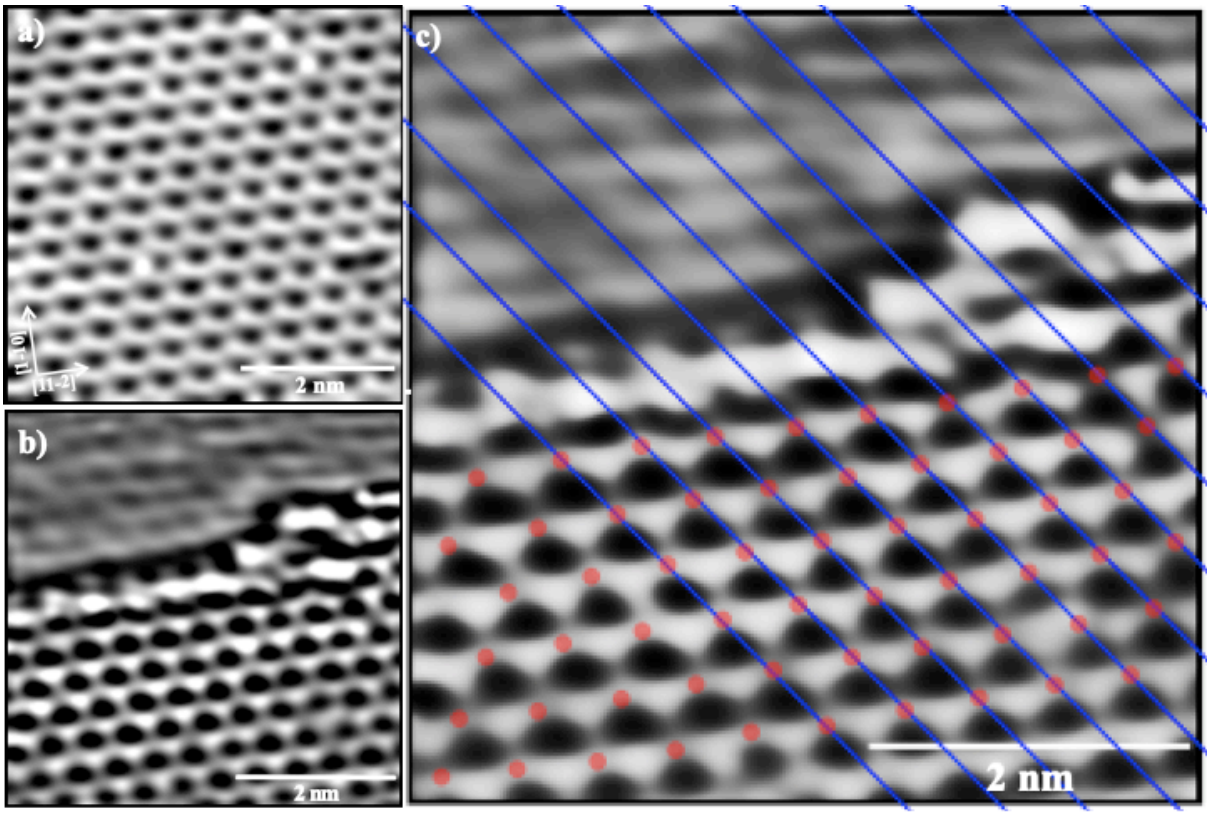

Figure 7. a) Clean (√3x√3)R30°-SnPt(111) surface imaged with Sn appearing as the dark site within the Pt honeycomb structure (77 K, -394 mV, 320 pA), b) the boundary between the bare SnPt substrate (top) and an island of first layer water (bottom), adsorbed on the alloy surface at 77 K after annealing to 120 K (77 K, 671 mV, 121 pA) and c) extrapolation of the Sn positions from the bare alloy terrace to the water layer, showing the location of the Sn atoms (red dots) underneath the low contrast sites of the hexagonal water network, which corresponds to flat water bound to Sn.

To understand how this first layer of water wets the alloy surface, the high resolution images seen in Figure 7 provide an insight into the surface registry. Figure 7a reveals the bare alloy surface imaged with a honeycomb contrast, described earlier in Section 3.3.3.1. In this contrast, surface Pt is imaged as an increased tunnel current, sited at the 6 bright corners of the hexagonal honeycomb matrix, whilst surface Sn is imaged as the dark ring centres. Figures 7b-c therefore provide an insight into the alignment of the first wetting layer with the underlying alloy substrate, where both structures are atomically resolved. The blue lines superimposed on Figure 7c correspond to the $[11\bar{2}]$ close-packed directions of Sn. The red

dots therefore represent the Sn sites in the underlying surface layer. This provides evidence that the hexagonal water rings are adsorbed on both Sn and Pt sites, with a bare surface Pt atom at the centre of the water hexamer. In turn, this confirms a commensurate arrangement between the first wetting layer and the underlying substrate.

A closer examination of this alignment also gives information regarding the 3-fold symmetry of the water network. Figure 6a reveals that the sites where water is adsorbed above surface Sn correspond to the fainter of the bright sites in the hexagonal ring structure. This means that the bright sites represent water adsorbed on Pt and it is the creation of these 2 distinct sites that fixes the rigid 3-fold symmetry of the water network. With these water molecules bonded in a flat orientation on Sn, the water network becomes locked into a fixed structure. The remaining water molecules then bond to Pt in a H-down orientation to complete the hydrogen-bonding network.

With this water network showing a clear 3-fold structure, the water molecules must be locked in a particular orientation (for example, flat, H-down or H-up) at particular binding sites and cannot interconvert, even in the presence of the STM tip. This observation supports water having different adsorption geometries at different binding sites, binding flat on Sn and H-down on Pt. If water was adsorbed solely on Pt, fast interchange between the different binding geometries can occur, with water able to rotate and change proton orientation as it is not locked in a particular geometry at a specific site. One would therefore expect no contrast differences between the 6 water sites, which is true for the hexagonal structures that form on Ru(0001), and also Pt(111) in the presence of hydrogen[53]. These water networks do not show internal structure, which leads to the assumption that the two water arrangements can interchange on the timescale of the STM measurement. This is not however the case for the SnPt system discussed here, where fast interchange between the two binding sites cannot occur.

Upon alloying, Sn donates charge density to Pt altering its electronic structure. The $1b_1$ lone pair orbital of water would usually donate electron density to Pt upon wetting, but this is now less favourable as a result of the charge density Pt has received from Sn, and instead the water molecule on Pt orients H-down. Meanwhile, the flat-lying water molecules above Sn can bind close to the surface, completing the hydrogen-bonding network. The Sn corrugation enables water to bond flat and reduces the repulsion between the lower hydrogen and the Pt

electron density, in turn allowing the entire oxygen network to remain flat[26]. This bonding arrangement is also influenced by the larger atomic size of Sn with respect to surface Pt. A LEED-IV study by McBride *et al*. reveals the outward expansion of Sn above the Pt surface layer to be 0.20±0.03 Å for the clean alloy surface. When a single layer of water is adsorbed, the displacement of Sn above the topmost Pt layer further increases to 0.36±0.03 Å[13]. This first layer wetting is consequently causing a 70-80 % increase in the displacement of Sn above the surface layer. This surface corrugation allows water to lie flat close to Sn, in turn providing enough space for the H-down orientation of water on Pt, while keeping the oxygen network almost completely flat.

3.3.2.2. Discussion of Defect Sites within the First Wetting Layer

Figures 5b and 8a reveal the presence of characteristic structural defects within the first wetting layer structure which are observed irregularly across the water layer. These sites appear as dark depressions in STM, with one water site imaging only very faintly and the surrounding water showing weaker contrast, appearing slightly 'blurred'. As they appear with a similar density and resemble the Sn vacancies seen for the bare SnPt surface (Figure 4c), they are most likely a result of a defect site in the underlying surface layer. Figure 8 reveals that this defect site in the first wetting layer is always situated at the fainter site of the hexagonal ring structure in the STM images. As this defect is proposed to be a result of a Sn vacancy, where a water molecule would usually be adsorbed flat above Sn, this supports the idea that the 3 less bright corners of the hexagonal rings correspond to flat water molecules atop Sn, whilst the 3 bright corners are H-down water on Pt. On this basis, the low contrast water molecule at the defect is fixed above this defect Pt site by the surrounding hydrogen-bonding network. However, with Pt being smaller than Sn, and lying in the plane of the other Pt, this flat water would be sited too high to bond directly to the metal substrate. It must therefore either relax towards the Pt or lose water-metal interaction at this site, both of which would reduce its contrast in STM. This means that water-tip interactions, water motion and/or relaxation during scanning could all influence proton orientation of this water molecule.

A more detailed examination of Figure 8 shows the defect site as a slightly blurred region in the STM image. This may be a result of either imaging conditions using a low tunnel current, labile water molecules on the surface or a combination of both. This water molecule is expected to be flat, fixed in this orientation by the neighbouring water molecules to maintain a complete hydrogen-bonding network. As this defect Pt site has not gained additional charge

transfer upon alloying, having no neighbouring Sn atoms, it could accept electron density from the $1b_1$ lone pair orbital of water as it adsorbs flat, forming a long, weak O-Pt bond. The blurred region of the STM image would then be a result of low tunnel current rather than labile water. Alternatively, since this defect site corresponds to a Sn vacancy in the underlying alloy surface, there is now enough space for this water to reorient to a more favourable H-down geometry. Being held in place by the surrounding hydrogen-bonding network, the neighbouring water molecules would become labile, in turn affecting the proton orientation of these adjacent water molecules because the hydrogen-bonding network will want to remain intact. The ability of this defect site to re-orient water may be the reason why both the site and surrounding area appear blurred. These two ideas give a plausible explanation as to why this defect site images as blurred in Figure 8, both in agreement that it is a result of a Sn vacancy in the underlying surface layer.

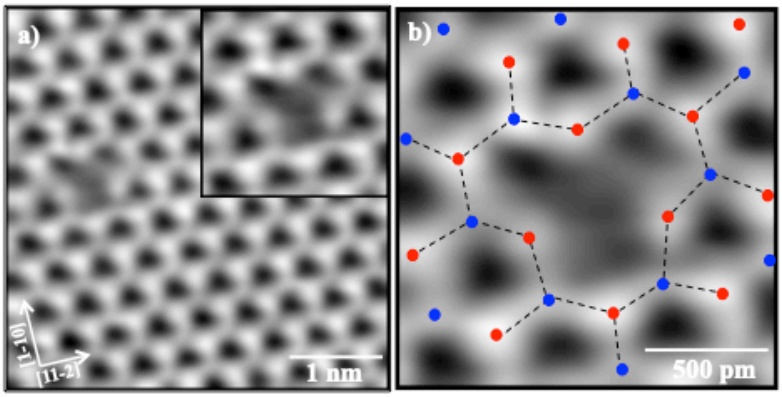

Figure 8. STM image shows a defect site in the first wetting layer structure, where b) highlights the bright H-down sites on Pt (red dots) and the fainter flat water sites on Sn (blue dots), revealing the fainter water site to be the defect site (77 K, 110 mV, 116 pA).

The only other possibility for this defect site is a missing water molecule within the first wetting layer structure. However, this would mean a single water molecule missing from the centre of an ordered network, which seems unlikely. At 77 K, water has enough thermal energy to move and reorient to its most favourable site and water is found to be mobile at 77 K, before surface annealing. It seems much more realistic that the water network would restructure to move the defect site to the edge of the water island, especially after annealing, producing a more stable hexagonal network at the centre of the water film. This idea was therefore discarded.

Following the discussion in this section, it seems most likely that the defect site observed in the first wetting layer on $(\sqrt{3}x\sqrt{3})R30°$-SnPt(111) is a result of a Sn vacancy within the

underlying alloy surface structure. This idea is therefore assumed for the remainder of this chapter.

3.3.2.3. Structural Comparisons to Other Water Systems

Defect sites have also been reported for the first layer wetting of other metal surfaces, most notably as Bjerrum defects on Cu(110)[54]. These have been observed for the partially dissociated c(2x2) overlayer, with a Bjerrum D-type defect occurring when 2 hydrogen atoms sit between an adjacent pair of oxygen atoms within a water network[55]. Forster *et al*. found both experimental and theoretical results favour a structure containing Bjerrum defects on Cu(110), formed from a 2:1 ratio of H_2O:OH[54]. Uncoordinated hydroxyl groups are the cause of these defect sites, stabilised by the formation of $(H_2O)_2$-OH trimer units within the water structure. These allow the hydroxyl group to act as a hydrogen bond acceptor to 2 water molecules, with a pair of these units creating a Bjerrum defect between the OH groups. Since the OH group is a poor proton donor but a very good acceptor, the loss of a H-bond between the O sites of OH is favourable, since it allows more strong donor bonds to OH[54]. In contrast, the intact wetting layer on (√3x√3)R30°-SnPt(111) has no hydroxyl groups, but Bjerrum defects might instead appear between water sites. Defect formation in this case would however mean sacrificing a water-water H-bond and this is not favourable. The theoretical simulation and model structure proposed by Forster *et al*. show the hexagonal rings in the c(2x2) overlayer are also slightly elongated in one direction, which is a result of the Bjerrum defect positioning on the substrate open face[54]. The hexagonal first layer which wets the (√3x√3)R30°-SnPt(111) surface, however, does not exhibit the same elongated hexamers, instead having a symmetrical structure. This again provides evidence to rule out the presence of Bjerrum defects in the first wetting layer structure on SnPt.

3.3.2.4. Summary of First Layer Wetting

This section describes the controlled growth of an ordered first wetting layer on a (√3x√3)R30° SnPt(111) template. STM analysis of the water network supports the intact structure previously reported by McBride *et al*.[13,26], with water adsorbed H-down on Pt and flat above Sn. Water is seen to form islands of a hexagonal network at a coverage less than 1 ML. The hexagonal rings exhibit a 3-fold structure displaying 3 bright and 3 less bright sites. Characterisation of this first layer structure reveals the bright sites correspond to H-down water on Pt, and the fainter of the 3-fold sites to flat water on Sn. Defect sites are also observed within the water islands which are assigned to Sn vacancy sites within the

underlying alloy surface. Now that the first wetting layer structure had been fully characterised and understood, investigation of multilayer surface wetting could proceed.

3.3.3. Multilayer Wetting of (√3x√3)R30°-SnPt(111)

With the underlying alloy surface and first wetting layer having the same (√3x√3)R30° periodicity as bulk hexagonal ice, this system provides a simple template to investigate multilayer surface wetting, with the aim of gaining a general insight into the initial growth of an ice film. Based on the evidence discussed above for first layer water on SnPt, it is possible that a second wetting layer might show ordered growth, since the first layer of water is tightly pinned commensurate with the substrate. The strong bond between water adsorbed flat in the first layer to Sn provides a constraint that is analogous to the strong pinning of water or OH on ionic or insulating surfaces, such as oxides. This suggests that this system may provide an insight into multilayer growth on materials with a much more corrugated potential than the widely studied close-packed metal surfaces. With this in mind, it is useful to assemble some initial thoughts for how growth of a second wetting layer might proceed on this surface.

The first aspect to consider is the hydrogen-bonding interaction between the first and second wetting layers and what constraints the structure of the first wetting layer might impose on second layer growth. In order to form a simple multilayer ice structure on this template, the second layer would want to bond to the wetting layer underneath by forming 3 hydrogen bonds between each hexagonal ring in the first and second layers. With the first layer found to have a H-down water structure, one might therefore expect the second layer to have 3 H-down water molecules forming hydrogen-bonds, leaving no free OH bonds to point into vacuum. This however assumes the first layer does not relax its orientation and that the first layer acts only as a H-acceptor. In practice, this will depend on the energy cost of reorienting water in the first layer and the stability of a hydrogen bond formed by donating to the first layer from the second layer, compared to that formed by donation to the second layer. A second factor to consider is the template size and its effect on the assembly of water within the second wetting layer. Although one might expect the second layer to favour commensurate stacking of the water layer in order to maximise hydrogen-bonding, this does not take into account any strain caused by this template. The first layer spacing is approximately 6 % greater than the lateral spacing in ice, and this layer is flat, not buckled, as it is in ice. Therefore, strain between the 3D ice structure and the simple hexagonal first

wetting layer may cause a change in the bonding network of second layer water in ways that are currently impossible to predict.

Multilayer surface wetting was investigated by controlling the exposure of the (√3x√3)R30°-SnPt(111) surface to water to achieve slow growth of an incomplete second wetting layer. High-resolution STM images revealed an ordered, yet complex structure of this second layer, differing from the simple (√3x√3)R30° hexagonal structure seen for a first layer of water discussed in the previous section. STM, LEED and electronic structure calculations reveal second layer water forms a complex hydrogen-bonded network, but one that is commensurate with the substrate. This structure contains 12 % more water than the first layer, with two additional water molecules incorporated within rows of linear defects, built from octamer rings linked by face-sharing water pentamers. These defect rows are linked by either three or four rows of hexagonal water to form a complete 2D hydrogen-bonding network, remaining in registry with the first wetting layer. These octamer-pentamer chains increase the water density, allowing the defect structure to bridge between the site density of the solid surface and that of a bulk ice film.

3.3.3.1. Structural Analysis of a Second Wetting Layer

An investigation into the initial stages of multilayer wetting on the (√3x√3)R30°-SnPt(111) surface was performed by restricting the water coverage to $1 < \Theta < 2$ ML and using low temperature STM to analyse the resulting surface structure. Figure 9a reveals a water film grown at 135 K at a coverage of approximately 1.6 ML, where both the first layer and an incomplete second layer are resolved. The second wetting layer forms extended 2D islands above the first wetting layer in Figure 9a, with the second layer completing before further adsorption occurs. The STM images show the second layer is built from three distinct domains, labelled α, β and γ in Figure 9b. These domains are aligned along the three $[11\bar{2}]$ symmetry directions of close-packed Sn, and have a domain size of approximately 10-20 nm measured across the rows.

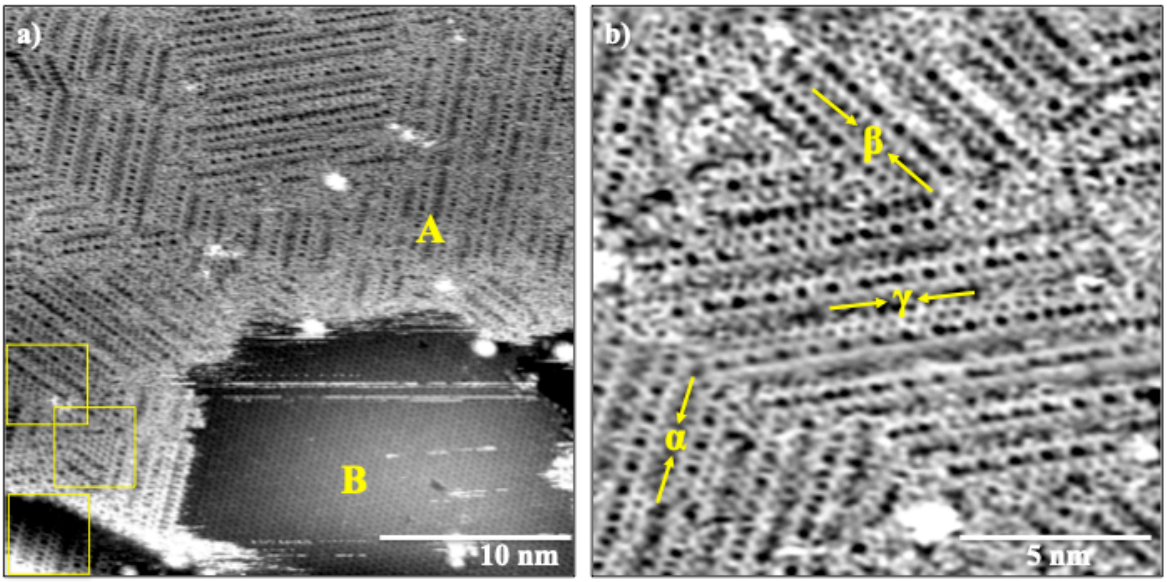

Figure 9. STM images showing second layer water growth, a) large scale image showing a second layer water island (A) growing on hexagonal first layer water (B), b) shows 3 intersecting domains. The highlighted frames of a) are shown with higher resolution in Figure 10. All images recorded at 77 K after growth at 135 K. a) (77 K, -173 mV, 22 pA), b) (77 K, -167 mV, 22 pA).

The three domains have an overall rectangular structure built from a combination of different sized water rings, seen more clearly in Figures 10d-e. The domains are characterised by rows of large, prominent rings with a unit repeat of $2\sqrt{3}a_{Pt}$ (where a_{Pt} is the atomic spacing of Pt, being 2.78 Å), highlighted by the ellipses in Figures 10d-e. Each row is separated from the next by a network of water rings, having a repeat distance of approximately $6a_{Pt}$, corresponding to a unit repeat of $4\sqrt{3}a_{Pt}$ along $[11\bar{2}]$ direction. Although the majority of the second layer has a well-defined repeat along the rows of large rings, the domains are less regular along the orthogonal direction. This is seen when each row of large, prominent rings are occasionally separated by $7.5a_{Pt}$, which is a consequence of disorder present within the domain. This separation corresponds to a unit repeat of $5\sqrt{3}a_{Pt}$ along $[11\bar{2}]$ direction, which maintains the registry with first layer water but demonstrates the complexity of the second wetting layer.

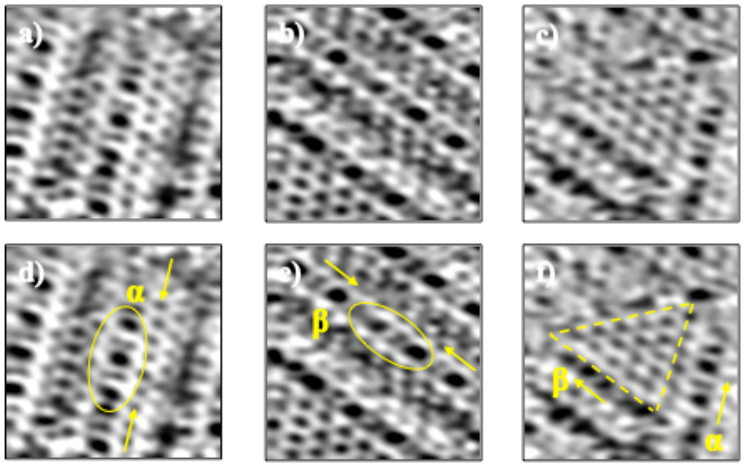

Figure 10. High resolution STM images of the highlighted frames in Figure 9a, where a-b) show 2 of the 3 domain directions and c) reveals a triangular region where different domains intersect (77 K, -173 mV, 22 pA).

Figures 10c/f show a small triangular region of hexagonal water, which is occasionally observed across the wetting layer at the point where different domains intersect. These regions are commensurate with the underlying (√3x√3)R30°-SnPt(111) substrate, closely resembling the first wetting layer structure discussed in detail in the previous section. Like the first layer, this two-layer structure shows a contrast alternation between the two water sites. The edges of this triangular patch are aligned along the rows of large rings allowing two or three symmetry related domains to link seamlessly together. However, the boundary between two intersecting domains in other regions of the second wetting layer can display less order.

3.3.3.1.1. In-Depth Analysis of Second Layer Structure

Increasing the tunnelling current and bias voltage when imaging the second wetting layer allows a closer examination of the structure with higher resolution. Figure 11 reveals the three distinct domains observed for the second layer, labelled α, β and γ in Figure 9b. The presence of these different domains allows optimisation of the density of second layer water, reducing the stress that has been created by adsorption on the SnPt template. Each domain images with a slightly different appearance, which is a consequence of the tunnelling conditions that cause the tip to interact with the water network, making the resulting image contrast sensitive to the scan direction. Different features are highlighted depending on the domain orientation, but this allows one to build a more thorough picture of the structure by using all three domains. That being said, this variable imaging contrast, weak lateral ordering of the second wetting layer and contrast variation between different images, presumably

caused by disorder in the hydrogen atom positions at particular water sites, does make it difficult to immediately understand the second layer structure.

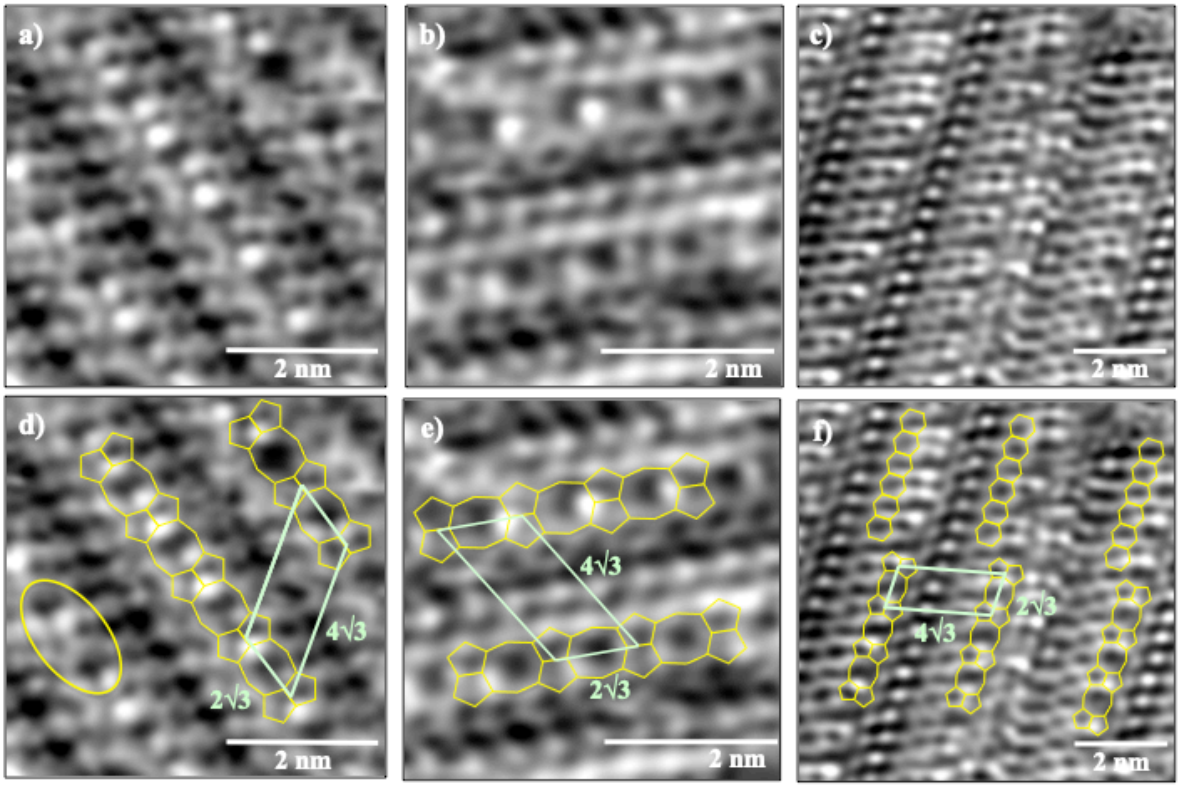

Figure 11. The 3 different symmetry directions of the second layer water domains with a horizontal scan direction, where d-f) have a superimposed structure on a-c). The defect rows are indicated by an overlay showing the large and small rings as octamer-pentamer rows, with the (2√3x4√3)R30° unit cell marked. The row of face sharing hexamer rings that runs alongside the defect row is indicated in frame f (top). a/d) (77 K, -845 mV, 26 pA), b/e) (77 K, -727 mV, 26 pA), c/f) (99 K, -748 mV, 30 pA).

Although complex, the STM images do reveal some indications as to the structure of this second wetting layer. With the domains characterised by rows of large, prominent rings, these are separated by an additional structure to give a unit repeat of $2\sqrt{3}a_{Pt}$ along the $[11\bar{2}]$ direction. These rows display sites with high contrast, suggesting the water molecules sited here protrude above the second layer plane. The structure separating these large rings is resolved in the high-resolution STM images of Figure 11, seen to be two small face-sharing rings. Taking into account the details of the STM images and supporting calculations, which are described in the next section, these defect rows are assigned to octamer water rings separated by two face-sharing pentagonal rings. This structure is highlighted by the yellow superimposed structure of Figures 11d-f, with these 1D defect rows forming a repeating (2√3x4√3)R30° unit cell along the $[11\bar{2}]$ symmetry direction. The remaining structure which

completes this second layer water network, connecting the defect rows, is however more difficult to interpret.

A well-defined chain of face-sharing hexagonal rings is found to run along one side of the defect octamer-pentamer rows, most noticeably highlighted in Figure 11e and by the yellow arrows in Figures 10d-e. The structure on the other side of these defect rows is however much less defined, showing a lower imaging contrast which is more difficult to resolve. Specific features appear to dominate the remaining structure, with these high contrast sites dependent on the imaging conditions. The structure separating the octamer-pentamer defect rows appears to have a simple $\sqrt{3}a_{Pt}$ periodicity, matching the first wetting layer and underlying SnPt surface structure. The separation of the defect rows is found to be approximately $6a_{Pt}$, which is equivalent to three rows of hexagonal rings, to form a structure that fits the $(2\sqrt{3}x4\sqrt{3})R30°$ unit repeat. However, this ordering is weak and incomplete, with a spacing of $7.5a_{Pt}$ observed for the occasional defective $(2\sqrt{3}x5\sqrt{3})R30°$ repeating unit. This separation is equivalent to four rows of hexagonal rings, suggesting that the octamer-pentamer chains are displaced by one $\sqrt{3}a_{Pt}$ unit.

3.3.3.1.2. Discussion of Disorder within the Second Wetting Layer

The presence of disorder within this second wetting layer could be a result of several causes. This includes strain relief within the second wetting layer, a compromise to maintain a complete hydrogen-bonding network within the water film, the accommodation of a higher density of water molecules within the second wetting layer and also the preservation of a commensurate registry between the first and second wetting layer structures with the SnPt surface. To gain a better understanding of the extent of disorder within the second wetting layer, the experimental STM images of this two layer structure can be directly related to LEED data previously reported for the growth of thin multilayer films on $(\sqrt{3}x\sqrt{3})R30°$-SnPt(111)[13,26,27]. McBride *et al*. found the first wetting layer exhibits a $(\sqrt{3}x\sqrt{3})R30°$ periodicity following a LEED investigation. Further growth above 2 ML, however, causes the appearance of $4\sqrt{3}$ diffraction features and streaking to become evident in the LEED pattern. This indicates disorder along the orthogonal $[10\bar{1}]$ directions, in agreement with the STM images and discussion above for second layer wetting. These additional features grow increasingly intense up to 5 ML, being slowly replaced by a weak hexagonal $(\sqrt{3}x\sqrt{3})R30°$ LEED pattern as the film grows to approximately 30 ML thick. Figure 12 shows a comparison of the experimental LEED and STM data, where a Fourier transform (Figure

12c) of the experimental STM image (Figure 12b) reproduces a diffraction pattern similar to the experimental LEED pattern for 2 ML of water, with the same additional 4√3 diffraction features and streaking observed.

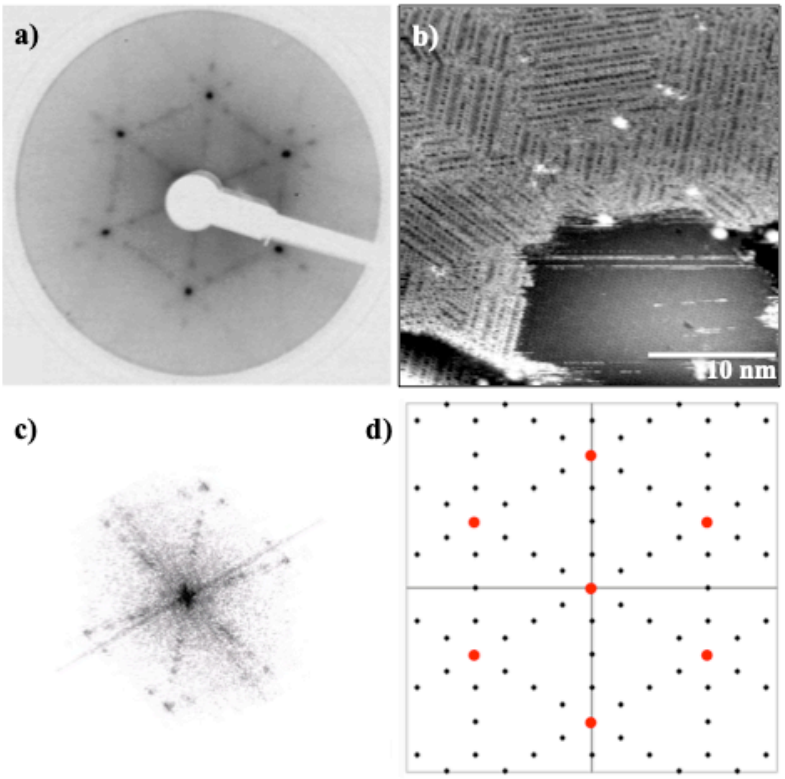

Figure 12. a) (√3x4√3)R30°-SnPt(111) LEED pattern for the adsorption of ≥ 2 layers of water (44 eV), b) STM image showing an island of second layer water after annealing to 135 K (77 K, -173 mV, 22 pA), c) Fourier transform of a two layer water domain shown in b), and d) schematic diffraction pattern for a (√3x4√3)R30°-SnPt(111) surface, with the √3 beams are highlighted in red.

3.3.3.1.3. Discussion of Surface Registry

Figure 12b reveals that exposed regions of the (√3x√3)R30° hexagonal first wetting layer structure remain unchanged upon second layer wetting. While this suggests that the water molecules in the first layer remain in their original sites above the alloy surface as the second wetting layer grows, we cannot confirm this directly. However, the close registry between the second layer and the (√3x√3)R30° SnPt, and the regular alignment of the domain edges of second layer water to the hexagonal first layer, all suggest there is minimal rearrangement of the underlying first water layer. The H-down first layer may relax or reorient to accommodate bonding to a second layer, particularly as the H-down first layer does not provide any free protons pointing into vacuum to facilitate second layer adsorption. With that being said, this

relaxation does not require much energy to allow the first layer structure to act as a template layer and facilitate multilayer ice growth.

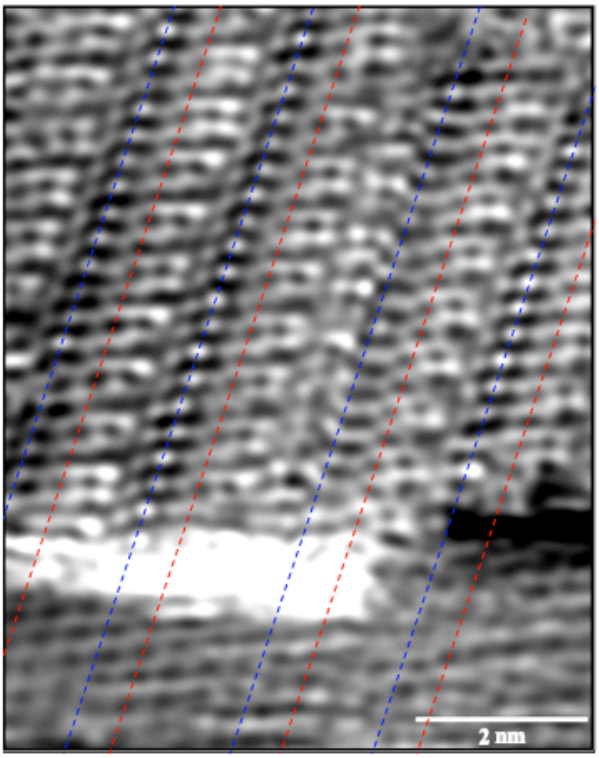

Figure 13. STM image showing the registry of the second wetting layer (top) with the underlying first wetting layer (bottom), grown at 90 K with annealing to 130 K (77 K, –767 mV, 27 pA).

The detailed registry between the first and second wetting layers can be determined by extrapolating across the edge of the second layer islands, where measurements find the rows of hexagonal rings in the second layer structure lie directly above first layer water rings, as shown in Figure 13. The superimposed lines provide information on the stacking of the water molecules within the ice film. The blue lines demonstrate that the bright √3 second layer features do not lie above the dark ring centers of the first wetting layer, but above a water molecule adsorbed on either Sn or Pt. As the 3-fold symmetry of the first wetting layer cannot be resolved in this image, one cannot distinguish if the site is Sn or Pt. The superimposed red lines show that the centre of the hexagonal rings in the second layer chain are aligned with the dark ring centre of the first wetting layer, locating the second layer hexagonal chains to be adsorbed directly above first layer water. This provides evidence that the second wetting layer is commensurate with the underlying first wetting layer, which supports the idea that the first wetting layer retains a (√3x√3)R30° structure with a lateral spacing matched to Pt.

A final constraint to consider when deliberating the second layer structure is the workfunction change during the growth of a multilayer film. The workfunction change was measured using a Kelvin probe as a thin water film was grown on (√3x√3)R30°-SnPt(111), with the results displayed in Figure 14. The value is sensitive to the average orientation of water and therefore gives an insight into the water structure as the thin film grows. A workfunction change of $\Delta\phi$ = -0.34 eV was recorded for the first wetting layer, consistent with the calculated value of $\Delta\phi$ = -0.50 eV calculated for a H-down water layer[13,26]. As a second layer wets the SnPt surface, the workfunction change increases to $\Delta\phi$ = -0.68 eV, reaching a limiting value of $\Delta\phi$ = -0.75 eV for a coverage > 2 ML of water. As the workfunction change is a global measurement, it will be influenced by regions which are not ordered within the structure. It can however be used to rule out structural models that possess too many water molecules in a H-up or H-down orientation, which would create workfunction changes that are not in agreement with experimental evidence.

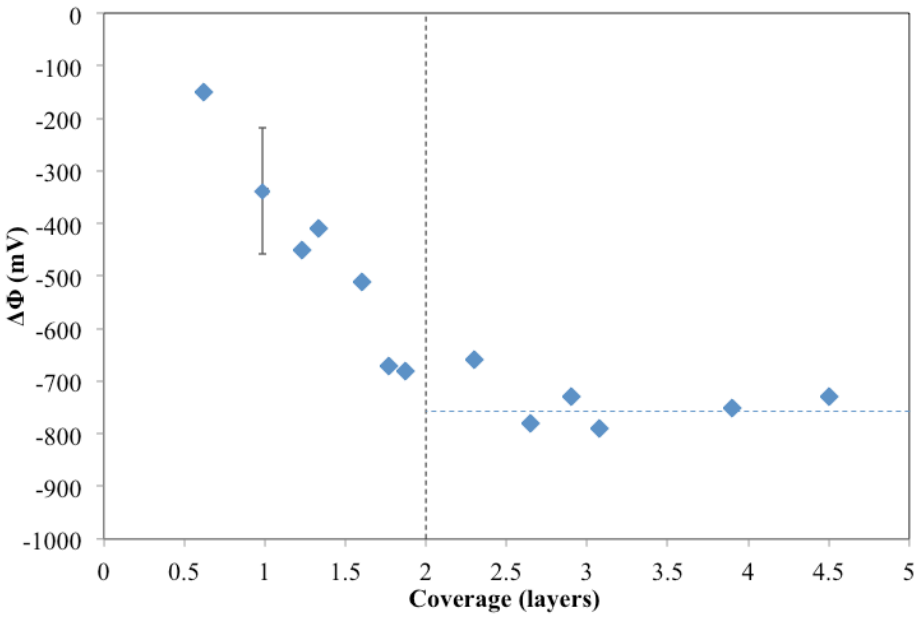

Figure 14. Workfunction change data for a thin water film grown on (√3x√3)R30°-SnPt(111), where the error bar indicates the full range for a series of measurements of $\Delta\phi$ for the complete monolayer whilst the limiting workfunction change for a thick film is indicated by the horizontal line.

3.3.3.2. Structural Models Proposed for Electronic Structure Calculations

With questions remaining with regards to the exact structure of this second wetting layer, it was essential to use electronic structure calculations to aid interpretation of the key features present within the second layer. Several models can be proposed to describe the features observed in the STM images, taking into account the rectangular (2√3x4√3)R30° domains,

the octamer-pentamer defect rows separated by a hexagonal network of water rings, and the overall registry between the two water layers and the underlying SnPt surface.

Three different types of second layer structures were simulated to gain a better understanding as to the density of water within the second wetting layer with respect to the underlying first layer. This included structures with a commensurate hexagonal second layer with a proton arrangement chosen to create the (√3x4√3)R30° superstructure, structures where a row of water molecules had been removed from the second wetting layer to form missing row structures, and finally, a structure where the density of the second layer was increased with respect to the first layer with two additional water molecules added to the (2√3x4√3)R30° unit cell. The most stable structure was found to be a complete hexagonal second layer, commensurate with the first wetting layer to form a sandwich structure. Although most stable energetically, this structure was not consistent with the complex second layer observed, and the STM simulation did not reproduce the key features observed in the experimental STM images. The latter was true for the missing row structures, with the STM simulations finding a large difference in appearance to the experimental STM images. These structural models were therefore discarded and theoretical calculations were concentrated on a (2√3x4√3)R30° second layer structure with an increased density of water molecules. The commensurate sandwich structure is discussed further in a later section, once the defect structure has been described in detail.

Having a structure with an additional two water molecules within the (2√3x4√3)R30° unit cell increases the water coverage to 0.75 ML, which is just 1 % less than the density of an ice $I_h(0001)$ surface. Figure 15 reveals four calculated structures that have this increased density. Here, two water molecules have been inserted into alternate face-sharing hexagonal rings to create the defect rows seen in the experimental STM images, consisting of a row of octamer rings separated by face-sharing pentamers. These structures have a similar binding energy to the commensurate hexagonal sandwich structure, being 13-28 meV/water less stable depending on the precise proton arrangement, but more importantly, the STM simulations reproduce many of the key structural features observed in the experimental images, unlike the sandwich structure. The rows of alternating large-narrow rings observed in the STM images (Figure 10) are reproduced in the STM simulated images, as well as displaying the high contrast sites present within the defect rows (Figure 10), highlighted in Figure 15 by the blue circles. These are associated with water sites which are buckled out of the second layer plane.

Also, the simulations show that the hexagonal chain along one side of the defect rows images with an increased contrast (see Figure 10/11).

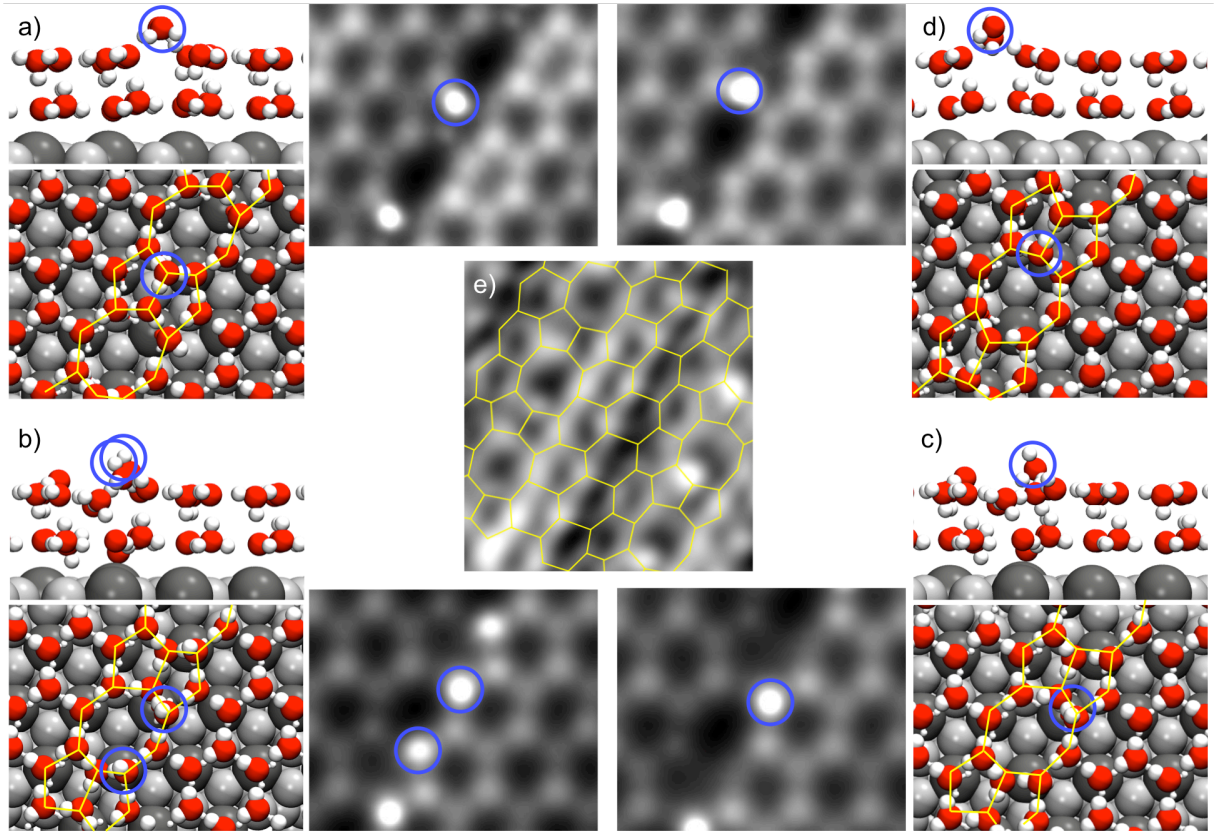

Figure 15. a-d) Calculated structures showing the formation of the defect octamer-pentamer rows between hexagonal domains adjacent to their simulated STM images, where e) provides a direct comparison to an experimental STM image where a (2√3 x 4√3)R30° water network has been schematically superimposed in yellow. Defect row structures (a-d) are formed by inserting a water dimer into alternate rings along a face-sharing hexagonal row, calculated in a (2√3 x 4√3)R30° unit cell, with a coverage of 0.75 ML. Water molecules that protrude above the second layer are marked by blue circles and image with a high contrast in the STM simulations.

The calculated workfunction change for these structures depends specifically on the exact hydrogen arrangement within the water network, but is found to lie within the experimental range, $\Delta\phi$ = -0.68 to -0.75 eV. This value proves useful to rule out structures which have incorrect hydrogen arrangements. Calculated work function changes lie in the range $\Delta\phi$ = -0.35 to -0.41 eV for defect row structures which have no H-up protons orientated towards the vacuum layer, increasing to $\Delta\phi$ = -1.04 eV as the number of H-up protons increases. Comparison with the observed workfunction change suggests at least some of the bright features observed by STM are likely to be H pointing into the vacuum, rather than simply

oxygen of water buckled water (although these cannot be distinguished by STM). Clearly the system retains considerable proton disorder, with various related hydrogen arrangements contributing.

3.3.3.2.1. Discussion of the Rejected Structural Models

The sandwich structure described above is found to the most stable two layer structure out of all of the models proposed from electronic structure calculations. This model is shown in Figure 16, being a fully hydrogen-bonding hexagonal network, commensurate with the underlying first wetting layer. It forms a highly symmetric structure with each water molecule within the first wetting layer having three in-plane hydrogen-bonds plus one H-up proton to bond to the second wetting layer. This structure, however, sacrifices bonding to the SnPt surface, losing the H-down bonding arrangement found to be most favourable for a single water layer. Although small commensurate regions of hexagonal second layer water are observed in the experimental STM images, such as the triangular region in Figure 10c, this is a minority structure across the second wetting layer occurring only at the point where different domains intersect. They also do not grow more than four or five units across before a defect row is formed. Figure 16 compares the experimental STM image of this region (Figure 16d) with the STM simulation for this structure (Figure 16c), which both show an alternation in intensity, with flat water molecules in the second wetting layer imaging with an increased contrast over the neighbouring H-down water molecule.

Similar hexagonal sandwich structures have been proposed for the adsorption of water on non-wetting surfaces, such as Au(111)[56] and graphite[57]. These structures possess weak water-surface interactions and hence do not form commensurate structures. Although the hexagonal first wetting layer does form a commensurate structure with the SnPt surface here, and has the correct symmetry to bind a hexagonal ice multilayer, the lattice spacing of Pt(111) is 6 % greater than that of a bulk ice structure. This creates lateral strain within the multilayer film which grows commensurate with the surface layer. The absence of extended hexagonal domains within the two layer water structure suggests that this lateral strain is sufficient to destabilize this structure on SnPt.

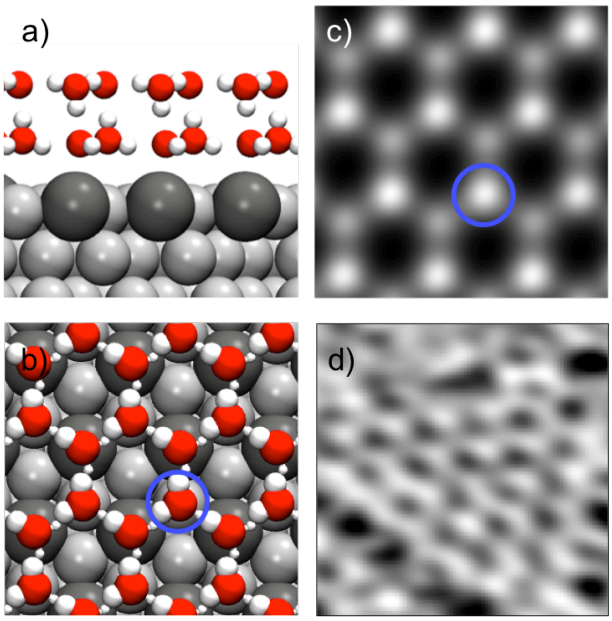

Figure 16. a-b) Calculated structure for the symmetric, two layer sandwich structure with the same water density as the first layer (0.67 ML) and a binding energy of E_{ads} = -0.70 eV/water, c) STM simulation showing the high contrast site marked by the blue circle and d) experimental STM image showing one of the small, minority triangular domains of second layer water with the same hexagonal (√3x√3)R30° alternation in site contrast (30 $Å^2$, 77 K, -173 mV, 22 pA).

3.3.3.2.2. Discussion of Most Feasible Model Structure

Considering the electronic structure calculations and STM simulations completed for the different types of structural models discussed earlier, the most feasible second layer structure is found to be one which has an increased density of water with respect to the first wetting layer. Here, two additional water molecules are inserted into alternate hexamers along the rows of hexagonal water rings to create large octamer rings which are separated by face-sharing pentamer rings, completing the hydrogen-bonding network. This produces a structure containing regularly spaced octamer-pentamer defect rows, separated by rows of hexagonal rings to create rectangular (2√3x4√3)R30° domains. The octamer-pentamer defect rows present within these structures reproduce the alternation between the large-small ring sizes that are observed experimentally by STM (Figure 10).

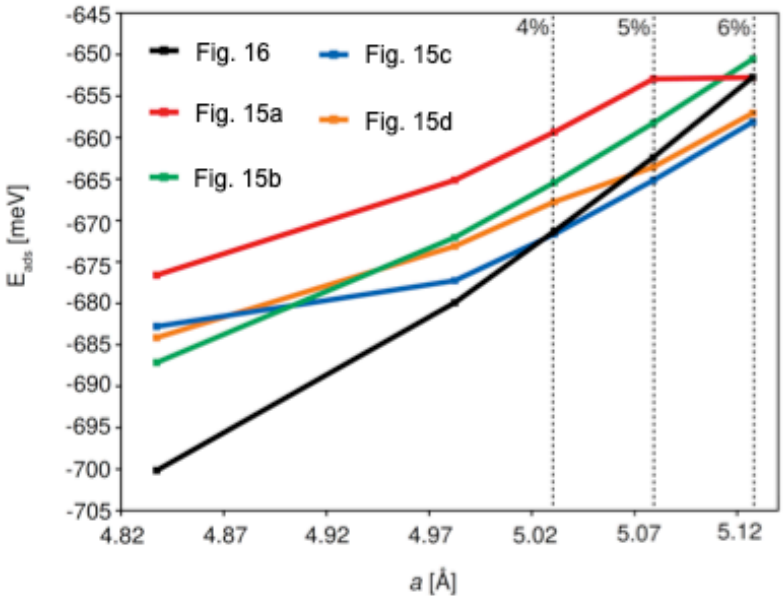

Figure 17. Change in adsorption energy for the structures shown in Figures 15a-d and 16 as a function of substrate lattice constant, *a*. Most of the defect row structures containing these octamer-pentamer rows become more stable than the sandwich structure (black line) within the strain range which has been tested (up to 6 %). Significant values of the substrate biaxial strain are indicated with black dotted lines. For the structure in Figure 15b, the sandwich structure is still more stable at 6 % strain, but the energy difference between the two decreases from 17 meV to 2 meV as the strain is increased, signaling a similar trend to the other defect structures.

Although the structures containing these octamer-pentamer defect rows (Figure 15) are found to be slightly less stable than the sandwich structure (Figure 16) discussed in the previous section, this energy difference is only small, being approximately 13 meV/water. Further analysis of the electronic structure calculations, however, reveal that the structures dominated by defect octamer-pentamer rows are actually more favourable when the lattice parameter is increased slightly, straining the substrate by approximately 5 %. This is observed in Figure 17, which shows an overall comparison between the different types of structures originally proposed when a lattice strain is applied. The trend implies that relaxation of the second wetting layer by increasing the water density allows stabilization of the defect structures, in turn, allowing them to become more stable (red line) than the simple hexagonal sandwich structure discussed earlier (black line). It should however be noted that DFT predicts this inversion in stability to occur at rather large tensile strains, which is mostly likely a consequence of DFT error in estimating the lattice constant of Pt and the hydrogen-bond length of the water network[58], and might appear at a different value of the biaxial strain in experiments.

3.3.3.3. Comparison to Other Systems

The defect rows of octamer-pentamer rings which form the (2√3x4√3)R30° rectangular domains are similar to the structure reported by Maier *et al*. for the adsorption of two layers of water on Ru(0001)[53]. Water adsorption on Ru(0001) sees the formation of growth domains which allow the low-lying rings of flat water molecules to sit in atop sites. Defect rows similar to those observed here for the SnPt system are seen where two domains meet to form an anti-phase boundary wall. Maier *et al*. also propose these defect lines to be an assembly of hexagonal units, linked by face-sharing pentamers and octamer water rings. These motifs allow the growth of an extended hexagonal lattice above the initial wetting layer on Ru(0001), whilst maintaining the hydrogen-bonding network and optimising the water-surface interaction.

Although both Ru(0001) and the SnPt system discussed here exhibit the same octamer-pentamer defect rows, the second wetting layer on Ru(0001) forms much larger hexagonal domains being around 10 units wide, separated by occasional defect rows aligned along the close-packed Ru direction. Maier *et al*. assign these rows to stacking faults within the water film, being a boundary wall between two out of phase domains, or associated with the formation of cubic ice[53]. The same structural defect rows on SnPt, however, are interpreted differently in this discussion, stabilising the wetting layer structure with the incorporation of two additional water molecules to increase the water density. Ru(0001) has a 3.7 % mismatch to ice, unlike Pt which has a much larger 6.3 % mismatch, thus a commensurate hexagonal network would therefore have less lateral strain on Ru(0001). This allows larger hexagonal domains to form on Ru(0001), staying commensurate with the underlying surface layer, before lateral strain becomes sufficient and the formation of an octamer-pentamer defect row occurs to allow relaxation within the wetting layer structure. With Pt having a much larger lattice mismatch to ice than Ru, this supports the idea of an increased lateral stress within a commensurate hexagonal water network on SnPt, and so, only three hexagonal rows can grow before formation of an octamer-pentamer defect row becomes favourable.

The first wetting layer structure on stepped Cu(511) also exhibits rows of octamer-pentamer rings, separated by a row of hexamers[59]. In this structure, however, the defect rows have a lower density of water molecules than the buckled hexagonal structure which forms as the first wetting layer completes, quite different to the situation on SnPt. Unlike SnPt, Cu(511) has a stepped structure separated by small terraces, with water tightly bound on the Cu step

sites. In this system, water exhibits a different strain relief mechanism as a lower density of water is required to relax the wetting layer to accommodate the short separation between the step sites. It appears that the formation of octamer-pentamer rows within a hexagonal water network is observed for a variety of wetting structures, with very different degrees of lattice mismatch present during surface wetting. Their formation offers a flexible, low energy strain relief mechanism between hexagonal rows to change the overall density and lateral registry of thin ice films, optimising the density of water to suit the surface involved.

3.3.3.4. Imaging of Thick Multilayer Films with STM

It was possible to image the second wetting layer of this system with high-resolution, but further multilayers proved more difficult. This was a consequence of interactions between the tip apex and water molecules within the ice film. The tip struggled to image thick water multilayers at the start of the *x*-scan direction, essentially being dragged through the water layers whilst trying to maintain the tunnel current parameter set in the constant-current working mode. Although we were sometimes able to obtain structures similar to those discussed above, any structural features observed in these STM images may correspond to the underlying first wetting layer or substrate being imaged through the thick film. This is reasonable as the tip is being pulled through the wetting layers, tunnelling into the states of the first wetting layer underneath which is tightly pinned to the substrate, or imaging of the (√3x√3)R30° SnPt(111) substrate itself.

3.3.3.5. Summary of Multilayer Water

Multilayer surface wetting was investigated by STM to reveal the growth of an ordered, yet complex second wetting layer, commensurate with the underlying first wetting layer. STM finds this second layer forms a structure built from three domains, with triangular patches of hexagonal water forming when the different domains intersect. The domains are built from defect rows of octamer-pentamer rings, separated by three rows of hexagonal water to form rectangular (2√3x4√3)R30° domains. Disorder is present within this second layer structure, creating occasional (2√3x5√3)R30° repeats by addition of an extra row of hexagonal rings. Evidence from electronic structure calculations reveals that the second wetting layer contains 12 % more water than the first layer structure, with two additional water molecules incorporated within the octamer-pentamer defect rows. These octamer-pentamer chains increase the density of the film, allowing the defect structure to bridge between the site density of the first layer water and that of a bulk ice film.

3.4. Conclusions

An investigation into the wetting of a template surface layer has been carried out using low temperature STM. Alloying Pt(111) with Sn creates a corrugated surface, matching the (√3x√3)R30° periodicity of hexagonal ice. This is an ideal structure to characterize a simple first wetting layer and provides a simple template of which to explore the growth of a multilayer film.

Depositing ≥ 0.33 ML Sn on Pt(111) and annealing to approximately 1000 K allowed the formation of a (√3x√3)R30°-SnPt(111) monolayer alloy surface. The surface structure was characterised by STM to reveal the growth of an ordered surface layer, in agreement with data reported in previous studies[13,26]. The surface can be imaged in two different imaging contrasts, either imaging Sn with an increased tunnel current so it appears as bright protrusions surrounded by dark neighbouring Pt atoms, or imaging the surface layer as a hexagonal honeycomb lattice where Pt is imaged as a bright matrix and Sn as the dark ring centres. STM analysis reveals both contrasts have the same (√3x√3)R30° structure and are a result of tip adsorbates. The bare surface shows faults such as Sn vacant sites and domain boundaries, all of which can be expected during formation of this substitutional alloy surface.

The formation of an ordered alloy surface allowed the chance to investigate surface wetting on a well-defined template that matches the spacing and symmetry of an ice film. In the first instance, surface wetting was restricted to a coverage slightly less than one complete monolayer to investigate the initial growth of a water film. The first layer wetting of (√3x√3)R30°-SnPt(111) sees the formation of a complete 2D network before the adsorption of an additional second layer. STM analysis reveals this first layer structure has a hexagonal arrangement of water molecules, built from interconnected 6-membered water rings, which remain commensurate with the underlying alloy substrate. Further analysis demonstrates a 3-fold symmetry of the hexagonal network, which is a result of flat water adsorbed on Sn whilst H-down water on Pt completes the hydrogen-bonding network. All data was in agreement with data previous reported by McBride *et al*[13,26]. Defect sites are also observed within the water islands which are assigned to Sn vacant sites within the underlying alloy surface. With the structure of this first wetting layer forming a simple hexagonal network, commensurate with the underlying surface, this provided a basis to investigate multilayer wetting in the hope of understanding how a thicker ice film can grow on this close-packed metal surface.

Finally, the growth of an ice film on a (√3x√3)R30°-SnPt(111) surface was investigated by STM. Surface wetting was restricted to the formation of just two layers of water in the hope of gaining an understanding as to the structure of a second wetting layer and its registry with the first wetting layer. High-resolution STM images revealed an ordered, yet complex structure in the second layer, accommodating the 6 % lateral expansion of the first wetting layer compared to bulk ice. Although commensurate with the first wetting layer, this second layer structure contains 12 % more water than the first layer, with these additional water molecules incorporated as linear defects to form rows of octamer rings linked by face-sharing water pentamers. These defect rows are linked by three or four rows of hexagonal water to form a complete, 2D hydrogen-bonding network in registry with the first wetting layer.

Overall, the results discussed in this chapter give an insight into the growth of an ice film on a solid template and how lateral strain can have a large effect on the structure which forms. The creation of octamer-pentamer face-sharing rows between hexagonal water domains provides a low energy, strain relief mechanism to vary the lateral density of water between the template and an ice film. We expect the same type of defect to appear in other systems where lateral strain requires a change in lateral density. These results demonstrate that in order to fully understand how surface wetting occurs, one is required to go beyond a description of the first water layer and develop techniques which can examine how the first few layers of water restructure during adsorption.

3.5. References

[1] Serov, C. Kwak, *Applied Catalysis B - Environmental*, 2009, **90**, 313-320.

[2] H. S. Liu, C. J. Song, L. Zhang, J. J. Zhang, H. J. Wang, D. P. Wilkinson, *Journal of Power Sources*, 2006, **155**, 95-110.

[3] E. Antolini, J. R. C. Salgado, E. R. Gonzalez, *Journal of Power Sources*, 2006, **160**, 957-968.

[4] E. Antolini, T. Lopes, E. R. Gonzalez, *Journal of Alloys and Compounds*, 2008, **461**, 253-262.

[5] J. Fearon, G. W. Watson, *Journal of Materials Chemistry*, 2006, **16**, 1989-1996.

[6] C. Panja, N. Saliba, B. E. Koel, *Surface Science*, 1998, **395**, 248-259.

[7] F. Vigier, C. Countanceau, F. Hahn, E. M. Belgsir, C. Lamy, *Journal of Electroanalytical Chemistry*, 2004, **563**, 81-89.

[8] E. Antolini, J. R. C. Salgado, E. R. Gonzalez, *Applied Catalysis B - Environmental*, 2006, **63**, 137-149.

[9] A. Hamnett, *Catalysis Today*, 1997, **38**, 445-457.

[10] T. Seiler, E. R. Savinova, K. A. Friedrich, U. Stimming, *Electrochimica Acta*, 2004, **49**, 3927-3936.

[11] S. Wasmus, A. Küver, *Journal of Electroanalytical Chemistry*, 1999, **461**, 14-31.

[12] R. Parsons, T. Vandernoot, *Journal of Electroanalytical Chemistry*, 1988, **257**, 9-45.

[13] F. McBride, G. R. Darling, K. Pussi, C. A. Lucas, Y. Gründer, M. Darlington, A. Brownrigg, A. Hodgson, *Journal of Physical Chemistry C*, 2012, **117**, 4032-4039.

[14] J. Kua, W. A. Goddard, *Journal of the American Chemical Society*, 1999, **121**, 10928-10941.

[15] T. Frelink, W. Visscher, J. A. R. Vanveen, *Electrochimica Acta*, 1994, **39**, 1871-1875.

[16] V. R. Stamenknovic, M. Arenz, C. A. Lucas, M. E. Gallagher, P. N. Ross, N. M. Markovic, *Journal of the American Chemical Society*, 2003, **125**, 2736-2745.

[17] T. E. Shubina, M. T. M. Koper, *Electrochimica Acta*, 2002, **47**, 3621-3628.

[18] B. E. Hayden, M. E. Rendall, O. South, *Journal of the American Chemical Society*, 2003, **125**, 7738-7742.

[19] B. E. Koel, *Model Systems in Catalysis: Single Crystals to Supported Enzyme Mimics*, ed. R. M. Rioux, Springer Science, New York, 2010, **Chapter 2**, 29-50.

[20] S. H. Overbury, D. R. Mullins, M. T. Paffet, B. E. Koel, *Surface Science*, 1991, **254**, 45.

[21] A. Atrei, U. Bardi, J. Wu, E. Zanazzi, G. Rovida, *Surface Science*, 1993, **290**, 286.

[22] M. Galeotti, A. Atrei, U. Bardi, G. Rovida, M. Torrini, *Surface Science*, 1994, **313**, 349-354.

[23] M. E. Gallagher, C. A. Lucas, V. Stamenkovic, N. M. Markovic, P. N. Ross, *Surface Science*, 2003, **544**, L729-L734.

[24] D. L. Doering, T. E. Madey, *Surface Science*, 1982, **123**, 305-337.

[25] J. Carrasco, A. Hodgson, A. Michaelides, *Nature Materials*, 2012, **11**, 667-674.

[26] F. McBride, G. R. Darling, K. Pussi, A. Hodgson, *Physical Review Letters*, 2011, **106**, 226101.

[27] A. Massey, F. McBride, G. R. Darling, M. Nakamura, A. Hodgson, *Physical Chemistry Chemical Physics*, 2014, **16**, 24018-24025.

[28] G. Kresse, J. Fürthmuller, *Computational Materials Science*, 1996, **6**, 15-50.

[29] G. Kresse, J. Hafner, *Physical Review B*, 1004, **49**, 14251-14269.

[30] G.Kresse, J. Hafner, *Physical Review B*, 1993, **47**, 558-561.

[31] J. Klimes, D. R. Bowler, A. Michaelides, *Physical Review B*, 2011, **83**, 195131.

[32] M. Dion, H. Rydberg, E. Schroder, D. C. Langreth, B. I. Lundqvist, *Physical Review Letters*, 2004, **92**, 246401.

[33] W. Lew, M. C. Crowe, C. T. Campbell, J. Carrasco, A. Michaelides, *Journal of Physical Chemistry C*, 2011, **115**, 23008-23012.

[34] C. J. Murphy, J. Carrasco, T. J. Lawton, M. L. Liriao, A. E. Baber, E. A. Lewis, A. Michaelides, E. C. H. Sykes, *Journal of Chemical Physics*, 2014, **141**, 014701.

[35] J. Carrasco, W. Liu, A. Michaelides, A. Tkatchenko, *Journal of Chemical Physics*, 2014, **140**, 084704.

[36] W. Liu, J. Carrasco, B. Santra, A. Michaelides, M. Scheffler, A. Tkatchenko, *Physical Review B*, 2012, **86**, 245405.

[37] M. L. Liriano, C. Gattinoni, E. A. Lewis, C. J. Murphy, E. C. H. Sykes, A. Michaelides, *Journal of American Chemical Society*, 2017, **139**, 6403-6410.

[38] J. P. Perdew, K. Burke, M. Ernzerhof, *Physical Review Letters*, 1996, **77**, 3865-3868.

[39] S. Grimme, S. Ehrlich, L. Goerigk, *Journal of Computational Chemistry*, 2011, **32**, 1456-1465.

[40] G. Kresse, D. Joubert, *Physical Review B*, 1999, **59**, 1758-1775.

[41] J.Tersoff, D. R. Hamann, *Physical Review B*, 1985, **31**, 805-813.

[42] B. E. Hayden, M. E. Rendall, O. South, *Journal of Molecular Catalysis A – Chemical*, 2005, **228**, 55-65.

[43] M. T. Paffett, R. G. Windham, *Surface Science*, 1989, **208**, 34-54.

[44] S. Speller, U. Bardi, *The Chemical Physics of Solid Surfaces*, ed. D. P. Woodruff, Elsevier, 2002, 10, **Chapter 6**, 184-224.

[45] M. J. Harrison, D. P. Woodruff, J. Robinson, *Surface Science*, 2004, **572**, 309-317.

[46] J. Kuntze, S. Speller, W. Heiland, A. Atei, I. Spolveri, U.Bardi, *Physical Review B*, 1998, **58**, 16005-16008.

[47] A. Atrei, U. Bardi, G. Rovida, M. Torrini, E. Zanazzi, P. N. Ross, *Physical Review B*, 1992, **46**, 1649-1654.

[48] M. Hoheisel, S. Speller, W. Heiland, A. Atrei, U. Bardi, G. Rovida, *Physical Review B*, 2002, **66**, 165416.

[49] A. R. Alexmozafar, X. C. Guo, R. J. Madix, *Surface Science*, 2003, **54**, L84-L88.

[50] J. Wintterlin, R. Schuster, D. J. Coulman, G.Ertl, R. J. Behm, *Journal of Vacuum and Science Technology B*, 1991, **9**, 902-908.

[51] Y. Kuk, F. M. Chua, P. J. Silverman, J. A. Meyer, *Physical Review B*, 1990, **41**, 12393-12402.

[52] A. K. Schmid, N. C. Bartelt, R. Q. Hwang, *Science*, 2000, **290**, 1561-1564.

[53] S. Maier, B. A. J. Lechner, G. A. Somorjai, M. Salmeron, *Journal of American Chemical Society*, 2016, **138**, 3145-3151.

[54] M. Forster, R. Raval, A. Hodgson, J.Carrasco, A. Michaelides, *Physical Review Letters*, 2011, **106**, 046103.

[55] M. Forster, R. Raval, J. Carrasco, A. Michaelides, A. Hodgson, *Chemical Science*, 2012, **3**, 93-102.

[56] D. Stacchiola, J. B. Park, P. Liu, S. Ma, F. Yang, D. E. Starr, E. Muller, P. Sutter, J. Hrbek, *Journal of Physical Chemistry C*, 2009, **113**, 15102-15105.

[57] G. A. Kimmel, J. Matthiesen, M. Baer, C. J. Mundy, N. G. Petrik, R. S. Smith, Z. Dohnalek, B. D. Kay, *Journal of the American Chemical Society*, 2009, **131**, 12838.

[58] Y. Fang, B. Xiao, J. M. Tao, J. W. Sun, J. P. Perdew, *Physical Review B*, 2013, **87**, 214101.

[59] C. Lin, G. Corem, O. Godsi, G. Alexandrowicz, G. R. Darling, A. Hodgson, *Journal of the American Chemical Society*, 2018 **140**, 15804-15811.

Chapter 4

An Investigation into the Structure of Water on the Open Ni(110) Surface and the Onset of Dissociation

4.1. Introduction

The adsorption of water on Ni has been of interest over recent years as it has relevance in fields of corrosion and catalysis. Studies on the close-packed hexagonal face of Ni(111) have shown that water adsorbs reversibly on this surface, remaining in its molecular state[1,2,3]. The open Ni(110) face, on the other hand, has been greatly deliberated as a result of its increased reactivity, having surface atoms with a lower coordination number with respect to close-packed Ni(111). Several investigations to probe the dissociation barrier of water on Ni(110) have appeared over recent years, but there is still much to be learnt about this system in terms of wetting at low temperatures.

The adsorption of water on this open-faced surface has been studied using a variety of surface characterisation techniques[4-9]. TPD data reported by Callen *et al*. reveals four desorption peaks, seen in Figure 1a, which were assigned to multilayer ice (180 K), water clusters (230 K), water dimers (280 K) and the disproportionation of OH_{ads} (400 K)[9]. LEED reveals a c(2x2) structure for the overlayer at adsorption temperatures 130 K and 180 K[7,10], with further evidence from Reflection Adsorption Infra-Red Spectroscopy (RAIRS) and Electron Stimulated Desorption Ion Angular Distribution (ESDIAD) leading to the belief that water was adsorbed with its molecular plane almost parallel to the surface with no intermolecular hydrogen-bonding[7,9,11-13]. Later studies, however, have proved this to be misguided[4,14].

Characterisation studies at higher temperatures revealed dissociation of water on Ni(110). Pirug *et al*. gained evidence from LEED, X-ray Photoelectron Spectroscopy (XPS), Ultraviolet Photoelectron Spectroscopy (UPS) and photoelectron diffraction

data to suggest that partial dissociation of water occurs when dosing above 180 K, resulting in a c(2x2) water/hydroxide structure[4]. Moreover, annealing above 200 K induces further dissociation to form hydrogen and hydroxide species according to High Resolution Electron Energy Loss Spectroscopy (HREELS) and Fourier-Transform Infrared Spectroscopy (FTIR) data[4,9,15,16]. Pirug *et al*. also proposed that water is in a dissociated state at temperatures as low as 120 K[4], demonstrating the continuing uncertainty as to what temperature water dissociates on Ni(110), or indeed if it ever adsorbs intact in a molecular state. Overall, there appears to be a consensus that water dissociates at temperatures above 200 K, but the nature of adsorption below 200 K remains ambiguous.

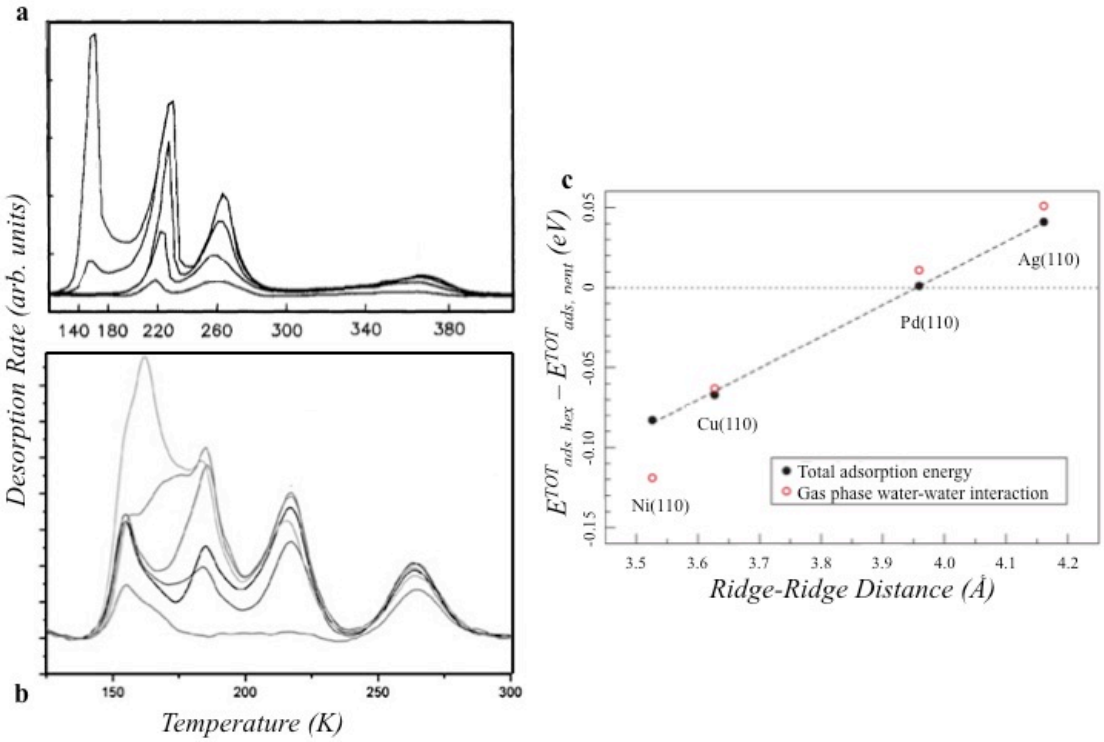

Figure 1. a) TPD of water/Ni(110), b) TPD of water/Cu(110) and c) adsorption energy difference between hexagonal- and pentagonal- based 1D chains as a function of metal substrate, where negative values represent a preference for pentagonal chains.
Adapted from a) B.W. Callen *et al.*, *Journal of Chemical Physics*, 1992, **97**, 3760-3774, b) M. Forster *et al.*, *Chemical Science*, 2012, **3**, 93, c) J. Carrasco *et al.*, *Nature Materials*, 2009, **8**, 427-431.

TPD data for water/Ni(110) is extremely similar to that of water/Cu(110)[17], as seen in Figures 1a-b, with both surfaces exhibiting four characteristic desorption peaks. These TPD peaks are shifted to a higher temperature on Ni(110) than Cu(110), which

indicates a stronger binding to the Ni surface. With both TPD plots having a similar shape, this does however raise the question as to whether the water structures found on Cu(110) also form on Ni(110), or whether stronger bonding to the Ni(110) substrate influences the structures formed.

Carrasco *et al*. showed that water does adsorb intact on Cu(110) at low temperature to form 1D chains of pentagonal rings[18]. These chains are found to lie along the [001] direction of the surface, perpendicular to the close-packed Cu rows. After DFT analysis of the atomic and electronic structures of several overlayers, it is believed that this pentagonal arrangement maximises the proportion of water molecules interacting with the substrate, whilst maintaining a relatively strong hydrogen-bonded system with minimal strain[18].

When assessing the possibility of water pentamers forming on other open-faced metal surfaces, DFT calculations indicate a strong correlation between the metal lattice parameter and relative stability of water hexamers versus pentamers[18]. This is displayed in Figure 1c, with calculations concluding that surfaces with a larger lattice constant, such as Ag(110), have a preference to form structures built from water hexamers. Equally, those with smaller lattice parameters like Cu(110) and Ni(110), are expected to favour the smaller pentagonal water units. As Ni has a lattice parameter which is 2.6 % smaller than Cu, this model suggests that Ni(110) may have an even larger preference than Cu(110) to form these smaller pentagonal building blocks.

Though this prediction seems reasonable, it does not fully consider the enhanced reactivity of Ni with respect to Cu, or the stability of other types of 1D chains. There is no clear evidence in the literature to demonstrate whether water does actually adsorb intact on Ni(110) or whether it dissociates immediately upon adsorption, leaving it unclear whether 1D pentamer chains of intact water could ever form on this surface or if any of the structural phases mimic those seen on Cu(110).

4.2. Experimental

4.2.1. Surface Preparation

The Ni(110) surface was polished to within 0.25 ° of the (110) face and initially cleaned by cycles of Ar^+ ion sputtering at 0.6 keV and annealing to approximately 950 K. The surface quality was firstly determined by LEED to give a sharp diffraction pattern, followed by STM to show large, clean terraces before beginning water adsorption experiments.

The adsorption of water on the Ni(110) surface was studied using a CreaTec low-temperature STM. The UHV chamber was equipped with a separate preparation chamber, as shown in Chapter 2, with both chambers exhibiting a base pressure of $4x10^{-11}$ mbar. Water films were grown using a molecular beam directed through the STM housing aperture towards the crystal face. The water exposure was quantified by STM, with one layer defined as covering the complete Ni(110) surface. The surface was annealed within the STM housing at various temperatures to order, dissociate or desorb the water structure. All experiments were performed in constant-current mode, with the exact temperature and tunnelling conditions stated in the figure caption.

4.2.2. Theoretical Calculations

DFT calculations have been carried out with Vienna Ab initio Simulation Package (VASP)[19-21] using the optB86b-vdW functional[22]. This exchange-correlation functional is a revised version of the van der Waals density functional of Dion *et al.*[23], which demonstrates a good agreement with experimental data for water adsorption on metal surfaces. Water adsorption was modelled with a (2x2) supercell in a 6-layer slab, fixing the bottom 3 layers using a (11x15x1) k-point mesh. Valence core electron interactions were included using the projector augmented wave method[24], with a plane wave cut off energy of 400 eV and dipole corrections perpendicular to the surface. STM images were simulated using the Tersoff-Hamann approximation implemented by Lorente and Persson[25]. The calculations described in this chapter are preliminary, and do not yet include spin polarisation. This is expected to have a relatively small effect on closed shell species like water, and initial tests suggest binding energies change marginally (~40 meV/water). More importantly, it is possible spin polarisation may slightly change the relative energy of different structures. Although calculations are continuing on both the intact and partially

dissociated structures observed by STM, with the aim to understand the differences between the structures formed on Ni(110) and Cu(110) in more detail, they are included here to aid discussion of the water structures.

4.3. Results and Discussion

4.3.1. Surface Wetting at Low Temperature (77 K)

4.3.1.1. Overview of Structures

To fully characterise the structure of water on Ni(110) at low temperature, a range of surface coverages were prepared between approximately 0.2 and 1.3 ML. Before discussing the STM images and structures observed in some detail, it is useful to briefly summarise our observations to indicate the overall behaviour observed. Adsorption at 77 K sees the formation of 2D islands extending along the $[1\,\bar{1}\,0]$ direction, following the close-packed Ni rows (Figures 2-3). This structure is very different to that which forms on Cu(110) at 77 K, with no evidence to suggest the formation of 1D pentagonal water chains. These islands continue to extend along the $[1\,\bar{1}\,0]$ direction of the surface as the coverage is increased, completing the first wetting layer, with additional adsorption forming second layer chains (Figure 4). Forming spontaneously at low temperature, there is no requirement for surface annealing above 77 K to order this 2D water structure.

Increasing the water coverage allows the 2D wetting layer to be imaged with higher resolution, revealing a structure which exhibits noticeably different ring sizes (Figures 4b-d). The majority of the overlayer appears to be built from 'zigzag' chains along the $[1\,\bar{1}\,0]$ direction, forming a network that contains a few additional dark voids as a minority structure. These large voids have flat edges that are aligned along the $[1\,\bar{1}\,0]$ direction, contrasting with the majority structure of the extended 2D islands. Although most of the large voids disappear slowly over time from the small water islands formed at low coverage, they remain stable within the large water terraces, and persist even as second layer chains grow above the first wetting layer. Based on the stability of different structures from DFT, and the presence of different water arrangements in STM, the structures are interpreted to be a result of flat 1D water chains bonded along alternate Ni rows.

4.3.1.2. Structural Analysis

4.3.1.2.1. Low Coverage Structure

Initially when water adsorbs on Ni(110) at 77 K, small 2D islands are formed, as seen in Figure 2a. The islands are elongated along the close-packed direction of the surface, being typically 300 Å long but only 50-120 Å wide. Analysis of the structure displayed in Figure 2b, reveals the islands are built from zigzag rows aligned along the $[1\,\bar{1}0]$ direction. There are darker ring features also present between the chains forming elongated rings. The edges of the islands appear blurred with the water molecules here being less tightly bound to the surface, and as a result, they are able to move and interact with the tip. Increasing the water coverage therefore gives better resolution of the structure, with an increased stability of the water network as the islands grow.

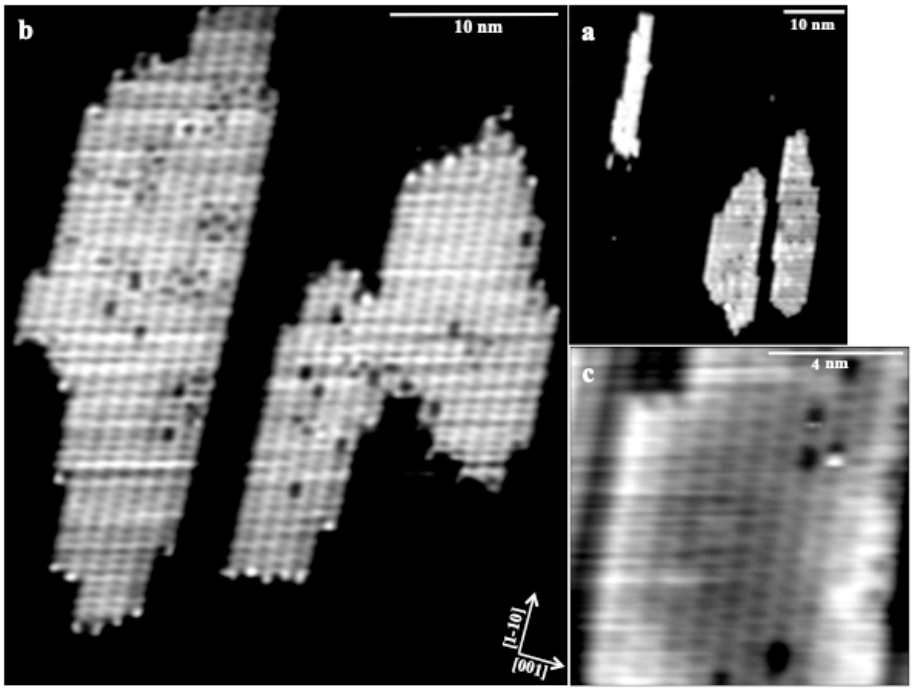

Figure 2. 'Zigzag' structure of 2D water islands grown at 77 K, with c) showing a close-up view of the island structure. a) (-101 mV, 142 pA), b) (-35 mV, 123 pA), c) (-76 mV, 248 pA).

The structure of these 2D water islands changes slightly over time, as displayed in Figure 3. When the surface is initially imaged after the adsorption of water at 77 K, the structure consists of both extended zigzag chains and dark, large ring features. However, over approximately 20 minutes, these features disappear. This produces a structure built almost exclusively from zigzag chains, becoming the majority structure

over this short time period. This effect is not induced by tip interaction as the majority of these dark, large ring features are only present during the first 40 minutes following water adsorption at 77 K, irrespective of whether the island has been imaged or not. As discussed earlier, the resulting 2D islands form spontaneously on Ni(110) with no need for surface annealing to order the water structure, so we assign this behaviour to a kinetic effect. Figure 3a shows the kinetic structure formed initially by growth at 77 K and Figure 3b the final thermodynamic structure which is dominated by these zigzag chain structure. Some large rings still remain locked into the structure even after a long period of time and are discussed in more detail later in the chapter.

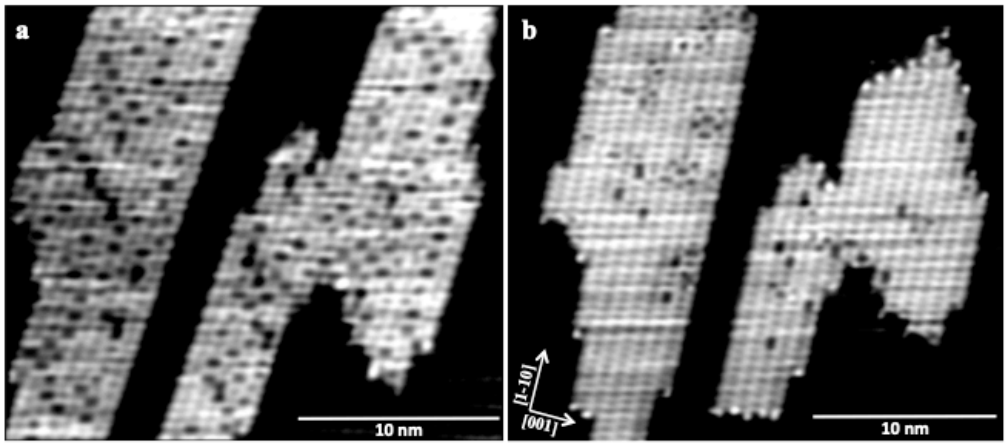

Figure 3. STM images of a 2D water island, imaged a) 30 minutes (-107 mV, 123 pA) and b) 50 minutes (-35 mV, 123 pA) after adsorption of water at 77 K. The second image shows a reduced number of large voids in the structure, compared to the first.

4.3.1.2.2. High Coverage Structure

Figure 4 displays a complete first wetting layer on Ni(110), with additional water forming second layer chains. Structural analysis of the first layer reveals the same 'zigzag' structure seen for the 2D islands at low coverage. The images also show the presence of the same dark large rings, which were previously assigned to the kinetic structure seen in the initial imaging of the 2D islands at low coverage (Figure 3a). At this higher water coverage, however, these features are stable with time, unlike at low coverage where they are seen to disappear (see Figure 3). This difference seems to be associated with the completion of the first wetting layer, which appears to make it more difficult for water to rearrange to form the more thermodynamically stable zigzag chains. Figure 4 also shows second layer water which images as bright chains in STM; these are discussed further in Section 4.3.1.7.

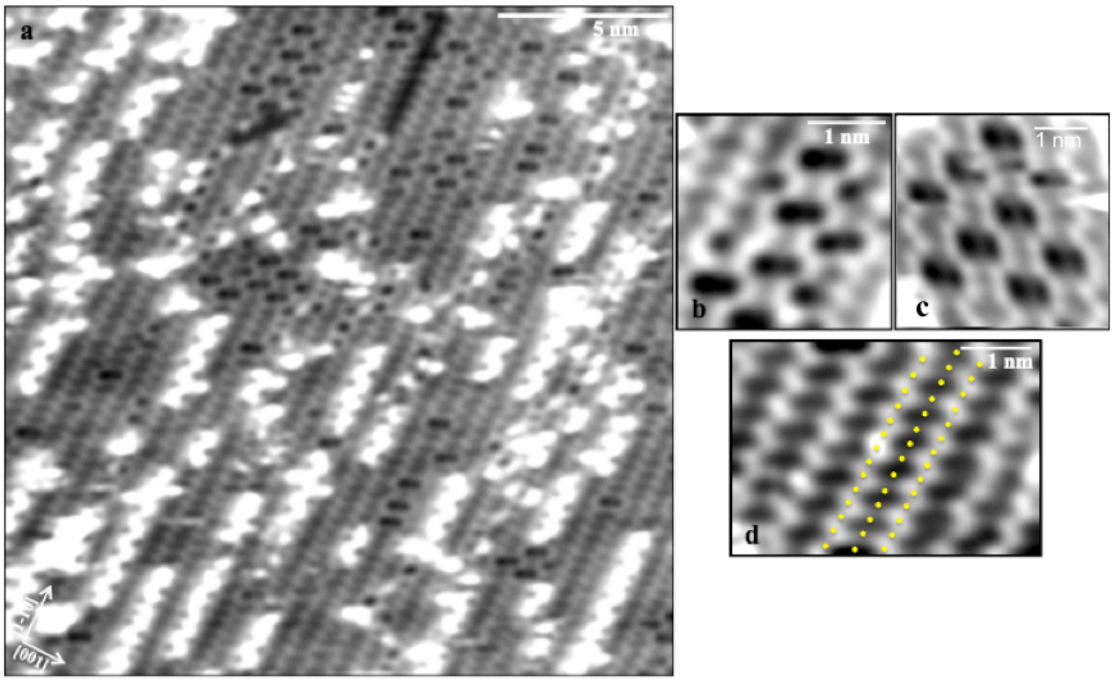

Figure 4. a) STM images showing a complete first layer and partial second layer during the surface wetting of Ni(110) at 77 K, b/d) close-up structure of the first wetting layer with the close-packed Ni arrangement indicated in d) as a series of dots, c) shows a different region where the large rings are aligned perpendicular to the Ni rows (77 K, -380 mV, 242 pA).

4.3.1.3. Structural Models for Intact Surface Wetting

Whereas Cu(110) forms chains of face sharing pentamers, the Ni(110) surface forms a 2D zigzag network, shown in Figures 2c and 4d. A structure built exclusively from face-sharing pentagonal rings can be disregarded because pentamer units cannot tessellate a 2D surface. There is also no evidence to support the presence of pentagonal rings in smaller clusters, or at the edges of islands, again reinforcing the unlikelihood of a pentagonal structure. Although the assembly of face-sharing water pentamers separated by octamer units would tessellate a 2D network, this can also be ruled out from the STM images. The octamer and pentamer units seen in the defect lines observed on Ru(0001)[26] and the (3 1, $\overline{3}$ 1) wetting layer structure on Cu(511)[27], image with the 8-membered rings being much larger in size than the smaller water pentamers, inconsistent with the zigzag structure reported here.

Measurements of the zigzag chains in Figure 4d reveal they are equally spaced by approximately 7 Å, along the [001] direction. However, one cannot discern from STM alone whether the zigzag chains are sited atop the Ni rows. With the [001] spacing of the Ni(110) lattice being 3.5 Å, this is roughly half that of the measured repeat of the

zigzag chains, confirming that the bright zigzag chains are arranged in registry with alternate close-packed Ni rows. Further analysis of the zigzag chains reveals the edges of the elongated rings, which point towards the [001] direction, are not aligned along the [001] direction and are actually offset from each other by one unit along the [1 $\bar{1}$ 0] close-packed direction. Although each ring has a repeating unit of approximately 5 Å along the [1 $\bar{1}$ 0] direction, consistent with that of a single water hexamer, the rings are too large in width to be single hexagonal units. With a measured width of approximately 7.5 Å along [001], this size suggests a face sharing, two-ring hexagonal unit, as shown in Figure 5a, where the central water chain bridging the two adjacent rings images with a low contrast in STM. This suggestion also explains why the edges of the elongated rings do not align along [001] but are offset from each other by one unit along the [1 $\bar{1}$ 0] close-packed direction. For this structure to be consistent with the experimental images would imply alternate water chains image bright and dark in STM. One suggestion to account for this difference between the chains is that these water molecules are bonded tightly to Ni in a flat orientation, creating a flat chain of water along the centre of the two rings. The surrounding water molecules are less tightly bound to the Ni(110) surface, most likely in a H-down orientation, and therefore appear as bright chains along the [1 $\bar{1}$ 0] direction, completing the hydrogen-bonding network.

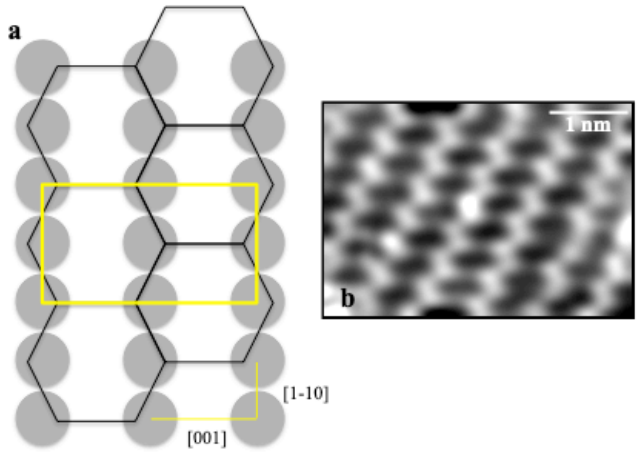

Figure 5. a) Schematic figure to show a water network consisting of zigzag chains along [1 $\bar{1}$ 0], bridging two hexagonal water rings, where the (2x2) unit cell is highlighted in yellow and b) STM image reveals these zigzag chains to have alternating bright and dark contrast (77 K, -380 mV, 242 pA).

This discussion suggests the best model for the 2D zigzag chain structure is likely to be a (2x2) two-ring structure of intact water molecules, directly analogous to the hexagonal networks originally proposed for wetting of these surfaces. This arrangement is built from two 6-membered water rings with the central zigzag chain containing solely flat water molecules. As this seems the most feasible, conventional water structure, this zigzag (2x2) model was explored by theoretical DFT calculations to determine the stability of this structure on Ni(110).

4.3.1.4. Theoretical Calculations

Theoretical calculations to understand the intact water structure are still on going and the results discussed here represent a snapshot of what has been learnt at the time of writing. Initial DFT calculations and STM simulations have investigated the stability of a zigzag hexagonal (2x2) water arrangement and if it is indeed the most favourable intact structure that can form on Ni(110).

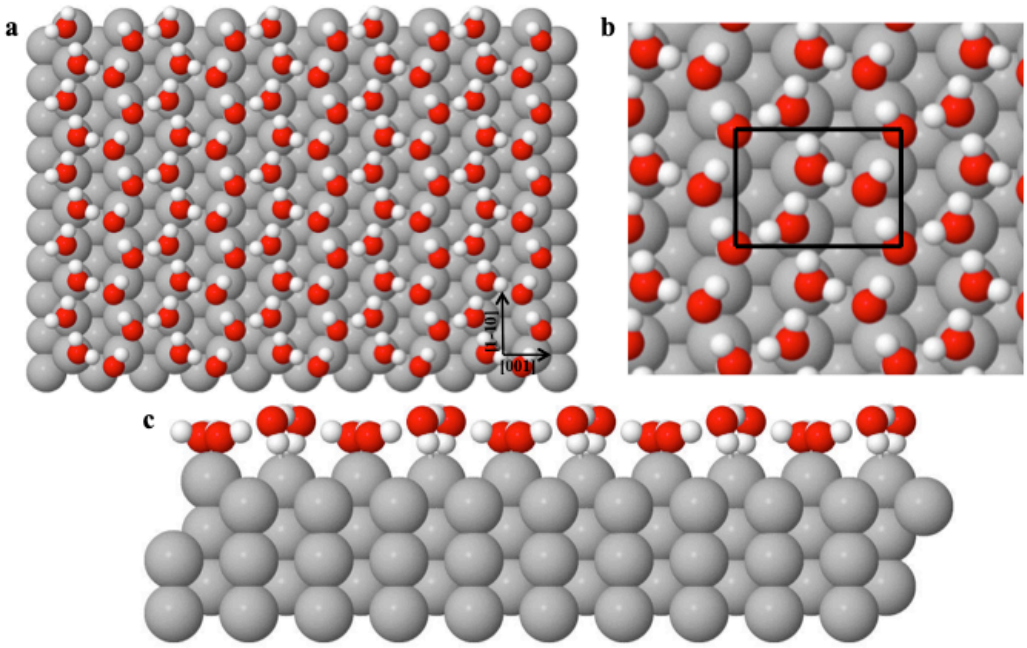

Figure 6. DFT structure calculations for a complete 2D hexagonal water network showing the favourable H-down model, a) top view, b) highlighted (2x2) unit cell, c) side view.

Assuming the zigzag structure is constructed from chains of water lying flat, close to the surface, binding tightly to Ni, the remaining water molecules which complete the hydrogen-bonding network can be arranged with their uncoordinated hydrogen atom oriented H-down towards the Ni surface or pointing H-up into vacuum. For this two-

ring zigzag structure, DFT calculations give a H-down and H-up binding energy of -0.836 eV/molecule and -0.684 eV/molecule, respectively. This confirms a large preference for H-down binding and produces an overlayer with a buckled arrangement of water molecules. This buckling is displayed clearly in Figure 6c, where the O-Ni bond length is measured at 2.06 Å in the flat arrangement, compared to 3.04 Å for the H-down water. Water binds very close to the Ni atoms, sitting nearly 0.2 Å closer to the metal than calculated for the intact water structures on Cu[27,28], reflecting a much stronger Ni-water bond.

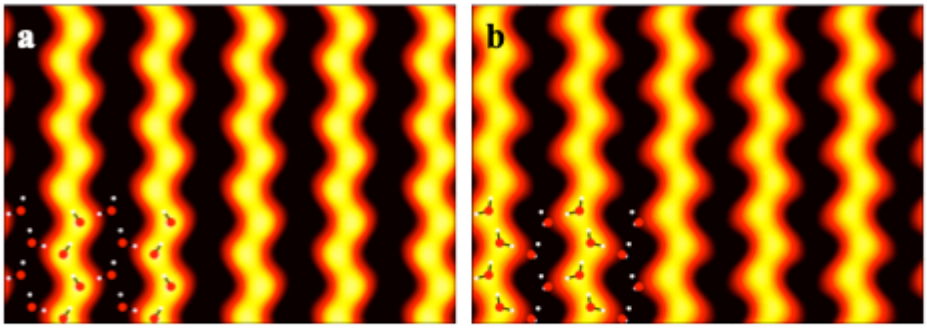

Figure 7. STM simulations of the model hexagonal (2x2) structure proposed for an intact first wetting layer on Ni(110), where filled states (a) image H-down water molecules as bright rows, whilst empty states (b) image the flat water rows.

In order to test this structure against the experimental STM images, simulations were performed using the Tersoff-Hamann approximation[25] to simulate how this structure would image in STM. The resulting simulations, reported in Figure 7, display alternate bright and dark chains along the close-packed [1 $\bar{1}$ 0] Ni direction. These chains exhibit a zigzag structure, and support the idea that a zigzag backbone of flat water molecules can sit between bright chains of H-down water and will image with low contrast, being effectively invisible under some scan conditions. However, the experimental STM images never showed any sign of the intermediate water chain, irrespective of bias voltage or tip changes, etc. Also, assigning the 2D zigzag islands (Figure 3b) to H-down water chains in a hexagonal water network leaves it unclear how to assign the voids formed initially (Figures 3a and 4b/c), since we can devise no equivalent flat (invisible) water structure that would create this pattern of H-down water to complete the structure.

The DFT calculations provide a further clue that the 2D zigzag islands may not be a conventional hexagonal water network. Calculations find 1D pentagonal chains, similar to those formed on Cu(110), are 40 meV/water more stable than the (2x2) structure on Ni(110). This is a relatively large energy difference by the standards of water-DFT studies, and one would normally consider a difference of this magnitude to be significant. These DFT functionals were successfully used to predict water structures on Cu[27,28] and produce a Ni lattice spacing (2.47 Å) that is very close to experiment (2.49 Å), so there is no obvious reason for this discrepancy between calculation and experiment. No evidence was however found for 1D [001] pentagonal chains in the STM images, even after annealing the water structures.

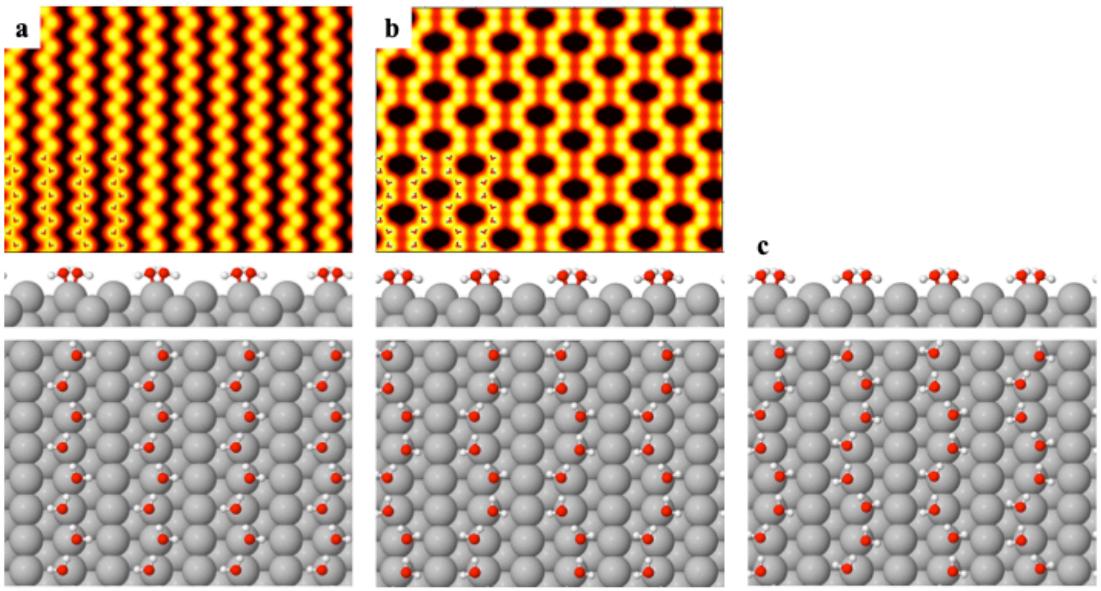

Figure 8. Calculated structures and STM simulations (filled state images) of intact water chains, showing three possible arrangements of water chains along alternate Ni rows, a) (2x2) unit cell, b) (4x4) unit cell and c) (4x8) unit cell.

In view of this discrepancy, calculations are continuing, but preliminary results offer a new explanation for the observed structure. If the water-Ni bond is sufficiently strong, it may be favourable to sacrifice hydrogen-bonding coordination number to optimise water-Ni bonding in the flat water chains. Calculations for the same chain of flat water but with no H-down water competing the network (Figure 8a), find that a flat chain is more stable than the complete 2D water network and is also just 10 meV/water less stable than the pentagonal chains. Water forms a zigzag chain that optimises the O-O separation while allowing water to bind close to the atop site of Ni.

Compared to the complete hydrogen-bonding network, the O atoms are offset slightly further from the chain axis and the uncoordinated hydrogen atoms point down towards the neighbouring Ni row, helping to screen and stabilise the OH dipole. This arrangement is similar to that adopted by water in the backbone of linear 1OH:1H_2O chains formed on Cu(110)[17].

4.3.1.5. Minority Structure Formed at Low Temperature

Models based on a 1D, not 2D, hydrogen-bonded structure, may also explain the dark voids seen in the STM images of Figures 4b/c for a short time. When compared directly to the spacing of the zigzag chains, the voids have a noticeably different structure and evidently a different arrangement of water molecules. Unlike the zigzag chains, these large rings have a flat edge along the $[1\,\bar{1}\,0]$ direction, which suggests they contain at least two additional water molecules possibly forming octamer 8-membered rings rather than water hexamers. However, it was not possible to find any arrangement of flat water molecules that would be (even partially) completed by a H-down water network of this form. In fact, no satisfactory interpretation could be found for the voids based on formation of a 2D hydrogen-bonded network, although several models were considered. Modelling the void structure as a series of unconnected 1D chains, however, does provide an immediate interpretation. There are two ways to form an intact chain along the Ni row, either with a two-unit repeat in the zigzag arrangement shown in Figure 8a, or with a four-unit repeat containing pairs of water on each side of the Ni row as in Figure 8b. This is again mimicking the two types of 1D water chain found for the OH/H_2O structures on Cu(110)[17]. A simulation of the STM image for this second type of chain (Figure 8b) creates features similar to the large dark voids seen initially by STM. This void structure is very slightly less stable (7 meV/water) than the zigzag arrangement, perhaps suggesting why the voids slowly disappear slowly with time without changing the size of the water islands.

STM images (Figures 4b/c) find the void structure may be either symmetric about the close-packed direction, or may have the long axis rotated off [001]. This is particularly the case when a few isolated voids are embedded in the zigzag structure, the axis tending to follow the same offset as the zigzags. The rotated arrangement can be achieved simply by displacing the water chains by one unit along the $[1\,\bar{1}\,0]$ direction, creating the structure shown in Figure 8c. Again, this structure has a similar

binding energy to the related 1D chains and STM simulations are in progress. Overall, local disorder seen in regions of the zigzag structure (Figure 4a) can invariably be explained by including short sections of the four-unit water chain into the zigzag network. There is no STM simulation reported for the structural arrangement in Figure 8c as this exhibits a (4x8) unit cell, which reaches the computational limitations of DFT. It is however included in this discussion as the arrangement of water chains gives the correct stacked oblique arrangement of water molecules to match the structure observed in the STM images.

4.3.1.6. Comparison to Other Structures

The evidence available indicates the intact 2D water islands found at 77 K are 2D assemblies of 1D water chains. Water forms hydrogen-bonded chains along alternate Ni rows, with the lateral assembly of the chains reliant on dispersion or through surface interactions. Preliminary calculations indicate only a very weak dependence of binding energy on chain separation, much weaker than the strong, long-range repulsion seen between pentamer chains on Cu(110)[17]. This is possibly a result of the unoccupied close-packed Ni rows screening the OH dipoles on neighbouring chains. We are not aware of any other system that adopts such a simple 1D chain structure in preference to forming high coordination structures. We tentatively attribute this behaviour to the strong water-Ni interaction, which favours flat water, and the short Ni lattice parameter which makes it difficult to complete a hydrogen-bonded network without buckling the water structure, reducing the ability of the flat water to bond to Ni.

Despite the increased binding energy of the 1D water chains over the 2D hydrogen-bonding network, the pentamer chain arrangement remains slightly more stable in this DFT calculation. While it is possible the 1D water chains form only because they are kinetically more accessible, we regard this as unlikely. We did not find a single pentamer ring or any fragment of chain aligned along [001], despite depositing and annealing water under many different conditions. This is not the first system where DFT calculations do not agree with the most stable structure found experimentally. A discrepancy between experimental and theoretical work has also been observed for structural calculations of water on a surface of Ru(0001)[29]. Haq *et al*. report an intact water layer from LEED, TPD and RAIRS experiments, exhibiting an ordered

(√3x√3)R30° structure for the adsorption of up to 0.67 ML at 140-160 K. The structure proposed from experimental work suggests disordered short chains of flat and H-down water molecules embedded within a honeycomb hydrogen-bonded network. This structure exhibits long-range order but allows for local disorder within the overlayer. Conversely, DFT predicts this intact structure should not have sufficient stability to wet the Ru(0001) surface, although experimental results prove otherwise, revealing the limitations of DFT when comparing very different structures (ie, 3D bulk ice versus water on a metal surface).

At 77 K, an increase in the water coverage on Cu(110) sees the spacing between the 1D pentamer chains reduce until they become less favourable, with water forming islands of a 2D structure. This resulting 2D overlayer has a (7x8) unit cell built from intact water molecules. STM images show a complex structure with rings of different shapes and sizes, but these prove difficult to analyse as a result of the large unit cell size and weak ordering. A definitive structure has therefore not been confirmed for this hydrogen-bonded overlayer, however it is clear that intact water on Cu(110) does not adopt the (2x2) ordering we find on Ni(110)

Although water remains intact on Cu(110) up to the monolayer desorption temperature of around 140 K, annealing above this temperature forms a partially dissociated c(2x2) structure. This water/OH overlayer shows little similarity to the intact (2x2) structure found here on Ni(110). Grown at 180 K on Cu(110)[30], water molecules partially dissociate to form distorted hexagonal rings with the same general alignment as for the zigzag chains on Ni(110). However, the 2:1 water/OH structure is flat with all oxygen atoms nearly coplanar, containing Bjerrum defects between OH groups to complete the hydrogen-bonding network. The network images as a distorted hexagonal network, with all the O sites visible, quite different from the intact (2x2) structure found on Ni(110), which is highly corrugated and does not show complete hexagonal rings.

4.3.1.7. Second Layer Adsorption

Following the completion of the 2D first wetting layer, water forms additional bright chains at a coverage above 1 ML, as seen in Figures 4a and 9. This second layer structure appears to be built from 1D chains of water molecules, adsorbed in the first

layer troughs, with the first wetting layer appearing unchanged following the adsorption of these second layer molecules (Figure 9). The growth of linear second layer structures reflects the highly corrugated, flat/H-down chain structure of the first water layer. The bright added row chains image with a contrast of roughly 0.8 (± 0.1) Å above the first wetting layer. This corrugation is similar to the 0.73 Å difference in O height between the flat water chains and H-down water seen in Figure 6. It seems likely that these water chains reflect decoration of the bare Ni rows found in the 1D chain structures shown in Figure 8, something that will be examined in future calculations.

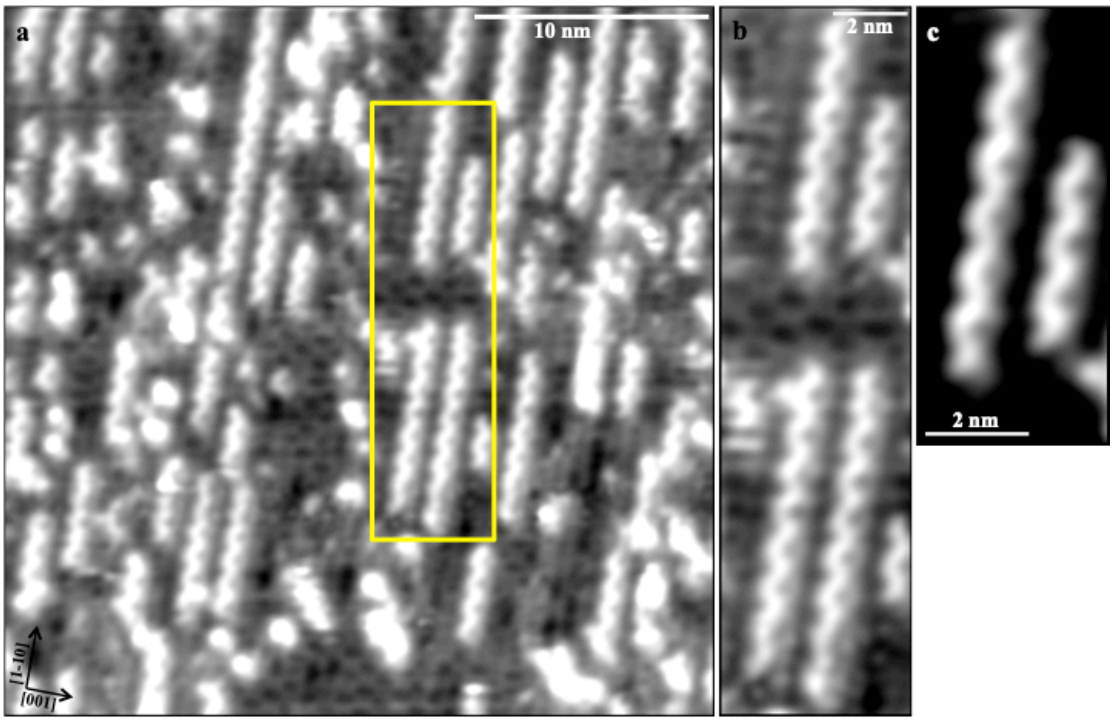

Figure 9. a) Complete first layer wetting of Ni(110) with some additional growth of second layer chains, b-c) close-up images of these second layer water chains showing structure and registry with first wetting layer, where b) shows the yellow highlighted region in a) (77 K, -138 mV, 192 pA).

The second layer growth mechanism is very different to that observed for the wetting of stepped Cu(511)[28], which also has a highly corrugated, anisotropic structure. The continuous 2D first wetting layer formed on Cu(511) adopts a structure built from hexagonal rings, interlinked by face-sharing pentamer-octamer rows. In order to facilitate further ice growth, however, this first layer must completely restructure to form a buckled hexagonal network. Water is then able to form a continuous second layer that grows into a commensurate ice multilayer. The first wetting layer formed

on Ni(110), on the other hand, has a much lower water density and would require considerable hydrogen-bond realignment to create a 3D structure. The STM images suggest that water does not immediately restructure the first layer but instead forms linear second layer chains that bind between the first layer water chains. However, since water dissociates on Ni(110) when the film is annealed, it is not possible to determine whether this structure is thermodynamically the most stable, intact high density structure.

4.3.1.8. Conclusions to Surface Wetting at Low Temperature

The data reported in this section shows the structure of water adsorbed on Ni(110) at 77 K. 2D water islands initially form and extend along the [1 $\bar{1}$ 0] direction as the first wetting layer completes. Experiments reveal a (2x2) 'zigzag' structure is formed, with voids in the structure annealing out for small water islands but not in extended 2D structures. While this (2x2) structure might be explained as a hexagonal water network built from alternating flat and H-down water chains, DFT suggests a different interpretation. The zigzag rows and different void structures formed can all be explained as assemblies of flat 1D water chains. This structure differs to that observed on Cu(110), or any other metal surface studied, but is similar to the water backbone found in 1D OH/H_2O chains on Cu(110)[17]. It is evident that the 1D chains of pentagonal water rings predicted by DFT[18] are not formed on Ni(110), although Ni has a smaller lattice parameter than Cu and this structure is predicted to be more favourable.

4.3.2. Surface Wetting at High Temperature (200-220 K)

4.3.2.1. Overview of Structures Observed

Annealing the surface results in the partial dissociation of water and in turn, a change in water structure. The resulting overlayer consists of 1D chains with a branched appearance, where the chain backbone is aligned along the [1 $\bar{1}$ 0] close-packed direction of Ni(110). There appears to be two types of this 1D chain structure coexisting on the surface, where the branches have a slightly different alignment. When annealed at 200 K, an additional structure is also observed in the STM images. These regions appear to have a distorted hexagonal 2D structure, with some periodic disruption in the overlayer along the [1 $\bar{1}$ 0] direction of the surface, thought to be a result of compressive strain. Surface annealing to a slightly higher temperature of 220

K sees this 2D hexagonal structure disappear to leave only the 1D branched chains. This higher anneal temperature also introduces additional bright chains in the STM images, which are later assigned to metallic Ni wires. These are a consequence of Ni atoms being removed from the terrace resulting from the dissociation of water, with increasing anneal temperature, to form wires along the close-packed Ni direction.

4.3.2.2. 2D Hexagonal Structure

Figure 10a shows an STM image after annealing the Ni(110) surface to 200 K for a water coverage close to saturation of the first layer. The insert of this image reveals domains of a 2D hexagonal structure and coexisting 1D chain structures, where the 2D phase is seen to disappear after annealing to 220 K. As the surface temperature is raised, water more readily dissociates into hydroxide, creating structures with a lower ratio of water to hydroxide. The 2D structure is seen to disappear steadily, leaving exclusively 1D branched chains that are identical to the $1H_2O$:1OH chains found on Cu(110) after surface annealing to remove excess water[17]. The 2D structure observed in the insert of Figure 10a is therefore assigned to a 2D hexagonal ($2H_2O$:1OH) phase that is analogous to the c(2x2) ($2H_2O$:1OH) structure reported by Forster *et al*. during the adsorption of water on Cu(110) at 180 K[30]. Both structures exhibit a 2D arrangement of flat, slightly distorted hexagonal rings growing along the close-packed direction of the metal surface. This suggests the partially dissociated hexagonal overlayer on Ni(110) also has an approximate 2:1 water/OH ratio. Further heating of this hexagonal structure desorbs and dissociates more water, leaving exclusively 1D branched chains of the 1:1 mixed structure.

4.3.2.3. 1D Branched Chains

The 1D chains observed in Figure 10a are aligned along the $[1\,\bar{1}\,0]$ direction of close-packed Ni. They possess a branched arrangement of molecules, with two slightly different structures, and are assigned to the partially dissociated, mixed water/hydroxide structures analogous to those reported by Forster *et al*. on Cu(110)[17]. These chains are built from a mixture of water and hydroxide in a 1:1 ratio and exhibit either a Pinched (P) or Zigzag (Z) arrangement. Although both the Z and P structures have the same binding energy on Cu(110), the Z arrangement appears to dominate the water/hydroxide overlayer in this Ni(110) system.

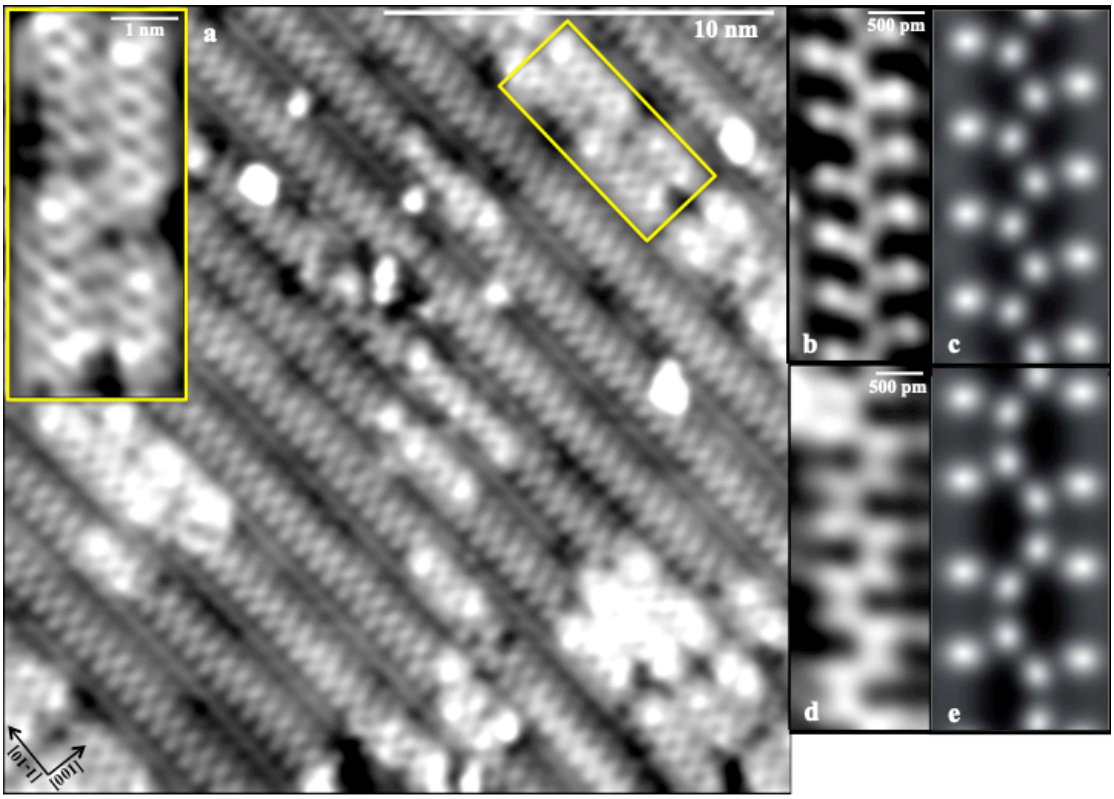

Figure 10. a) Partially dissociated water structure which forms on Ni(110) after annealing to 200 K, showing coexisting 1D branched chains structures and a 2D hexagonal structure (insert) (77 K, -59 mV, 208 pA), b) experimental STM image of the Z arrangement on Ni(110) (77 K, -41 mV, 181 pA), c) STM simulation of the Z arrangement on Cu(110), d) experimental STM image of the P arrangement on Ni(110) (77 K, -87 mV, 192 pA), e) STM simulation of the P arrangement on Cu(110).
c/e) Adapted from M. Forster *et al.*, *Chemical Science*, 2012, **3**, 93.

Both the Z and P structures have a backbone built from an intact water chain that lies along the [1 $\bar{1}$ 0] close-packed Ni row. The branches attached to this backbone, however, differ between the P and Z arrangements. With the Z chain, the branches are aligned to either all point up or all point down along the close-packed Ni row. The hydroxide molecule at the end of this branch is then bound to Ni at the bridge site. In contrast to this, the branches of the P chain do not point in the same direction. They are found to alternate either pointing up or pointing down to produce an alternating, irregular branched structure with two different spacings.

Figure 10b displays a high resolution STM image of a Z chain where the individual water/OH molecules are visible. It has a regular structure where the branches are directional with a spacing of approximately 5.05 Å, equivalent to two Ni lattice constants in the [1 $\bar{1}$ 0] direction. The image shows the branches are slightly skewed

along the chain, and are therefore not perfectly aligned along the [001] direction. A high resolution STM image of the P chain, on the other hand, is displayed in Figure 10d. This confirms an irregular structure where the branches are pointing alternatively up and down the chain with a spacing of approximately 10 Å, four times the Ni lattice spacing in the [1 $\bar{1}$ 0] direction.

The two different structures have the OH molecules adsorbed each side of a water chain, at the same Ni bridge site, but the water molecules that form the backbone of these branched chains sit in a slightly different arrangement above Ni, making the Z and P chains slightly different. With the Z chain, the water molecules forming the chain backbone sit close to atop Ni, alternating towards the left and right of the surface Ni atoms in a regular zigzag arrangement. The P chain, on the other hand, has these water molecules arranged with two sited towards the left and then two sited towards the right of the atop Ni site, regularly alternating every two water molecules rather than every one. Both structures are in good agreement with the water/Cu(110) data reported by Forster *et al*.[17], including their STM images and the theoretical structures calculated from DFT and STM simulations (Figures 10c/e).

The high-resolution STM image in Figure 10a also shows that the 1D branched chains occasionally switch between two different close-packed Ni rows. As Ni has a small lattice parameter, it is thought that the water backbone occasionally bonds across adjacent rows of Ni to accommodate the hydrogen-bonding network and relieve compressive strain along the chain. This is not restricted to a specific chain structure and is seen for both the Z and P branched arrangements. Such a shift in close-packed rows was not reported to occur on Cu(110), but Ni has a lattice constant 2.6 % smaller than Cu, causing a greater lateral buckling of water along the chain and allowing this new strain relief mechanism.

4.3.2.4. Ni Wires

Annealing the surface to temperatures above 210 K results in the appearance of bright, featureless rows, displayed in Figure 11. These appear to coexist with the 1D branched water/OH chains, also aligned along the [1 $\bar{1}$ 0] direction of close-packed Ni. Analysis of this structure reveals that these rows are approximately 3 Å high, which is roughly double the height of the branched chains and therefore cannot be assigned to

first layer water. Second layer water can also be ruled out because the anneal temperature is too high for multilayer wetting, hence any second layer water molecules would have desorbed before reaching 210 K. Experimental analysis reveals that as more water is driven off the surface, more of these bright rows form. They are therefore a consequence of water desorption and/or dissociation.

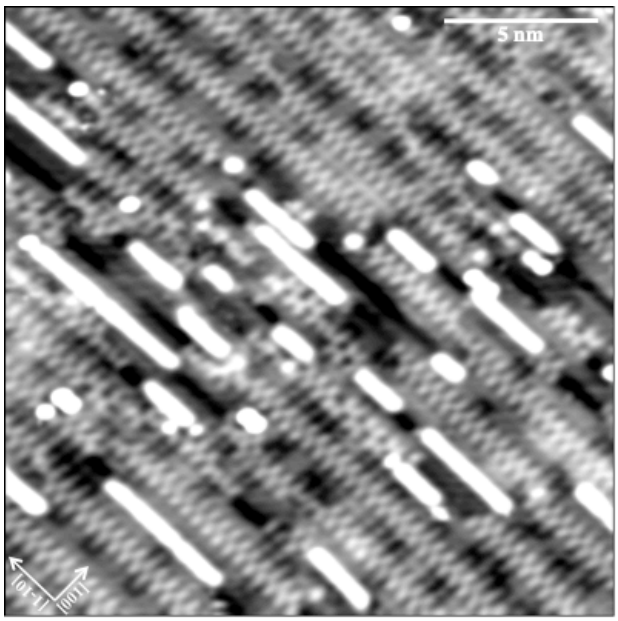

Figure 11. Formation of Ni wires after annealing to 210 K (77 K, -69 mV, 215 pA).

Similar bright rows have also been observed during the dissociation and desorption of water on Cu(110)[33]. Pang *et al*. assign these bright rows to Cu metal wires formed by the dissociation and desorption of water at 200 K. Although similar in appearance, there are some differences between the formation of these chains on Cu(110) and Ni(110). Firstly, the majority of the 1D branched water/OH chains have disappeared on Cu(110) after annealing to 200 K. This differs from Ni(110) were these 1D partially dissociated water chains are still present after annealing to 220 K. This indicates a stronger bonding between the 1D branched chains and the Ni(110) surface compared to Cu(110). Another observation by Pang *et al*. is that the Cu wires are stabilised by 1D P branched chains, which are found to grow along each side of the Cu wires. This is not true on Ni(110), however, where the metal wires are seen to grow without stabilisation from the 1D branched water chains. Heating above 220 K on Cu(110) sees the disappearance of both the bright Cu wires and 1D branched water chains as water dissociates and desorbs from the surface. Pang *et al*. report the

formation of Cu-O rows along the [001] direction of the surface, resulting from water/OH dissociation. Ni(110), on the other hand, has both the Ni wires and 1D water/OH chains still present on the surface after annealing to 220 K, and evidence of Ni-O row formation is not seen until a much higher anneal temperature. These discrepancies again demonstrate that the increased reactivity of Ni compared to Cu has an effect on the stability of the OH/H_2O structures that grow on this metal surface.

4.3.3. Further Annealing above 300 K

4.3.3.1. Overview of Structures

A TPD study by Guo *et al*. investigating water/Ni(110) reveals the evolution of hydrogen with increasing temperature[34]. Although the peak maxima is observed at approximately 340 K, the onset of hydrogen formation appears from around 270 K, as seen in Figure 12c. It is therefore evident that hydrogen is produced with the dissociation of water. Here, we find annealing the surface to approximately 340 K results in the complete dissociation of water from the Ni(110) surface. Figure 12a shows a STM image of the resulting species present on the surface after the dissociation of this water layer. As water fully dissociates to form oxygen and hydrogen, annealing to 340 K will see desorption of hydrogen from the surface, but this temperature is too low to desorb the remaining oxygen atoms. Evidence to support this comes from the short dark rows aligned along the [001] direction, highlighted by the yellow arrows in Figure 12a, which correspond to Ni-O chains.

Figure 12a also displays bright and dark rows elongated along the $[1\,\bar{1}\,0]$ close-packed direction of Ni, a result of water dissociation with increased surface annealing. The bright rows are assigned to rows of Ni metal atoms, forming Ni wires above the surface terrace with a height roughly equivalent to the Ni lattice spacing (2.49 Å). One explanation for the formation of these Ni wires is that Ni atoms are liberated from the Ni-O chains discussed above, with a proposed reaction of $H_2O + NiO \rightarrow Ni + 2OH$, similar to that reported by Pang *et al*. for an analogous reaction on Cu(110)[33]. This provides free Ni atoms which can coalesce on the surface terrace to form these resulting bright rows.

This reaction does not however explain the formation of the dark rows in the STM images, which have a measured depth roughly equivalent to the Ni lattice spacing

(2.49 Å). As these dark rows have the same height below the topmost surface layer as the bright rows do above the topmost surface layer, it is reasonable to suggest that they are a result of Ni removal from the terrace and coalescence above the surface. An explanation for this would be that the bright and dark rows are a product of the water dissociation reaction which results in Ni becoming mobile within the surface layer. These mobile Ni atoms are now free to diffuse across the terrace and coalesce to form the bright rows observed in Figure 12a. In turn, dark vacant rows are produced within the surface layer as a result of the Ni atoms that have been removed from the terrace, also observed in Figure 12a. The bright rows correspond to the same Ni metal wires discussed in Section 4.3.2.4, which are also seen to coexist with the 1D branched water/OH chains at 210 K in Figure 11.

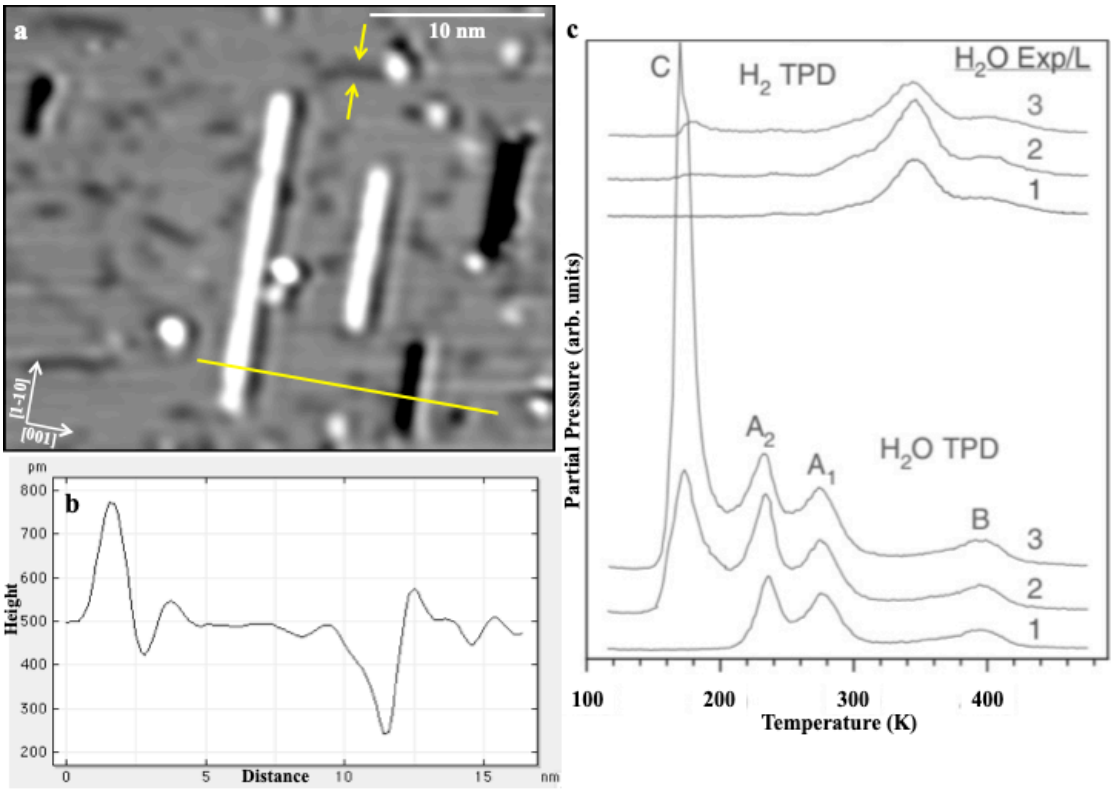

Figure 12. a) STM image of the Ni(110) surface after annealing the water layer to 340 K (77 K, -294 mV, 128 pA), b) a height profile across the yellow cross-section of a) and c) TPD showing hydrogen desorption from the water/Ni(110) surface.

c) Adapted from H. Guo *et al.*, *Catalysis Letters*, 2003, **88**, 95-104.

As discussed above, a similar structure is reported on Cu(110) by Pang *et al*. but at a slightly lower temperature. This is expected as the dissociated phases observed here on Ni(110) are all evident at a higher temperature than that reported on Cu(110)[33],

attributed to a stronger binding of water to the Ni(110) surface. Again, this shows the similarities between the structure of water adsorbed on Ni(110) and Cu(110) at higher temperatures when dissociation is initiated, unlike the very different behaviour which exists at low temperatures for intact water.

4.4. Conclusions

This chapter examines the adsorption of water on an open-faced surface of Ni(110). At 77 K, intact water forms 2D islands with a (2x2) hexagonal structure. These islands extend along the $[1\,\bar{1}\,0]$ direction of close-packed Ni as the wetting layer completes, forming spontaneously at low temperature. Initially, the 2D islands form a kinetic structure with some larger rings presents within the 2D network. However, at least in small islands, these larger ring features disappear over a short period of time to form a structure built almost exclusively from 'zigzag' chains. Theoretical studies suggest that this zigzag arrangement is a result of flat 1D water chains extending along the $[1\,\bar{1}\,0]$ direction of the surface, tightly bound to the Ni surface atoms and loosely assembled into a (2x2) symmetry by long range dispersion or through surface interactions. Further adsorption at 77 K sees the completion of this first wetting layer with additional growth forming second layer chains. The larger ring features that make up the minority structure in small islands do not disappear as the layer completes. These features are formed by flat 1D water chains that have a four times repeat along the close-packed direction, rather than the two times repeat found in the zigzag structure. Second layer growth results in high contrast chains decorating the bare Ni rows, but the extent of their interaction with the first layer water remains to be discovered.

Annealing the surface to higher temperatures (200-220 K) results in the partial dissociation of water. The resulting overlayer consists of 1D chains with a branched appearance, where the chain backbone is aligned along the $[1\,\bar{1}\,0]$ close-packed direction of Ni(110). There are two types of this 1D chain structure coexisting on the surface, with the branches having a slightly different arrangement of water/OH molecules to give either a Zigzag or Pinched structure. The water backbone in these two structures exactly mimics the 1D water chains proposed for the intact water phase. When the surface is annealed to the slightly lower temperature of 200 K, an additional structure is observed in the STM images. This is assigned to a c(2x2)

distorted hexagonal 2D structure, with some disruption in the structure along the [1 $\bar{1}$ 0] direction of the surface. This structure is thought to be a result of compressive strain and disappears when the surface anneal temperature is increased to 220 K.

Surface annealing above 340 K introduces the presence of bright and dark rows in the STM images, which have a respective height and depth roughly equivalent to the Ni lattice spacing (2.49 Å), and are attributed to two possible explanations. The first explanation involves the liberation of Ni atoms from the Ni-O chains seen in the experimental STM images by the proposed reaction, $H_2O + NiO \rightarrow Ni + 2OH$. This provides free Ni atoms which can coalesce on the surface terrace to form the resulting bright rows, similar to that reported by Pang *et al*. for an analogous reaction on Cu(110)[33]. This does not however explain the formation of the dark rows in the STM images, which leads to the suggestion that they are a result of removal of Ni from the terrace (dark rows) which then coalesce above the surface layer (bright rows). Although debatable, both explanations are proposed as a result of water dissociation and desorption.

Overall, this study has provided evidence to support the adsorption of intact water on Ni(110) at low temperature. Although pentagonal rings were expected to be the most favourable structure, based on DFT predictions, the first wetting layer is actually built from zigzag chains of flat and H-down water molecules to create a (2x2) unit cell. Surface annealing initiates the partial dissociation of water to form a c(2x2) distorted hexagonal structure and 1D branched chains, with Ni metal wires forming as a result of water dissociation and desorption from the surface as the anneal temperature is increased further. These (partially) dissociated structures are analogous to that reported on Cu(110)[17,30,33], but they are observed at a slightly higher anneal temperature on Ni, which is a result of the stronger binding of water to the Ni(110) surface.

4.5. References

[1] L. Zhu, C. Liu, X. Wen, Y Li, H. Jiao, *Catalysis Science and Technology*, 2019, **9**, 199-212.

[2] T. Pache, H. P. Steinrück, W. Huber, D. Menzel, *Surface Science*, 1989, **224**, 195-214.

[3] M. Schulze, R. Reißner, K. Bolwin, W. Kuch, *Fresenius' Journal of Analytical Chemistry*, 1995, **353**, 661-665.

[4] G. Pirug, O. Knauff, H. P. Bonzel, *Surface Science*, 1994, **321**, 58-70.

[5] B. W. Callen, K. Griffiths, P. R. Norton, D. A. Harrington, *The Journal of Physical Chemistry*, 1992, **96**, 10905-10913.

[6] H. Seenivasan, A. K. Tiwari, *The Journal of Chemical Physics*, 2014, **140**, 174704.

[7] B. W. Callen, K. Griffiths, U. Memmert, D. A. Harrington, S. J. Bushby, P. R Norton, *Surface Science*, 1990, **230**, 159-174.

[8] C. Benndorf, T. E. Madey, *Surface Science*, 1988, **194**, 63-91.

[9] B. W. Callen, K. Griffiths, R. V. Kasza, *Journal of Chemical Physics*, 1992, **97**, 3760-3774.

[10] K. Griffiths, U. Memmert, B. W. Callen, P. R. Norton, *Journal of Vacuum Science and Technology A*, 1989, **7**, 2001.

[11] B. W. Callen, K. Griffiths, P. R. Norton, *Physical Review Letters*, 1991, **66**, 1634-1637.

[12] M. Kovar, R. V Kasza, K. Griffiths, P. R. Norton, G. P. Williams, D. Van Campen, *Surface Review and Letters*, 1998, **5**, 589-598.

[13] B. W. Callen, K. Griffiths, P. R. Norton, *Surface Science*, 1992, **261**, L44-L48.

[14] A. Hodgson, S. Haq, *Surface Science Reports*, 2009, **64**, 381-451.

[15] L. Ollé, M. Salmeron, A. M. Baro, *Journal of Vacuum Science and Technology A*, 1985, **3**, 1866-1870.

[16] M. Hock, I. Bassignana, K. Wagemann, J. Küppers, *Surface Science*, 1986, **177**, L978-L982.

[17] M. Forster, R. Raval, J. Carrasco, A. Michaelides, A. Hodgson, *Chemical Science*, 2012, **3**, 93.

[18] J. Carrasco, A. Michaelides, M. Forster, S. Haq, R. Raval, A. Hodgson, *Nature Materials*, 2009, **8**, 427-431.

[19] G. Kresse, J. Furthmuller, *Computational Materials Science*, 1996, **6**, 15-50.

[20] G. Kresse, J. Hafner, *Physical Review B*, 1994, **49**, 14251-14269.

[21] G. Kresse, J. Hafner, *Physical Review B*, 1993, **47**, 558-561.

[22] J. Klimes, *Physical Review B*, 2011, **83**, 195131.

[23] M. Dion, H. Rydberg, E. Schröder, D. C. Langreth, B. I. Lundqvist, *Physical Review Letters*, 2004, **92**, 246401.

[24] G. Kresse, D. Joubert, *Physical Review B*, 1999, **59**, 1758-1775.

[25] J. Tersoff, D. R. Hamann, *Physical Review B*, 1985, **31**, 805-813.

[26] S. Maier, B. A. J. Lechner, G. A. Somorjai, M. Salmeron, *Journal of the American Chemical Society*, 2016, **138**, 3145-3151.

[27] C. Lin, N. Avidor, G. Corem, O. Godsi, G. Alexandrowicz, G. R. Darling, A. Hodgson, *Physical Review Letters*, 2018, **120**, 076101.

[28] C. Lin, G. Corem, O. Godsi, G. Alexandrowicz, G. R. Darling, A. Hodgson, *Journal of the American Chemical Society*, 2018, **140**, 15804-15811.

[29] S. Haq, C. Clay, G. R. Darling, G. Zimbitas, A. Hodgson, *Physical Review B*, 2006, **73**, 115414.

[30] M. Forster, R. Raval, A. Hodgson, J. Carrasco, A. Michaelides, *Physical Review Letters*, 2011, **106**, 046103.

[31] D. L. Doering, T. E. Madey, *Surface Science*, 1982, **123**, 305-337.

[32] E. D. Williams, *Journal of Vacuum Science and Technology A*, 1983, **1**, 1188.

[33] Z. Q. Pang, S. Duerrbeck, C. Kha, E. Bertel, G. A. Somorjai, M. Salmeron, *Journal of Physical Chemistry C*, 2016, **120**, 9218-9222.

[34] H. Guo, *Catalysis Letters*, 2003, **88**, 95-104.

Chapter 5

An Investigation into the Structure of Water on a Stepped Surface of Pt(211)

5.1. Introduction

The adsorption of water on stepped surfaces has become of interest over recent years in hope of gaining a better understanding as to what makes a good ice-nucleating agent. Having investigated the compatibility of flat surfaces to nucleate and grow ice[1-8], none of the multilayer structures that form on these ideal templates actually match that of a true ice-like layer. Those studying ice-nucleating proteins have suggested that symmetry and corrugation are key requirements for a surface to be a good ice-nucleating agent[9,10], concepts which had not really been considered previously. In light of this, the suitability of stepped surfaces to nucleate ice has gained great attention, with the hope of corrugated surface symmetry providing a basis to grow true ice-like layers.

With stepped surfaces influencing the binding sites of water, it seems likely that the structures which form will deviate significantly from the molecular ordering of bulk hexagonal ice[11]. On a flat Pt(111) surface, water forms a (√37x√37)R25.3° structure at low coverage, restructuring to a (√39x√39)R16.1° arrangement as the wetting layer completes[12,13]. This overlayer is built from a combination of flat water hexamers tightly bound to Pt, higher-lying hexagonal rings arranged H-down and rotated 30° with respect to the tightly bound hexamers, and a combination of pentagonal and heptagonal rings which bridge these two types of hexagonal units. However, studies on stepped Pt surfaces have shown considerable differences to this 2D network, with the reactive step edges dominating the binding site of water and the structures formed reported to be one dimensional chains[14-16].

Two interesting stepped Pt surfaces to consider are Pt(211) and Pt(221) which both have extremely narrow terraces. Figure 1a displays a comparison of TPD data for

both of these surfaces, along with Pt(111), revealing a large difference between the adsorption of water on flat and stepped Pt[16]. All three surfaces show significant differences in terms of the TPD plots. Pt(111), highlighted in black, shows multilayer desorption at around 160 K and a monolayer peak at a slightly higher temperature of approximately 175 K. The small tail present at 190 K is thought to be a result of surface imperfections, such as step sites and kinks[16-18]. The temperature difference between the two peak maxima is only 15 K, significantly different to that of the Pt(211) surface, highlighted in red. This plot also displays two desorption peaks, again corresponding to multilayer and monolayer desorption, but the temperature spread is much greater. With the multilayer peak at around 150 K and monolayer at 194 K, this leads to a maxima spread of approximately 45 K, three times that of the Pt(111) plot. This discrepancy suggests that the known 2D structure which forms on Pt(111), does not form on Pt(211), or one would expect the TPD data to look more similar.

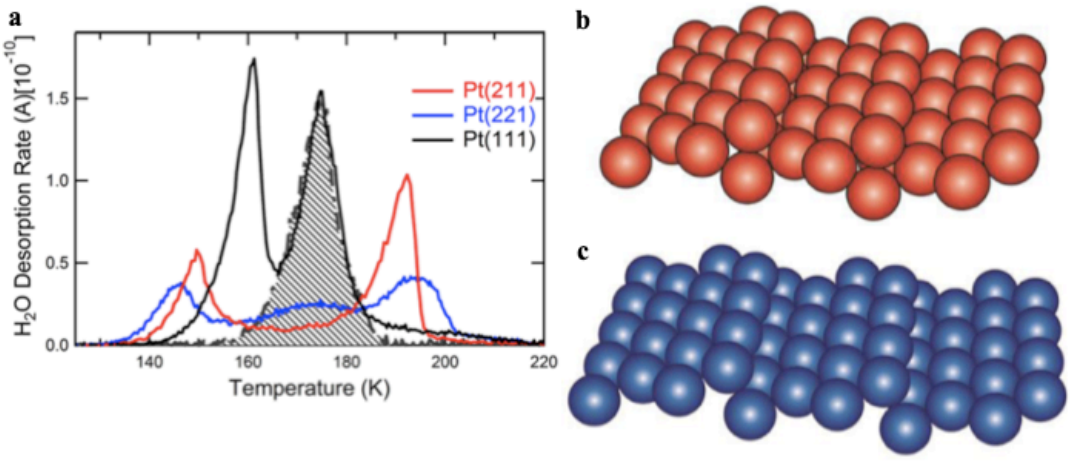

Figure 1. a) Comparison of TPD data for 1-2 ML water on flat Pt(111), stepped Pt(211) and stepped Pt(221) surfaces at 0.91 K/s, b) schematic of Pt(211), c) schematic of Pt(221).
Adapted from a/c) C. Badan *et al.*, *Journal of Physical Chemistry Letters*, 2016, **7**, 1682−1685 and b) C. Badan *et al.*, *Journal of Physical Chemistry C*, 2015, **119**, 13551-13560.

The other stepped surface investigated in this study is the Pt(221) surface, which is similar in structure to Pt(211). As seen in Figure 1b-c[16,19], both these surfaces exhibit a (111) terrace symmetry, but Pt(211) has only three-atom wide terraces with (100) step sites whereas Pt(221) has four-atom wide terraces with (111) step sites. This slight change in terrace width and step symmetry is sufficient to significantly change

the bonding structure on the surface. Pt(221) displays an additional broad desorption peak at around 170 K in the TPD plot, similar to that from Pt(111), which is not observed for Pt(211)[16]. This suggests that water forms a different structure on Pt(221) at low coverage (≤1 ML), with the exact terrace width and step symmetry playing a significant role in determining the structure which forms on these stepped surfaces.

Further analysis of the TPD data reveals more information about the structure of water on Pt(211). Multilayer water is less tightly bound to the surface, desorbing at a lower temperature than the monolayer water peak on Pt(111). The second TPD peak appearing at 194 K is described as water desorption from the favourable surface step sites[16]. As there is only one peak observed for the desorption of the entire first monolayer of water, it appears all of the water molecules in this first layer structure desorb simultaneously, which suggests there is only one structure forming for the first wetting layer.

An initial DFT study by Fajin *et al*. concluded that water would not dissociate on Pt(211) without a promoter[20], but this was contradicted by Badan *et al*., with TPD experiments indicating that first layer water partially dissociates into hydrogen and hydroxide species[19]. More recent studies were performed by Peköz *et al*. in the hope of understanding the surface wetting of Pt(211) to a greater extent[21,22]. They concluded that the partial dissociation of water on Pt(211) was facilitated by the increased surface reactivity and hydrogen-bonding cooperative effects. Overall, these studies indicate the disagreement within the literature to describe what is actually occurring when water adsorbs on this surface. These DFT and Molecular Dynamics (MD) calculations did however find that water more favourably adsorbs at the (100) step edges, but is weakly bound, giving an insight into the preferred binding site of water on this stepped Pt surface[22].

The findings reported in this chapter demonstrate inconsistencies between the results described here and those discussed in the literature. From STM analysis, it appears that water initially clusters at the step edges, forming a 2D structure which extends across more than one terrace as the wetting layer grows. This implies water is able to

bond across the (111) terraces of Pt(211) to form a structure larger than the simple 1D chains proposed in previous studies.

5.2. Experimental

5.2.1. Surface Preparation

The Pt(211) surface was initially cleaned by cycles of Ar^+ ion sputtering at 1 keV and annealing to approximately 1000 K. The surface quality was firstly determined by LEED to give a sharp diffraction pattern, followed by STM to show large, clean terraces before beginning water adsorption experiments.

The adsorption of water on the Pt(211) surface was studied using a CreaTec low-temperature STM. The UHV chamber was equipped with a separate preparation chamber, as shown in Chapter 2, with both chambers exhibiting a base pressure of $4x10^{-11}$ mbar. Water films were grown using a molecular beam directed through the STM housing aperture towards the crystal face. The water exposure was quantified by STM, with one layer defined as covering the complete Pt(211) surface. The surface was annealed within the STM housing at various temperatures to order the water structure. All experiments were performed in constant-current mode, with the exact temperature and tunnelling conditions stated in the figure caption.

5.3. Results and Discussion

5.3.1. Analysis of Clean Pt(211) Surface

5.3.1.1. Ordered Surface Structure

Pt(211) is a stepped surface built from extremely narrow terraces and regular step edges. The terraces exhibit a hexagonal (111) symmetry, being only three-atoms wide, whilst the step sites have a square (100) symmetry and are the more reactive, favourable site for water adsorption[19]. STM reveals formation of large flat terraces under the above preparation conditions, which are ideal to investigate the adsorption of water on this stepped surface. The STM features are separated by a step spacing of 6.8 Å, meaning the bright rows in the STM images (Figure 2a) are displaying single height Pt steps. Evidence to support that these regions are flat comes from there being no contrast difference between the (100) step edges in the STM images.

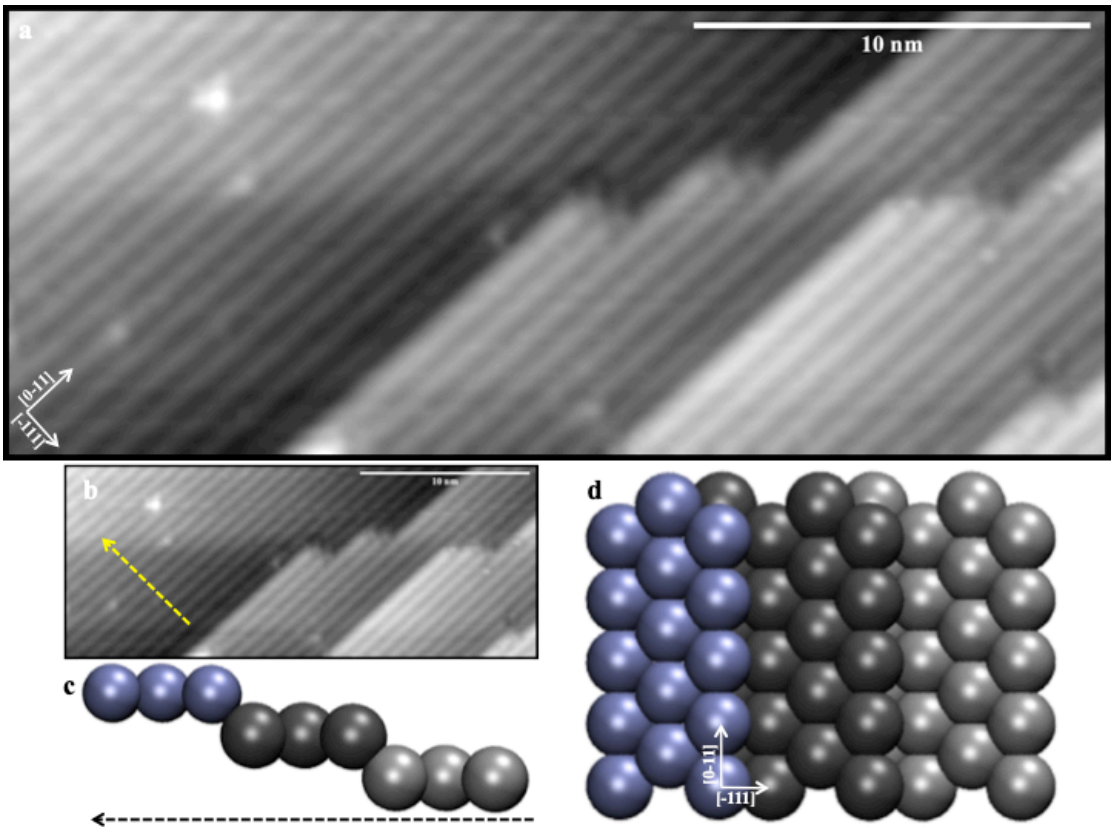

Figure 2. a) STM image of Pt(211) showing flat surface preparation before water adsorption experiments, with the step-up direction highlighted by the dashed arrow in b) (77 K, 74 mV, 53 pA), c) side-view and d) top-view of the Pt(211) surface with the 'step-up' direction highlighted from right to left in c), as described in the text.

c/d) Adapted from R. Peköz *et al.*, *Journal of Physical Chemistry C*, 2017, **121**, 16783-16791.

Analysis of the STM images gives further information about the structure of the surface layer. By examining the close-packed direction of the terrace, it is possible to understand the direction in which the steps grow. The surface schematic in Figure 2d demonstrates the close-packed direction along the step is the $[0\,\bar{1}\,1]$ direction. The direction across the step edge/terrace, on the other hand, is the perpendicular $[\,\bar{1}\,11]$ direction. The 'step up' direction, highlighted in Figure 2c, is the direction across the surface layer where the height of the topmost layer increases with each step edge. When examining the height profile obtained across the surface layer, the direction which shows a steady increase in the overall height of the topmost surface layer, is indicated by the dashed yellow arrow in Figure 2a. This corresponds to the 'step up' direction, which is the direction running from right to left in the schematic structure seen in Figure 2c.

5.3.1.2. Surface Roughness

Whilst perfecting the surface preparation, some regions appeared to have a rough surface in STM but give an ordered LEED pattern when analysed before transferring the sample into the characterisation chamber. This surface roughness is indicated by an alternation in contrast between different (100) step edges in the STM images. Figure 3a demonstrates this problem where the bright rows, corresponding to (100) steps, display different contrast. This is also supported by further height analysis where the profile of the area shows variation in the terrace sizes, measuring between two, three and four atom wide terraces across the surface layer. This discrepancy implies that the surface is not well ordered or one would expect the terrace sizes to be exclusively three atoms wide over the majority of the surface layer.

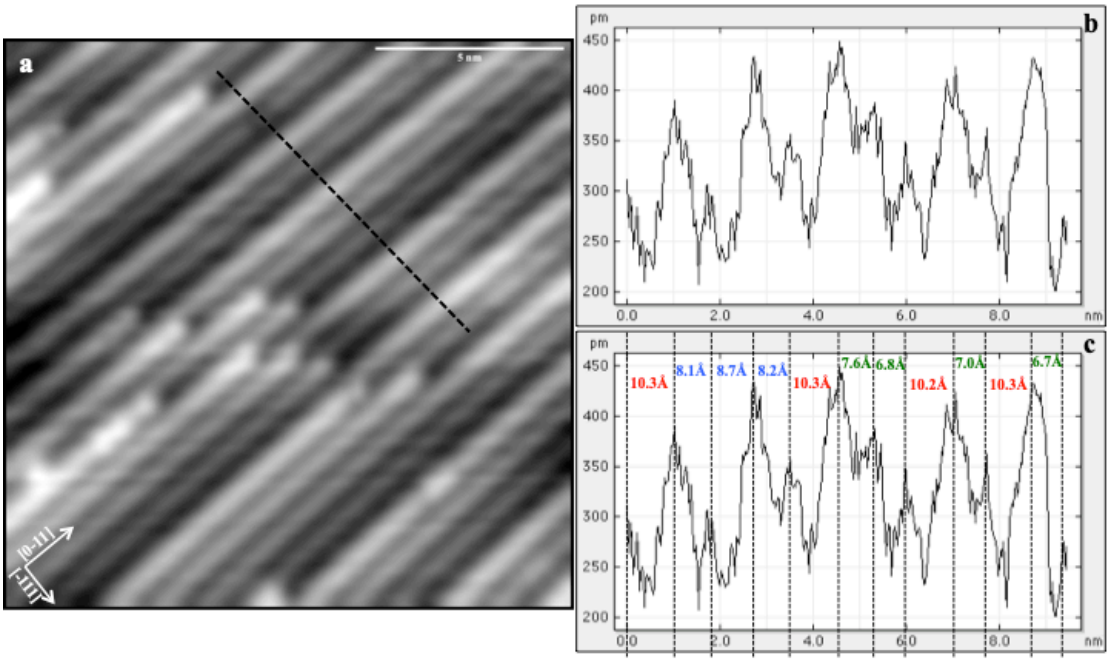

Figure 3. a) STM image of Pt(211) surface showing surface roughness when preparation conditions are not optimum (77 K, 1.14 V, 45 pA), b) height profile from the dashed line superimposed on a), c) highlighted terrace sizes for this region of interest showing different terrace widths.

This problem was avoided by increasing the anneal temperature slightly to obtain an overall flat surface, shown in Figure 2a, which did not show this surface roughness. Water adsorption experiments could then begin with confidence that the terraces had an optimum width of three atoms.

5.3.2. Adsorption of Water

To gain an understanding of how water initially wets the stepped surface of Pt(211), it was essential to initially expose the surface to only a small amount of water. At this low coverage, water clusters at the larger step edges, as seen in Figure 4a. These step sites are the most favourable sites for water adsorption, exhibiting a (100) symmetry.

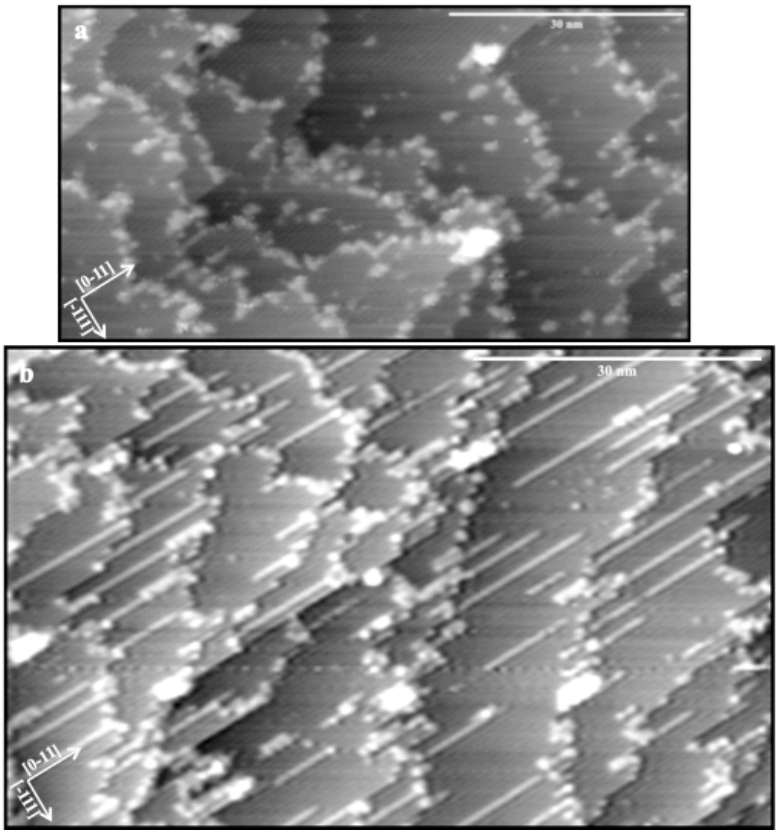

Figure 4. a) Low coverage water clusters at the step edges of the Pt(211) surface after surface annealing to 145 K (77 K, 1.47 V, 46 pA), b) shows the growth of water chains extending along the $[0\,\bar{1}\,1]$ direction of the surface as the coverage is increased (77 K, 1.43 V, 50 pA).

Increasing the water coverage sees the formation of long extended chains along the $[0\,\bar{1}\,1]$ direction of the Pt(211) surface. The STM images reveal a structure which appears wider than that of a simple 1D chain. This is seen in Figure 5a where the wetting structure extends across more than one terrace, suggesting the water molecules are able to bond across the (111) terraces, unlike previously anticipated[14,16,19,22,23]. This structure forms in preference to the growth of a larger, continuous 2D network across the surface layer, demonstrating the influence these hydrophilic step sites have on the growth of a water network.

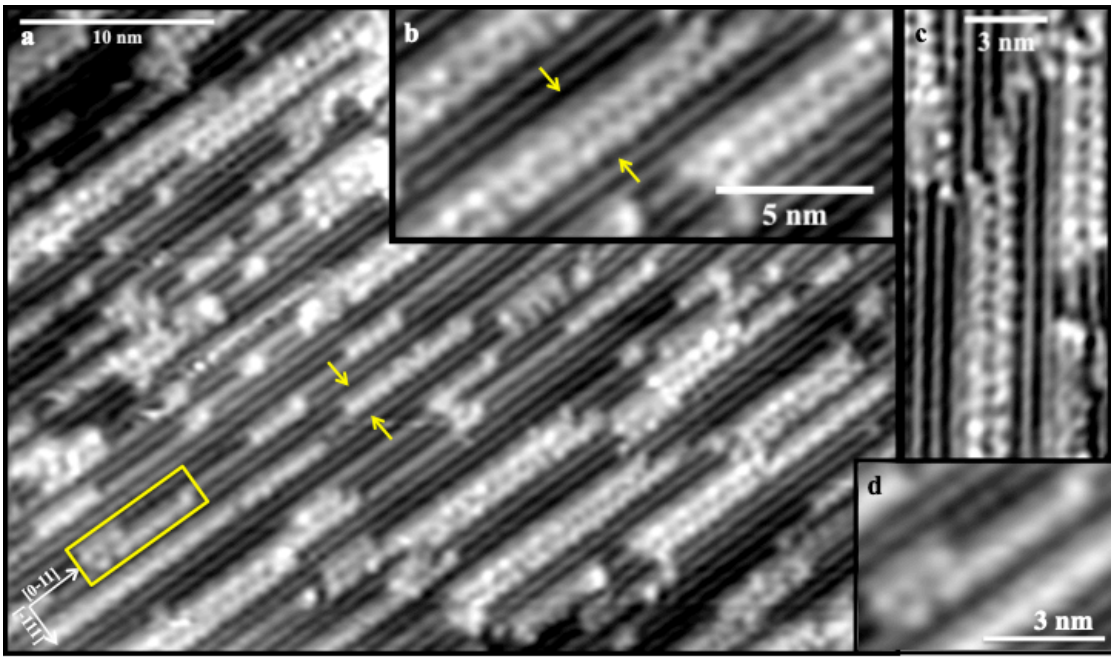

Figure 5. Water adsorption at 77 K on Pt(211) after surface annealing to 148 K, c) has been rotated for clarity of alignment with Pt(211) step sites and d) is a close-up of the intermediate structure highlighted by the yellow box in a) (77 K, 900 mV, 40 pA).

From the STM images, it seems that there are two types of structures present on this surface. The chain highlighted by the yellow arrows in Figure 5a reveals a narrow structure showing one bright side and a faint structure on the other side. The most common structure is the wider chains, one of which is highlighted by the yellow arrows in Figure 5b and seen as a filtered image in Figure 5c. These wide chains are reproducible and are seen throughout the surface layer, with an overall width of roughly 14-15 Å along the $[\bar{1}11]$ direction, extending across three rows of step sites. This is evident from the STM images in Figure 5 as the underlying (100) step edges are displayed as the bright rows in the STM image. There is little evidence of any islands wider than this three step width, and no extended 2D domains are found.

5.3.2.1. Discussion of the Structure

The measurements obtained from the STM images provide evidence that water forms a small 2D structure on Pt(211), extending along the $[0\,\bar{1}\,1]$ step direction. The structure bridges across three rows of step edges, confirming the expected preference for water to bind to stepped sites. The structure, however, does not extend wider than three rows of step sites, which suggests that growth into a continuous 2D layer is unfavourable.

The narrow structure highlighted by the yellow arrows Figure 5a, appears to bridge across a maximum of two rows of step sites, averaging a spacing of roughly 8-10 Å in width. It is thought this minority structure is formed initially and would disappear as the water coverage is increased to favour formation of the wider 2D chain structure discussed above. There are also additional structures present that seem to be intermediate structures between the narrow and wider chains. An example of this structure is highlighted by the yellow box in Figure 5a, and is shown as a close-up image in Figure 5d. This appears to be an intermediate in the growth of the three step wide water clusters, representing an intermediate growth structure as the wider cluster grows from the narrow chain, increasing the average hydrogen-bond coordination towards that of a 2D structure.

Previous experimental and theoretical work reports that water forms 1D chains along the step edges of Pt(211) and will not bridge across the (111) terraces to form a 2D structure[14,16,19,22,23]. This directly contrasts the STM data reported in this chapter, which clearly shows structures larger than a simple 1D array of water molecules, bonded between at least two neighbouring step edges. The most obvious explanation for this is that water adsorbed on the terrace is stabilised by the water molecules adsorbed at the step sites. These step bound water molecules lock the hydrogen-bonding network and stabilise the water that binds above the (111) terraces, creating a network that is more stable than the simple 1D chain anticipated from calculations. This behaviour has been reported for other structures, including the 2D network which forms on Cu(511), where water bonds across both the hydrophilic step sites and hydrophobic terrace regions[9,24]. The linear structures formed on Pt(211) may remain favourable over a full 2D network because these narrow clusters contain a higher proportion of water adsorbed at the stable step sites, compared to that in an infinite 2D network. An alternative explanation may be that the narrow width of the clusters allows the water network to accommodate lattice mismatch to the substrate that would otherwise destabilise an extended 2D network. These questions will be addressed in future by DFT calculations to explore the structures observed.

5.3.2.2. Comparison with Cu(511)

Lin *et al*. investigated the structure of a 2D [3 1, $\bar{3}$ 1] wetting layer on Cu(511)[9]. Also a stepped surface, Cu(511) exhibits narrow three-atom wide terraces with a (100) structure. These sites are hydrophobic and therefore unfavourable to bind water, but by binding tightly to the step edges, water is able to form a stable 2D layer. This 2D network requires only three water molecules to sit at unfavourable terrace sites and bridge the network between seven water molecules adsorbed along the step edges. The stability of the step sites, combined with the high degree of hydrogen-bonding, is sufficient to support surface wetting, resulting in the formation of a 2D layer that could not be predicted from theory. The Cu(511) terrace arrangement is very similar to the Pt(211) surface being investigated here, both having three-atom wide terraces between low coordinate step sites. It is therefore feasible for the water network to bridge across the hydrophobic (111) terraces to bind to the more favourable (100) step sites.

The structure which forms on Pt(211), however, clearly favours formation of narrow water chains in place of a continuous 2D network. This is different to that seen on Cu(511) and is thought to be a result of a stronger binding of water to the steps of Pt with respect to Cu[9]. Previous experiments find the steps on Pt stabilise significantly more water than can be associated with a simple linear chain[15-17,19,25], and electronic structure calculations by Kolb *et al*. proposed interlinked rings growing along the steps[15,25]. Other theoretical work suggests that water will bind flat atop the step and H-down beside it, which places the water and step dipoles in opposition[15,26]. This encourages the water molecules to preferentially form extended 2D chains, aiding the strain relief of the water structure along the [0 $\bar{1}$ 1] step direction. Wheras a 2D network can form on Cu(511) with little distortion from the bulk ice spacing (just 2.1 %)[9,24], the clusters formed on Pt(211) remain linear, with the step sites clearly defining the width of the structures formed. This suggests the larger lattice spacing of Pt causes the 2D layer to be too strained to remain stable.

5.3.2.3. Comparison to Pt(533)

Pt(533) has a very similar structure to Pt(211), both exhibiting reactive (100) step sites, but with a slightly different terrace width; Pt(211) has three-atom wide terraces, whereas Pt(533) has slightly wider four-atom terraces. Overall, this can make a large

difference in adsorption as the terraces are already extremely narrow. On Pt(533), Kolb *et al*. report the formation of linear double stranded water chains forming along the favourable (100) step edges, with tetramer units linking flat chains on the step edge to a H-down chain below it[15]. With Pt(533) having four-atom wide terraces, these may be too large to form a stable water structure that bridges across two or more step edges. Instead, water bonds at the preferred step sites, and apparently, a strained tetramer unit completes the hydrogen-bonding network. Pt(211), having a smaller terrace width, is able to form a 2D network across at least 2 or 3 steps, but does not create a full, extended 2D network across many steps.

5.4. Conclusions

The adsorption of water on a stepped surface of Pt(211) has been investigated in the hope of understanding how corrugated surfaces can influence the structures adopted by water. Although only a low coverage of water has been studied here, being less than 1 ML, it has already revealed an exciting insight into the structure that water forms on this stepped surface.

With the low coordinate step sites being the most favourable site for water adsorption, water preferably binds here at very low coverage. As the coverage is increased, long 2D chains extend along the $[0\,\bar{1}\,1]$ direction of the Pt(211) surface, forming linear structures which are rather wider than the 1D chains originally proposed in the literature[14,16,19,22,23]. This is thought to be a result of water binding above the terrace sites, bridging between two or three steps to form narrow, linear structures.

Badan *et al*. proposed that the three-atom wide terraces of the Pt(211) surface are too narrow to support a favourable hexagonal base unit to grow crystalline bulk ice, without seeing interference from the reactive (100) step sites[16,19]. The results reported in this chapter, however, reject the idea that the terraces are intrinsically too narrow to bind water, as structures wider than simple 1D rows are observed in STM. It appears that water is able to bridge across the three-atom wide (111) terraces, although via a less favourable binding site, forming small 2D structures. This has also been observed on other stepped surfaces such as Cu(511)[9], but in the case of Pt(211), the islands are elongated along the step direction to maximise the fraction of the water that is bound to the step site.

This study concludes that water does not form simple 1D chains on Pt(211), as originally proposed. Instead, wider chains form which bridge across three rows of steps sites, thought to be the most favourable structure. This wetting behaviour is quite different from any other system we have previously seen and brings questions about both surface and step reactivity influencing the binding site of water and the structures that form. We hope that future work on this system will reveal more insight into this unusual behaviour and reveal the hydrogen-bonding structures involved in wetting this surface.

5.5. References

[1] A. Hodgson, S. Haq, *Surface Science Reports*, 2009, **64**, 281-451.

[2] J. Carrasco, A. Hodgson, A. Michaelies, *Nature Materials*, 2012, **11**, 667-674.

[3] M. Henderson, *Surface Science Reports*, 2002, **46**, 5.

[4] S. Maier, B. A. J. Lechner, G. A. Somorjai, M. Salmeron, *Journal of the American Chemical Society*, 2016, **138**, 3145-3151.

[5] A. Massey, F. McBride, G. R. Darling, M. Nakamura, A. Hodgson, *Physical Chemistry Chemical Physics*, 2014, **16**, 24018.

[6] J. Stachler, M. Mehlhorn, U. Bovensiepen, M. Meyer, D. O. Kusmierek, K. Morgenstern, M. Wolf, *Physical Review Letters*, 2007, **98**, 206105.

[7] K. Thürmer, N. C. Bartelt, *Physical Review Letters*, 2008, **100**, 186101.

[8] K. Thürmer, S. Nie, *Proceedings of the National Academy of Science of the United States of American (PNAS)*, 2013, **110**, 11757-11762.

[9] C. Lin, N. Avidor, G. Corem, O. Godsi, G. Alexandrowciz, G. R. Darling, A. Hodgson, *Physical Review Letters*, 2018, **120**, 076101.

[10] R. Pandey, K. Usui, R. A. Livingstone, S. A. Fischer, J. Pfaendtner, E. H. G. Backus, Y. Nagata, J. Frohlich-Nowoisky, L. Schmuser, S. Mauri, J. F. Scheel, D. A. Knopf, U. Poschl, M. Bonn, T. Weidner, *Science Advances*, 2016, **2**, e1501630.

[11] L. B. F. Juurlink, *Journal of Physics – Condensed Matter*, 2018, **30**, 090301.

[12] S. Nie, P. J. Feibelman, N. C. Bartelt, K. Thürmer, *Physical Review Letters*, 2010, **105**, 026102.

[13] K. Thürmer, N. C. Bartelt, *Physical Review Letters*, 2008, **100**, 186101.

[14] M. Nakamura, N. Sato, N. Hoshi, J. M. Soon, O. Sakata, *Journal of Physical Chemistry C*, 2009, **113**, 4538-4542.

[15] M. J, Kolb, R. G. Farber, J. Derouin, C. Badan, F. Calle-Vallejo, L. B. F. Juurlink, D. R. Killelea, M. T. M. Koper, *Physical Review Letters*, 2016, **116**, 136101.

[16] C. Badan, Y. Heyrich, M. T. M. Koper, L. B. F. Juurlink, *Journal of Physical Chemistry Letters*, 2016, **7**, 1682−1685.

[17] M. L. Grecea, E. H. G. Backus, B. Riedmüller, A. Eichler, A. W. Kleyn, M. Bonn, *Journal of Physical Chemistry B*, 2004, **108**, 12575-12582.

[18] A. T. Gee, B. E. Hayden, C. Mormiche, T. S. Nunney, *Journal of Chemical Physics*, 2000, **112**, 7660-7668.

[19] C. Badan, M. T. M. Koper, L B. F. Juurlink, Journal of Physical Chemistry C, 2015, **119**, 13551-13560.

[20] J. L. C. Fajin, M. N. D. S. Cordeiro, J. R. B. Gomes, *Journal of Physical Chemistry A*, 2014, **118**, 5832-5840.

[21] R. Peköz, S. Wörner, L. M. Ghiringhelli, D. Donadio, *Journal of Physical Chemistry C*, 2014, **118**, 29990-29998.

[22] R. Peköz, D. Donadio, *Journal of Physical Chemistry C*, 2017, **121**, 16783-16791.

[23] O. Endo, M. Nakamura, R. Sumii, K. Amemiya, *Journal of Physical Chemistry C*, 2012, **116**, 13980-13984.

[24] C. Lin, G. Corem, O. Godsi, G. Alexandrowicz, G. R. Darling, A. Hodgson, *Journal of the American Chemical Society*, 2018, **140**, 15804-15811.

[25] A. den Dunnen, M. van der Niet, C. Badan, M. T. M. Koper, L. B. F. Juurlink, *Physical Chemistry Chemical Physics,* 2015, **17**, 8530.

[26] M. J. Kolb, J. Wermink, F. Calle-Vallejo, L. B. F. Juurlink, M. T. M. Koper, *Physical Chemistry Chemical Physics*, 2016, **18**, 3416.

Summary

Summary of Thesis

The analysis and characterization of water/metal interfaces is essential to understand important processes which occur in science, nature and technology, not only overcome undesirable outcomes such as corrosion, but also to enhance industrial applications including heterogeneous catalytic reactions. Water/metal interfaces have therefore been studied for many years in hope of developing an insight into surface wetting and subsequent ice growth. Surface analysis techniques have been key to this field, focusing on ideal surface reactions using well-defined single crystal surfaces in Ultra High Vacuum systems. By taking this approach, the water/metal interfaces which form can be analysed and interpreted within this ideal perfect system, without the complication of contaminants effecting the reaction, before applying this information to the macroscopic world. High-resolution Scanning Tunnelling Microscopy provides a direct route to do this, allowing direct investigation of water and its hydration at solid interfaces.

This thesis discusses the surface wetting of close-packed, open-faced and stepped metal surfaces and the variation in structures that form in this interfacial layer. It takes into account how specific sites can provide preferential binding, how the reactivity of different metals can have an effect on the structures which form and whether this influences dissociation. It also deliberates factors that help make a good ice nucleating agent and whether a surface can act as a template to grow an ordered multilayer film. Tackling a variety of different surface characteristics, the discussions in this thesis give a good overview of the field, but also the on-going issues and difficulties which still need to be addressed and hopefully overcome in the future.

Future Experiments and Data Analysis

Future experiments with regards to the SnPt(111) alloy system discussed in Chapter 3, could involve the use other surface analysis techniques to analyse the monolayer alloy structure which forms. Although we believe this system forms only a monolayer

surface alloy, the development and recent optimisation of gas cluster ion sources would allow the removal of material from the surface without causing damage to the bulk structure as seen with monatomic etching. Using depth profile experiments, one could gently etch away the topmost surface layers and use X-ray Photoelectron Spectroscopy to rule out the presence of Sn in the bulk Pt structure.

Further data analysis of this system would allow one to work out whether the second layer domains grow from the triangular defects discussed in Chapter 3, or whether they terminate the second wetting layer. As a first thought, it is more likely that they terminate the second layer domain structure as there are not many present in the STM images included in this thesis. However, one could reanalyse the data recorded to rule out the nucleation of water from these sites, and to also gain an insight into the kinetics behind the growth of this strained second layer structure.

Future work on the water/Ni(110) system from Chapter 4 would be to analyse the structures which form at low temperature with Low Energy Electron Diffraction. This would be a useful approach to confirm the formation of the (2x2) structure seen for the low coverage 2D islands at 77 K, and their transformation into the (4x4) structure as the coverage is increased. A measurement of the exact coverage at which these structures form could provide confirmation of the type of structures formed.

Future experiments also involves completing the investigation into the surface wetting of Pt(211) seen in Chapter 5. Only a preliminary study was included in this thesis as a result of time restrictions, which involved the analysis of only a partial monolayer coverage of water. To aid understanding of this system, one would need to examine the adsorption of a higher water coverage, up to and maybe beyond a complete monolayer of water. It would be extremely interesting to see how the structure of water persists on the surface as the coverage is increased and how repulsive interactions prevent the water layer from forming a continuous 2D layer when space is limited.